Optimised Active Fault Detection for an Open Loop Stable System

by

Regardt Busch

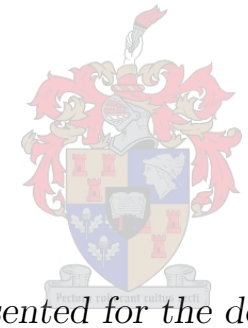

Dissertation presented for the degree of Doctor of Philosophy in Engineering in the Faculty of Engineering at Stellenbosch University

Supervisor: Prof. T. Jones

December 2016

Declaration

By submitting this dissertation electronically, I declare that the entirety of the work contained therein is my own, original work, that I am the sole author thereof (save to the extent explicitly otherwise stated), that reproduction and publication thereof by Stellenbosch University will not infringe any third party rights and that I have not previously in its entirety or in part submitted it for obtaining any qualification.

Date: .....

Abstract

Optimised Active Fault Detection for an Open Loop Stable System

R. Busch

Department of Electrical and Electronic Engineering,
University of Stellenbosch,
Private Bag X1, Matieland 7602, South Africa.

Dissertation: PhD

November 2016

Active fault detection for a stable open-loop linear time invariant system is considered. The optimal active fault detection setup is developed around an estimator based architecture. The auxiliary signal and estimator are then designed in order to maximize detection performance.

Equations are derived which relate the estimator design to the nominal residual signal covariance. The relationship between the auxiliary input and the system performance degradation constraint is considered. The effect of estimator gain and excitation signal frequency on the dual Youla-Jabr-Bongiorno-Kucera parameter is investigated.

An LTI input shaping filter is added to allow for added MIMO system complexity. Theory developed for the general output zeroing problem is combined with the extended MIMO architecture in order to arrive at a solution without the nominal performance penalty usually associated with active fault detection. Furthermore, the effect of the control input is considered and formulated as an additional optimisation criterion, resulting in an average-case optimisation scenario.

The effect of the excitation signal frequency on detector performance is investigated, and a minimum targeted detection time parameter is introduced. This set of equations is then used to minimise the fault detection time for fixed performance constraints and minimum targeted detection time.

A conceptual Active Fault Tolerant Control Framework is developed for a small unmanned aerial vehicle, emphasising the role of fault detection. The theoretical framework is then applied to this UAV, illustrating the applicability of the proposed AFD framework to more complex practical problems.

Uittreksel

Geoptimeerde Aktiewe Vout Deteksie vir n Ooplus Stabiele Stelsel

("Optimised Active Fault Detection for an Open Loop Stable System")

R. Busch

Departement Elektries en Elektroniese Ingenieurswese,
Universiteit van Stellenbosch,
Privaatsak X1, Matieland 7602, Suid Afrika.

Proefskrif: PhD

November 2016

Aktiewe foutdeteksie vir 'n stabiele oop-lus liniere tyd-onafhanklike stelsel word oorweeg. Die optimale aktiewe foutdeteksie stelsel word ontwerp rondom 'n beramer-gebaseerde argitektuur. Die hulpsein en beramer word dan ontwerp om opsporingsvermoe te maksimeer.

Vergelykings wat die verband tussen die beramerontwerp en die nominale residuele sein se kovariansie beskryf word afgelei. Die verhouding tussen die hulpsein en die beperking op die stelsel se prestasie agteruitgang word oorweeg. Die effek van beramer aanwins en die hulpsein frekwensie op die dubbel-Youla-Jabr-Bongiorno-Kucera parameter word ondersoek.

'n Liniere tyd-onafhanklike insetvormende filter word bygevoeg om die addisionele multi-inset multi-uitset kompleksietyd te hanteer. Teorie wat ontwikkel is vir die algemene uitset nulstellingsprobleem word gekombineer met die uitgebreide multi-inset multi-uitset argitektuur om 'n oplossing to vind sonder enige van die nominale stelselprestasie agteruitgang wat gewoonlik geassosieer word met aktiewe foutdeteksie. Verder word die effek van die beheerinset

oorweeg, en geformuleer as ’n addisionele optimiseringskriterium, wat lei tot gemiddelde-geval optimisering.

Die effek van die hulpsein frekwensie op die foutdeteksie prestasie word ondersoek, en ’n minimum teiken opsporingsparameter word ingestel. Hierdie stel vergelykings word dan gebruik om die foutdeteksie tyd vir vaste prestasiebeperkings en minimale geteikende deteksie tyd so laag as moontlik te kry.

’n Konseptuele Aktiewe Foutverdraagsame Beheerraamwerk is ontwikkel vir ’n klein onbemande lugvoertuig, wat die rol van foutdeteksie beklemtoon. Die teoretiese raamwerk word dan tot hierdie onbemande lugvoertuig aangewend, om sodoende die toepaslikheid van die voorgestelde Aktiewe Foutdeteksie raamwerk op meer ingewikkelde praktiese probleme te illustreer.

Acknowledgements

I would like to express my sincere gratitude to the following people and organisations:

- Dr. Iain K. Peddle for his support and guidance during the first few years of this project.
- Prof. Thomas Jones for his continued support as my study leader during the latter part of this project, as well as his insights and supervisory role throughout the entire project.
- My lovely wife Charmaine, for her continued encouragement, her steadfast faith in me, and the provision of her superior linguistic skills when they were most needed.
- My loving parents for supporting me whenever I may have needed them. Without your continued support none of this would have been possible.
- The DPSS at the CSIR, as well as Department of Science and Technology, for their much needed financial support.
- The Department of Electrical and Electronic Engineering for providing an environment conducive to advanced research.

Contents

List of Figures

List of Tables

Nomenclature

Vectors and Tensors

$G_{ed}(s)$	System from Disturbance Input to Error Output
$G_{eu}(s)$	System from Actuator Input to Error Output
$G_{yd}(s)$	System from Disturbance Input to Sensor Output
$G_{yu}(s)$	System from Actuator Input to Sensor Output
$P_{ed}(s)$	System from Disturbance Input to Error Output
$P_{e\eta}(s)$	System from Auxiliary Input to Error Output
$P_{rd}(s)$	System from Disturbance Input to Residual Output
$P_{r\eta}(s)$	System from Auxiliary Input to Residual Output
A, B, C, D	State Space System Matrix
Θ	Parametric Fault Matrix
η	Auxiliary Input Signal
r	Residual Output Signal
d	Disturbance Signal
$H_u(s)$	Control Input Shaping Filter
$H_\eta(s)$	Auxiliary Input Shaping Filter
$D_r(s)$	Detector Dynamics

Variables

Λ_0	Nominal Disturbance Constraint
Λ_1	Faulty Disturbance Constraint
ν_0	Nominal Detection Signal
ν_1	Faulty Detection Signal

$\omega_{L_{opt}}$	Optimal Estimator Bandwidth
$\omega_{\eta_{opt}}$	Optimal Excitation Frequency
t_d	Targeted Detection Time
c_l	Detector Leakiness Factor
P, Q, R	Roll, Pitch and Yaw Rate
$\dot{P}, \dot{Q}, \dot{R}$	Roll, Pitch and Yaw Acceleration
B_w	Lateral Acceleration
C_w	Normal Acceleration
α	Angle of Attack
β	Angle of Sideslip

Acronyms

6DOF	Six Degrees of Freedom
AFD	Active Fault Detection
AFTC	Active Fault Tolerant Control
CUSUM	Cumulative Sum
FDD	Fault Detection and Diagnoses
FTC	Fault Tolerant Control
IFAC	International Federation of Automatic Control
ILC	Inner-Loop Controller
IMM	Interacting Multiple-Model
LFT	Linear Fractional Transform
LTI	Linear Time Invariant
LQ	Linear Quadratic
LQG	Linear Quadratic Gaussian
MIMO	Multiple Input Multiple Output
MIT	Massachusetts Institute of Technology
MRAC	Model Reference Adaptive Control
OLC	Outer-Loop Controller
PCA	Principal Component Analysis

SDG	Signed Digraphs
SISO	Single Input Single Output
UAV	Unmanned Aerial Vehicle
YBJK	Youla-Bongiorno-Jabr-Kucera

Chapter 1

Introduction

This chapter begins by providing background information to the Active Fault Detection research presented in the remainder of this thesis. A brief history to the wider field of Fault Tolerant Control and more specifically Fault Detection is provided. Next, a detailed motivation for implementing an Active Fault Detection system is provided. The research presented here is then related to previous research performed at Stellenbosch University. Finally, a brief thesis outline is provided.

1.1 Background

1.1.1 Definition

Active fault detection (AFD) is the technique of detecting anomalous changes by means of injecting an external excitation signal into the system and then monitoring the system's response to this excitation signal.

1.1.2 History of Fault Tolerant Control and Fault Detection

With the ever increasing levels of automation and control came ever increasing demands on sophistication, performance, availability, and reliability of these automated systems.

One of the first research fields spawned by this search was adaptive control. The earliest adaptive controllers were the results of autopilot research in the 1950s. The first Model Reference Adaptive Control (MRAC) designs were based on the Massachusetts Institute of Technology (MIT) rule, and later on the optimal Linear Quadratic (LQ) solution [1]. However from the 1970s onwards a number of concerns were raised about the stability problems associated with the adaptive control schemes of the time.

Around the same time the field of Robust Control started to produce practically applicable theory. With robust control, the control law remains fixed but uncertainty is explicitly considered during the design phase. Robust control was born from the failures and disappointments experienced when attempts were made in the mid 1970s to apply Linear Quadratic Gaussian (LQG) control to practical problems including submarines and aircraft[2]. Robust control research has lead to a number of frequently used design tools and concepts such as: Multi-variable stability margins; H^2 synthesis; H^∞ optimal synthesis; and later H^∞ loop shaping.

Both adaptive and robust control theory are attempts to deal with the uncertainty problem but solves the problem using entirely different approaches. Both these approaches have there own advantages and disadvantages, and from the 1980s onwards attempts were made to combine the strengths of both into what is known as Robust Adaptive Control [2] [3] [4].

Both Adaptive Control as well as Robust Control theory can be used to develop so called Passive Fault Tolerant Control Systems (PFTC). This is usually done by modelling system failures as parametric variations. These PFTC systems do not employ fault detectors or online parameter estimation, and they do not actively reconfigure the control law after a failure.

Research into Active Fault Tolerant Control (AFTC), and the subsystems required to make it viable, was sparked by a number of air transport incidents in the 1970s which made it clear that using the remaining actuators in an unconventional manner could save the vehicle after a serious failure. It was quickly realised that the limiting factor to the success of these AFTC systems was fast and accurate fault detection [5] [6].

Not surprisingly, research into fault detection also started in the 1970s with the development of observer based detectors. Later in the same decade, system

identification based methods also started to appear. The parity-equation based methods that are currently popular first appeared in the mid 1980s. Activity started to gather pace in the early 1990s with the International Federation of Automatic Control (IFAC) holding symposiums and later establishing a technical committee for the rapidly progressing research field[7].

The first publications in the field of active fault detection started in the late 1980s with the publication of research on auxiliary signal design by Zhang [8] [9]. This was followed by more research on the design of auxiliary input signals including the research published by Keresteciogl u [10] [11] in the early 1990s. Research in the field accelerated rapidly from the late 1990s onwards with a number of significant publications including, numerous publications by Nikoukhah and/or Campbell [12] [13] [14] [15] [16].

1.1.3 Motivation for Active Fault Detection

A key element of an AFTC system is a reliable and efficient fault detector. Fault Detection Approaches can be subdivided into passive or active fault detection. With passive fault detection the system response is simply monitored, while for active fault detection additional stimuli are injected. Both approaches come with their own advantages and disadvantages. However, the primary reason for using active fault detection is that it provides the ability to provide guarantees on the detection performance independently of control inputs.

The main disadvantage of using active fault detection is the negative effect this additional excitation has on the other system performance parameters, while passive fault detection imposes no such penalty. This negative effect can however be minimised to such a degree that it imposes a very small performance penalty, and in some cases even completely eliminated.

1.1.4 Control and Systems Research at Stellenbosch University

Extensive research has been conducted in the related fields of control and general systems research at Stellenbosch University's Electronic Systems Lab-

oratory (ESL).

Most of the research conducted in the ESL since 2001 has emphasized Aerospace applications, in particular Unmanned Aerial Vehicles, which include both fixed and rotary wing vehicles [17] [18] [19] [20] [21]. Some of the most notable research conducted has been on Manoeuvre Autopilot Design and Application [22] [23] [24] [25] [26] [27].

From 2010 onwards the research performed started to focus more on Fault Tolerant Control and related fields, in particular applied to Unmanned Aerial Vehicles. Initially the research focused on system identification [28], post failure actuator reallocation [29], and standard adaptive control solutions [30]. Following this, research was performed on more complex asymmetric failure cases [31], online system identification [32], and a comparison of available fault detection methods applicable to actuator failures [33].

1.2 Literature Review

Classifying fault detection systems into exact groupings is often a difficult task as different aspects of the fault detection system may be classified into different groups. According to a review paper by Zhang and Jiang [34] fault detection systems may be classified by using a number of different metrics, these include: Model vs Data based; Qualitative vs Quantitative; by residual generation technique; and by residual evaluation technique. A similar grouping is also proposed in an extensive review paper by Venkatasubramanian et al.[35] [36] [37]. Each of these groupings can again be subdivided into a number of subgroups. In addition to the groupings proposed in [34] and [35] [36] [37] it is also useful to group the schemes based on the type of excitation used, i.e passive vs active excitation. This distinction provides many of the basic axioms underlying the research to follow, and therefore will form the basic viewpoint of this review. Below follows a summary of the various fault detection schemes, based on the groupings suggested in [35].

- **Quantitative Model-Based:** In a quantitative model a priori knowledge is usually expressed in terms of input-output relations. These models closely resemble the well known classical and modern control models.

The quantitative model based methods exploit some form of analytical redundancy, and can be grouped as follows:

  - **Observers or Estimators:** Observers or Estimators may be used to estimate the plant output. This estimate is then compared to the measured output generating a residual signal from a mismatch. A form of feedback is usually employed to provide robustness against mismatched initial conditions, model uncertainties, as well as noise sources.
  - **Parity Space:** Parity Equations are derived from modified input-output relations. These parity relations are designed to be theoretically zero in the fault-free case, while resulting in non-zero residual in the faulty case. In practice, however, the residuals will never be zero due to modelling errors, as well as various noise sources.

- **Qualitative Model-Based:** Qualitative models are more conceptual in nature, and describe the available a priori knowledge in more abstract terms. Popular qualitative model-based schemes may be grouped as follows:

  - **Signed Digraphs:** Signed Digraphs are directional cause-effect relations which can be used to describe the possible faults in a system. This qualitative modelling technique has been most widely used in the field of process control.
  - **Qualitative Simulations:** QSIM models are derived by approximating the physical model. These models are often highly inaccurate and may contain only partial information. This method has proved popular in the process control filed.

- **Knowledge- or History-Based:** No explicit models are available. The available a priori knowledge is in the form of large amounts of historical data. Popular knowledge-based schemes may be grouped as follows:

  - **Expert Systems:** Expert systems attempt to duplicate the methods used by a expert human operator in detecting and analysing

fault conditions. These systems are popular due to their well defined behaviour and relatively simple implementation.

- **Principal Component Analysis:** PCA and other statistical extraction methods are widely applied to complex process control problems. These methods monitor a few key statistical metrics, providing a overview of the system's health.
- **Neural Networks:** Artificial Neural Networks are used as building blocks for a self learning system. A lot of interest has been shown in applying these networks to the fault detection problem. A major problem with these systems is the difficultly in providing deterministic performance guarantees.

A categorised summary of some of the most notable and relevant contributions to the field of fault detection is shown in Table 1.1.

With reference to Table 1.1 it can be seen that numerous approaches have been attempted to perform fault detection. However, for the research presented here, the actively excited quantitative model-based are the most relevant. Therefore, these methods are now discussed in more detail.

When compared to the classic quantitative model-based passive fault detection methods, relatively few papers have been published on active fault detection. Some research has been published augmenting the well known Interacting Multiple-Model (IMM) based methods using active excitation[51]. Of the most notable publications on the topic are those by Niemann and Poulsen [54][55][56][57] based on the dual Youla-Bongiorno-Jabr-Kucera (YBGK) parametrisation [69][70][71]. In [54][55] Niemann considers Active Fault Diagnosis in open loop and closed loop systems based on the YBGK parametrisation. In [56] the previous research is expanded by giving some consideration to auxiliary signal design. These ideas are further extended by Niemann and Poulsen in [57] by focusing on the isolation and diagnosis of faults from stochastic signals using Cumulative Sum (CUSUM) tests. Of less relevance to the research presented here, but by no means less notable, are numerous works published by Campbell, Nikoukhah, et el. These include a number of publications on active failure detection, with a specific focus on auxiliary signal design [14][15][72].

	Passive Fault Detection	**Active Fault Detection**
Quantitative Model-Based	General Observer Based Fault Detection [38] [39]. IMM based methods, including research presented in [40] [41] [42]. Parity Relation based Fault Detection methods, including [43] [44] [45]. LMI based methods, including the research presented in [46] [47]. Fault Detection Using Sliding Mode Observers [48] [49] [50].	General Observer Based Fault Detection with active excitation [14] [16]. Active IMM based methods, including research presented in [51] [52] [53]. Actively excited YBJK parametrization based, including research by Niemann and Poulsen [54] [55] [56] [57].
Qualitative Model-Based	SDG based methods, including [58] [59]. Qualitative simulation based fault diagnosis methods, including research presented in [60] [61].	
Knowledge or History Bases	Expert System Based Fault Detection, including the frameworks and systems presented in [62] [63] [64]. Neural-Network Based Schemes, such as the research presented in [65] [66]. PCA based fault detection methods, including research presented in [67] [68].	

Table 1.1: Basic Approaches in fault detection grouped according to the type of model and excitation used

1.2.1 Novelty of Approach

For the research presented in this dissertation it is considered that an estimator can be designed for the sole purpose of fault-detection. This allows the estimator to be optimised for AFD instead of being fixed due to control system requirements.

In order to simplify the AFD system the focus is initially shifted to the open-loop case, which leads to significant simplifications of the optimal AFD solution. Considering the AFD system in the open loop case ensures that the solution is not skewed by the controller dynamics. Considering the more complex problem from the start increases the risk that a major problem may be missed. Additionally, it is shown that the effect of closing a control loop around the system can be quantified and is often of little consequence. Exten-

sion and considerations for the closed loop case will be the subject of further research. Furthermore, it is shown that, by employing these simplified open-loop equations, a simple optimal observer based AFD system can be realised.

With the extra degree of freedom this provides, the optimising equation of [54] yields a trivial solution unless augmented with a final constraint that captures the detector dynamics. The theory is therefore extended in order to take the dynamics of the detector into consideration by analysing the effect of the excitation signal on the detector performance. To quantify this effect a parameter called the minimum targeted detection time is introduced. This parameter is related to the detector dynamics, and places a lower limit on the excitation signal frequency, thereby allowing a non-trivial optimal AFD solution to be obtained.

The theory developed is extended to take advantage of certain Multiple Input Multiple Output (MIMO) system properties, making it possible to excite the fault dynamics without introducing additional disturbances into the nominal system as is always the case in for Single Input Single Output (SISO) systems. A zero disturbance AFD system based around the general output zeroing problem [73] is developed.

The resulting optimisation framework employs relatively simple to apply frequency domain optimisation techniques. Furthermore , the fault detection system requires relatively few run-time resources as it primarily consists of a linear estimator and a bi-directional cumulative sum detector.

1.3 Thesis Overview

Earlier in chapter 1 the theoretical background required for the active fault detection problem and related research is introduced in the form of a detailed literature review.

In Part 1 the active fault detection problem is introduced. Next, the theoretical AFD framework developed. This framework is then used to arrive at an optimal estimator based AFD solution for both MIMO as well as simplified SISO systems.

In Part 2 the theoretical research presented in Part 1 is applied to a number of illustrative SISO and MIMO examples of increasing complexity.

In Part 3 the optimal AFD problem is applied to a larger Unmanned Aerial Vehicle (UAV)-centric case study. This case study illustrates the effectiveness of applying the optimal AFD solution to practical problems.

Finally, in Part 4 a conclusion is provided, and possible future research efforts discussed.

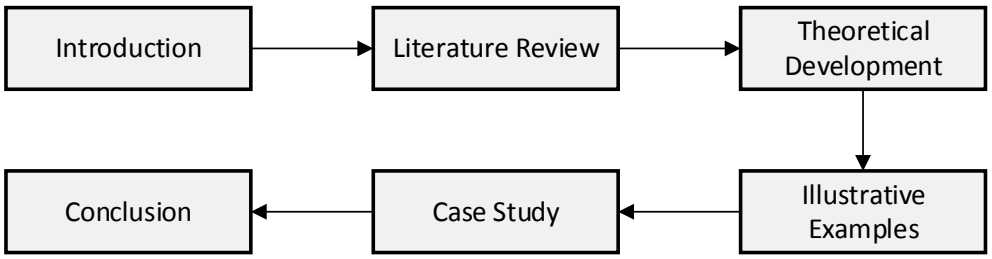

Figure 1.1: Thesis overview.

1.3.1 Theoretical Development

Chapter 2 deals with the theoretical framework development and optimisation problem. The chapter starts by describing the basic AFD framework and associated theory. Next, in Chapter 3 the full MIMO AFD optimisation is derived. This includes the Standard as well as Zero Disturbance AFD cases. In Chapter 4 this optimisation problem is then considered for SISO systems leading to substantial simplifications. Finally, in Chapter 5 the developed framework is summarised and discussed.

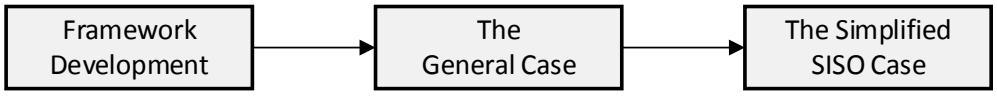

Figure 1.2: Theoretical development overview.

1.3.2 Practical Application

Chapter 6 and 7 deals with the application of the theoretical framework developed in part 1. Chapter 6 starts by considering basic SISO applications. This is then followed by more complex MIMO examples. Chapter 7 provides

background to the application of fault detection for UAVs and then applies the framework to a larger, more practical UAV example.

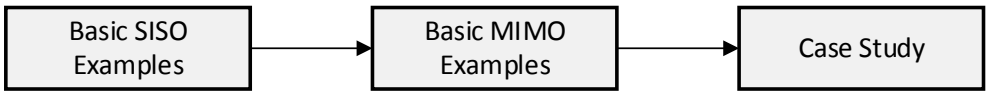

Figure 1.3: Illustrative examples and practical application overview.

Part I

Theoretical Development

Chapter 2

An Architecture for Active Fault Detection

In this chapter, the system setup used for Active Fault Detection is derived. During this process, a number of key aspects are addressed. Amongst these core aspects are:

- The introduction of an auxiliary fault detection signal into the system, while minimizing the negative effects of this additional excitation signal;
- The generation of a residual signal, to be used for the purpose of fault detection;
- The development of a fault detector which interprets the residual signal for the purpose of fault detection;
- The calculation of the Dual Youla parameter which describes the parametric faults in the system;
- The calculation of output zeroing inputs is considered as these can be used to arrive at an AFD solution without the nominal performance degradation usually associated with active fault detecting schemes.

2.1 Definitions

A number of concepts extensively used throughout this chapter are now briefly defined:

- **Nominal System:** The state a system was designed to operate in. Most systems spend the majority of time in this state.
- **Faulty System:** Any operating state other than the nominal. The system might be in a degraded operational state, but this is not a pre-requisite.
- **Linear Fractional Transform:** A conformal mapping of the from $\zeta = \frac{as+b}{cs+d}$ which maps lines to circles and vice versa [74]. The commonly used S- to Z-plane bilinear transformation is an example of such a transformation.
- **Auxiliary Input:** A signal injected into the system for the purpose of fault detection. This signal is injected in addition to any required control inputs.
- **Residual Generation:** An output generated from the system, related to the parametric faults in the system. The signal is ideally zero in nominal case, and non-zero in the faulty case.
- **Dual Youla Parametrisation:** A parametrisation of all systems which can be stabilised by a single controller in terms of a single stable parameter [71].

2.2 System Setup

A generic two port model with uncertain parameters is given in transfer matrix form as

$$E(s) = G_{ed}(s, \Theta)D(s) + G_{eu}(s, \Theta)U(s) \tag{2.2.1}$$

$$Y(s) = G_{yd}(s, \Theta)D(s) + G_{yu}(s, \Theta)U(s) \tag{2.2.2}$$

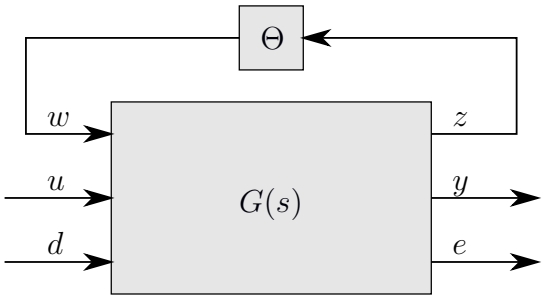

Figure 2.1: System model described in terms of the nominal plant $G(s)$ and the deviations from the nominal plant given by Θ

By using a linear fractional transform [3], the uncertain model parameters are removed from the primary plant model and placed in a feedback path. This modified setup is shown in figure 2.1.

$$Z(s) = G_{zw}(s,\Theta)W(s) + G_{zd}(s,\Theta)D(s) + G_{zu}(s,\Theta)U(s) \tag{2.2.3}$$

$$E(s) = G_{ew}(s,\Theta)W(s) + G_{ed}(s,\Theta)D(s) + G_{eu}(s,\Theta)U(s) \tag{2.2.4}$$

$$Y(s) = G_{yw}(s,\Theta)W(s) + G_{yd}(s,\Theta)D(s) + G_{yu}(s,\Theta)U(s) \tag{2.2.5}$$

Or, alternatively a state-space realisation of this uncertain plant is given by

$$\dot{x} = Ax + B_w w + B_u u + B_d d \tag{2.2.6}$$

$$z = C_z x + D_{zw} w + D_{zu} u + D_{zd} d \tag{2.2.7}$$

$$y = C_y x + D_{yw} w + D_{yu} u + D_{yd} d \tag{2.2.8}$$

$$e = C_e x + D_{ew} w + D_{eu} u + D_{ed} d \tag{2.2.9}$$

where $d \in \mathbb{R}^r$ is the disturbance input, $e \in \mathbb{R}^q$ the error output, $u \in \mathbb{R}^m$ the actuator input, $y \in \mathbb{R}^p$ the sensor output, $w \in \mathbb{R}^k$ an external input, and $z \in \mathbb{R}^k$ an external output. The loop from z to w is closed through Θ, where the diagonal elements of Θ describe the parametric faults of the system and is nominally equal to zero.

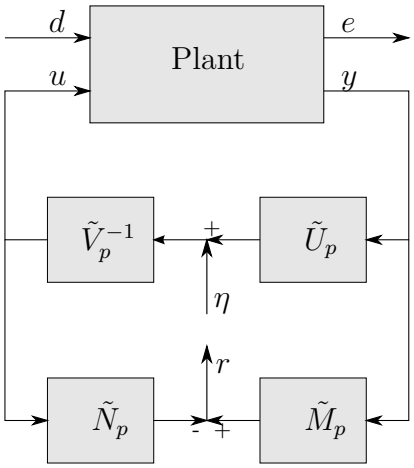

Figure 2.2: System setup used for AFD in co-prime factors form. The auxiliary input (η) as well as the residual signal (r) are also shown.

2.3 Coprime Factorisation

Given that the plant is stabilised by a controller $K(s)$, a coprime factorisation of the system $G_{yu}(s)$ and $K(s)$ is given by [55]

$$G_{yu} = N_p M_p^{-1} = \tilde{M}_p^{-1}\tilde{N}_p \qquad N_p, M_p, \tilde{N}_p, \tilde{M}_p \in RH_\infty \tag{2.3.1}$$

$$K = U_p V_p^{-1} = \tilde{V}_p^{-1}\tilde{U}_p \qquad U_p, V_p, \tilde{U}_p, \tilde{V}_p \in RH_\infty \tag{2.3.2}$$

where the eight matrices must comply to the double Bezout equation, given by

$$\begin{bmatrix} \tilde{V}_p & -\tilde{U}_p \\ -\tilde{N}_p & \tilde{M}_p \end{bmatrix} \begin{bmatrix} M_p & U_p \\ N_p & V_p \end{bmatrix} = \begin{bmatrix} M_p & U_p \\ N_p & V_p \end{bmatrix} \begin{bmatrix} \tilde{V}_p & -\tilde{U}_p \\ -\tilde{N}_p & \tilde{M}_p \end{bmatrix} = \begin{bmatrix} I & 0 \\ 0 & I \end{bmatrix} \tag{2.3.3}$$

This coprime factorisation setup is shown in figure 2.2. It is important to note that the coprime factors are systems, which may be realised as either transfer matrices or state-space systems.

Assuming that observer based feedback control is applied, this coprime

factorisation is equivalent to the following state space representation [75] [1]

$$\begin{bmatrix} M_p & U_p \\ N_p & V_p \end{bmatrix} = \left[\begin{array}{c|cc} A + B_u F & B_u & -L \\ \hline F & I & 0 \\ C_y + D_{yu} F & D_{yu} & I \end{array}\right] \tag{2.3.4}$$

$$\begin{bmatrix} \tilde{V}_p & -\tilde{U}_p \\ -\tilde{N}_p & \tilde{M}_p \end{bmatrix} = \left[\begin{array}{c|cc} A + L C_y & -(B_u + L D_{yu}) & L \\ \hline F & I & 0 \\ C_y & -D_{yu} & I \end{array}\right] \tag{2.3.5}$$

where the feedback gain (F) and observer gain (L) are chosen such that both $A + B_u F$ and $A + L C_y$ are stable.

From this point on, the Active Fault Detection problem is considered in the open-loop case for the following reasons:

- Considering the active fault detection problem in the open-loop case removes the solution's dependency on the chosen control law, thereby greatly simplifying the result.
- Using an open-loop setup removes the risk of the control law obscuring the underlying system dynamics.
- It is possible to add a feedback control system separately if adequate care is taken not to deteriorate the AFD performance significantly.
- Alternatively, the feedback control system may be designed first and this controlled system can then again be considered as a open-loop system for the purpose of AFD.

From the arguments given above it is now assumed that G_{yu} is open-loop stable and therefore that AFD can be applied in the open-loop case. From this point on, the value of the controller gain (F) is assumed to be zero[2]. Given

[1] The equations above are given in block partition format with the vertical and horizontal lines separating the matrix into the four standard state space matrices.

[2] In the open-loop case no feedback control is applied, therefore the feedback gain is zero.

these assumptions, the equations given in [75] can be simplified as follows

$$\begin{bmatrix} M_p & U_p \\ N_p & V_p \end{bmatrix} = \left[\begin{array}{c|cc} A & B_u & -L \\ \hline 0 & I & 0 \\ C_y & D_{yu} & I \end{array}\right] \tag{2.3.6}$$

$$\begin{bmatrix} \tilde{V}_p & -\tilde{U}_p \\ -\tilde{N}_p & \tilde{M}_p \end{bmatrix} = \left[\begin{array}{c|cc} A+LC_y & -(B_u+LD_{yu}) & L \\ \hline 0 & I & 0 \\ C_y & -D_{yu} & I \end{array}\right] \tag{2.3.7}$$

From (2.3.6) and (2.3.7) it can be shown that,

$$M_p = \tilde{V}_p = I \qquad\qquad U_p = \tilde{U}_p = 0 \tag{2.3.8}$$

Furthermore, it can easily be shown that,

$$\left[\begin{array}{c|cc} A+LC_y & -(B_u+LD_{yu}) & L \\ \hline 0 & I & 0 \\ C_y & -D_{yu} & I \end{array}\right] \left[\begin{array}{c|cc} A & B_u & -L \\ \hline 0 & I & 0 \\ C_y & D_{yu} & I \end{array}\right] = \begin{bmatrix} I & 0 \\ 0 & I \end{bmatrix} \tag{2.3.9}$$

and,

$$\left[\begin{array}{c|cc} A & B_u & -L \\ \hline 0 & I & 0 \\ C_y & D_{yu} & I \end{array}\right] \left[\begin{array}{c|cc} A+LC_y & -(B_u+LD_{yu}) & L \\ \hline 0 & I & 0 \\ C_y & -D_{yu} & I \end{array}\right] = \begin{bmatrix} I & 0 \\ 0 & I \end{bmatrix} \tag{2.3.10}$$

therefore, (2.3.6) and (2.3.7) comply with the requirements stipulated by (2.3.3).

2.3.1 Introducing the Auxiliary Input and Residual Output

A residual vector can be generated by using the co-prime factors as follows [54]

$$R = \tilde{M}_p Y - \tilde{N}_p U \tag{2.3.11}$$

It can be shown that this is equivalent to the vector r shown in figure 2.3 [4].

With reference to figure 2.3 an auxiliary signal η is introduced which excites both the plant and estimator. This signal has no affect on r in the nominal

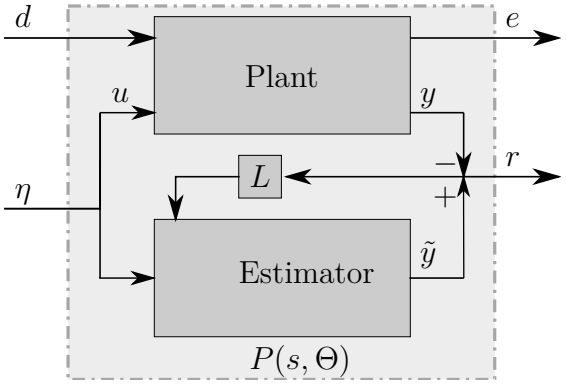

Figure 2.3: System setup used for AFD in state space form. The plant is defined as in figure 2.1. The auxiliary input (η) as well as the residual signal (r) are also shown.

case, but affects the residual signal if a postulated fault has occurred. In this research, only single frequency periodic signals of the form

$$\eta = \begin{bmatrix} A_1 \sin(\omega t + \phi_1) & \dots & A_m \sin(\omega t + \phi_m) \end{bmatrix}^T \tag{2.3.12}$$

will be considered. This may also be given in terms of a single input signal as,

$$\mathcal{H} = H_\eta(s)\mathcal{L}\{\sin(\omega t)\} \tag{2.3.13}$$

where $H_\eta(s)$ is a stable LTI shaping filter[3].

Next, define the system $P(s)$ as

$$E(s,\Theta) = P_{ed}(s,\Theta)D(s) + P_{e\eta}(s,\Theta)\mathcal{H}(s) \tag{2.3.14}$$

$$R(s,\Theta) = P_{rd}(s,\Theta)D(s) + P_{r\eta}(s,\Theta)\mathcal{H}(s) \tag{2.3.15}$$

This is often written in the more compact form as,

$$\begin{bmatrix} E \\ R \end{bmatrix} = \begin{bmatrix} P_{ed} & P_{e\eta} \\ P_{rd} & P_{r\eta} \end{bmatrix} \begin{bmatrix} D \\ \mathcal{H} \end{bmatrix} \tag{2.3.16}$$

where the dependence on s and Θ is not explicitly given. As is common place in the literature, the dependence on s is often not explicitly shown in this dissertation.

[3]The capital letter of η is technically H, but in order to avoid confusion $\mathcal{H}$ is used instead.

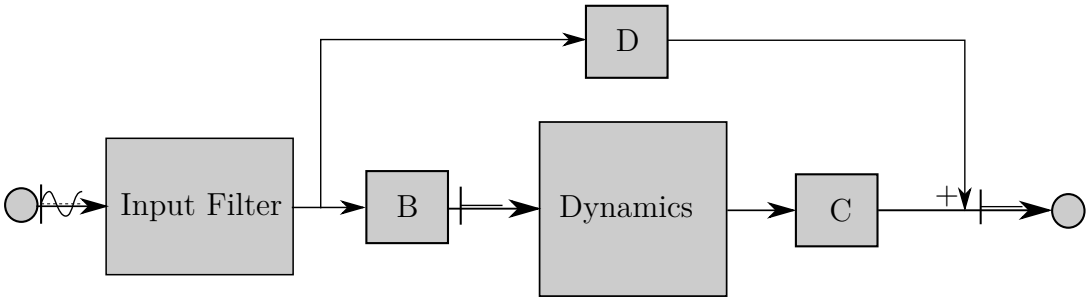

Figure 2.4: System setup illustrating the basic principle behind input cancellation. Note the zeroed signal after the B and D gains.

According to [54], the four transfer functions from the two inputs to both outputs are given by

$$P_{ed}(\Theta) = G_{ed}(\Theta) \tag{2.3.17}$$

$$P_{e\eta}(\Theta) = G_{eu}(\Theta) \tag{2.3.18}$$

$$P_{rd}(\Theta) = G_{yd}(\Theta) \tag{2.3.19}$$

$$P_{r\eta}(\Theta) = G_{yu}(\Theta) - N_p = G_{yu}(\Theta) - G_{yu}(0) \tag{2.3.20}$$

where the simplifications obtained in equation (2.3.8) have been applied to the equations given in [54]. Again, the dependence on s is not explicitly given.

In [54] it is noted that $P_{r\eta}$ is equal to the dual Youla parameter S. According to [71] and [54] it is possible to rewrite S or $P_{r\eta}$ as

$$P_{r\eta}(\Theta) = \tilde{M}_p G_{yw}(0)\Theta \left(I - G_{zw}(0)\Theta\right)^{-1} G_{zu} \tag{2.3.21}$$

where the simplifications obtained in (2.3.8) have been applied to the equations given in [54]. For further background on the Youla parametrisation please refer to [69] and [70].

2.4 Output Zeroing Input in MIMO Systems

2.4.1 Output Zeroing Input for a Nominal System with Redundant Actuators

MIMO systems with redundant actuators can be excited by injecting disturbances into the null-space of the control matrix. It is important to note that

using this method only allows for the detection of control or actuator faults, and not changes in the other system matrices.

The system is excited in such a way as not to cause any nominal disturbance, therefore

$$|P_{e\eta}(j\omega)\mathcal{H}(j\omega)| = |G_{eu}(j\omega)\mathcal{H}(j\omega)| = 0 \tag{2.4.1}$$

with, $s = j\omega$.

Figure 2.3 shows that the signals η and u are equal. It is further assumed that the error signal is a function of a reference and the plant output, therefore equation (2.4.1) implies

$$B_u\eta = 0 \qquad\qquad D_{eu}\eta = 0 \tag{2.4.2}$$

with

$$B_u \neq 0 \qquad\qquad \eta \neq 0 \tag{2.4.3}$$

Equations (2.4.2) and (2.4.3) are satisfied if

$$\eta \in (\ker B_u) \cap (\ker D_{eu}) \tag{2.4.4}$$

where *ker* is the kernel or null space of the given matrix. In other words the input zeroing signal must be within the kernel of both B_u and D_{eu}.

2.4.2 Output Zeroing Input for an Output nulling MIMO System

In some MIMO systems it is possible to use output cancellation in order to employ zero disturbance AFD without the limitations of using input cancellation. The discussion provided here is based on the general output zeroing problem discussed in [73].

In this section output zeroing inputs are derived for the excitation signal. From equation (2.3.18), the auxiliary input to error output dynamics can be described by the following state space model.

$$\dot{x_0} = Ax + B_u\eta \tag{2.4.5}$$

$$e = C_e x + D_{eu}\eta \tag{2.4.6}$$

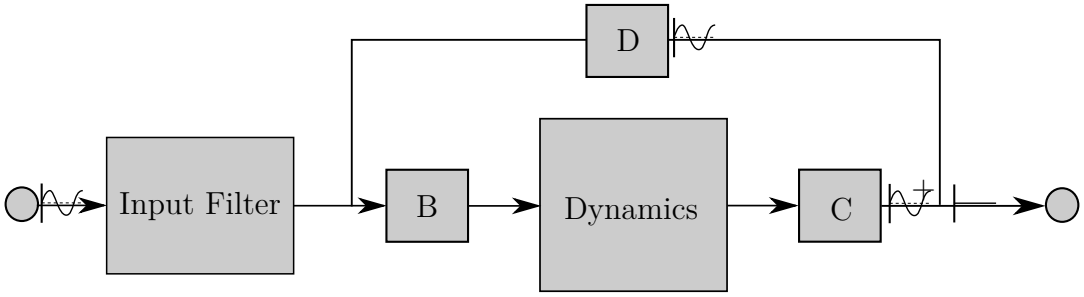

Figure 2.5: System setup illustrating the basic principle behind output cancellation. Note the non-zero signal after C and D, and zeroed signal at the output. This setup can be slightly altered for strictly proper systems.

with $e = 0 \quad \text{for} \quad t \geq 0$.

The investigation provided here is divided into proper and strictly proper systems[4].

2.4.2.1 Strictly Proper Systems

For strictly proper systems, the first non-zero Markov parameter, at index k, is given by, [73]

$$C_e A^k B_u \neq 0 \tag{2.4.7}$$

where $0 \leq k \leq n-1$.

Further define the matrix [73]

$$K_k = I - B_u (C_e A^k B_u)^+ C_e A^k \tag{2.4.8}$$

Now, for strictly proper systems the output zeroing states are entirely contained within the subspace [73]

$$x_0(t) \in \bigcap_{l=0}^{k} \ker C_e A^l \tag{2.4.9}$$

and define the initial condition as,

$$x_0(0) = x^0 \tag{2.4.10}$$

[4]The results provided here can be simplified for certain systems. Also note that the output zeroing solution does not necessarily span the entire complex plain. For further details refer to [73].

Furthermore, the output zeroing states can be described by [73]

$$x_0(t) = e^{tK_kA}x^0 + \int_0^t e^{(t-\tau)K_kA}B_u\eta_h(\tau)d\tau \tag{2.4.11}$$

while the output zeroing excitation input is given by,

$$\begin{aligned}\eta(t) = &-(C_eA^kB_u)^+C_eA^{k+1}e^{tK_kA}x^0 \\ &- (C_eA^kB_u)^+C_eA^{k+1}\int_0^t e^{(t-\tau)K_kA}B_u\eta_h(\tau)d\tau \\ &+ \eta_h(t)\end{aligned} \tag{2.4.12}$$

with $\eta_h(t) \in U$ which satisfies

$$C_eA^kB_u\eta_h(t) = 0 \tag{2.4.13}$$

2.4.2.2 Proper Systems

For proper systems the output zeroing states are entirely contained within the subspace [73]

$$x_0(t) \in \ker(I_r - D_{eu}D_{eu}^+)C_e \tag{2.4.14}$$

where I_r is the right identity. Define the initial condition as,

$$x_0(0) = x^0 \tag{2.4.15}$$

Furthermore, the output zeroing states can be described by [73]

$$\begin{aligned}x_0(t) = &e^{t(A-B_uD_{eu}^+C_e)}x^0 \\ &+ \int_0^t e^{(t-\tau)(A-B_uD_{eu}^+C_e)}B_u\eta_h(\tau)d\tau\end{aligned} \tag{2.4.16}$$

while the output zeroing input is given by,

$$\begin{aligned}\eta(t) = &-D_{eu}^+C_ee^{t(A-B_uD_{eu}^+C_e)}x^0 \\ &- D_{eu}^+C_e\int_0^t e^{(t-\tau)(A-B_uD_{eu}^+C_e)}B_u\eta_h(\tau)d\tau \\ &+ \eta_h(t)\end{aligned} \tag{2.4.17}$$

with $\eta_h(t)$ some piecewise continuous function which satisfies

$$D_{eu}\eta_h(t) = 0 \tag{2.4.18}$$

2.5 Summary

During this chapter the basic theoretical framework used to construct the optimised AFD system was introduced and briefly discussed. The following key concepts were considered:

- The introduction of an auxiliary fault detection signal into the system. This signal is given by:

$$\mathcal{H} = H_\eta(s)\mathcal{L}\{\sin(\omega t)\} \tag{2.5.1}$$

- The generation of a residual signal, to be used for the purpose of fault detection. This signal is defined as:

$$R = \tilde{M}_p Y - \tilde{N}_p U \tag{2.5.2}$$

- The calculation of auxiliary signal inputs is considered for output as well as input zeroing excitation schemes.
  - An input zeroing auxiliary signal is a signal which complies with,

$$\eta \in (\ker B_u) \cap (\ker D_{eu}) \tag{2.5.3}$$

  - An output zeroing auxiliary signal is a signal which complies with,

$$\begin{aligned}\eta(t) = &-(C_e A^k B_u)^+ C_e A^{k+1} e^{tK_k A} x^0 \\ &- (C_e A^k B_u)^+ C_e A^{k+1} \int_0^t e^{(t-\tau)K_k A} B_u \eta_h(\tau) d\tau \\ &+ \eta_h(t)\end{aligned} \tag{2.5.4}$$

    for strictly proper systems, or

$$\begin{aligned}\eta(t) = &-D_{eu}^+ C_e e^{t(A - B_u D_{eu}^+ C_e)} x^0 \\ &- D_{eu}^+ C_e \int_0^t e^{(t-\tau)(A - B_u D_{eu}^+ C_e)} B_u \eta_h(\tau) d\tau \\ &+ \eta_h(t)\end{aligned} \tag{2.5.5}$$

    for proper systems.

Chapter 3

Optimal Open-Loop Active Fault Detection: The General Case

In this chapter optimal open-loop AFD is investigated for general MIMO systems by making use of the theory presented in the previous chapter. In the open-loop case accurate state estimation is not of primary importance, since a separate state estimator for the purpose of applying feedback control can be employed. Therefore, the estimator gains can be designed to optimise for AFD performance. With this extra design freedom both the estimator as well as the auxiliary signal can be designed to optimise for AFD performance, as opposed to [54] where the estimator is treated as a fixed attribute of the pre-existing control system.

Furthermore, optimal open-loop AFD is investigated in the presence of a control input signal. It is assumed here that the primary source of excitation is from the control input and not from any additional auxiliary signal. When taking the control input as the primary source of excitation the optimising is effectively performed for the average-case, as opposed to the worst-case scenario when only the auxiliary input is considered.

Keeping this in mind, the following design goals are considered important during the design of the optimal estimator and auxiliary signal pair:

1. Design the estimator gain so that $A + LC_y$ is stable. This is a necessary

and sufficient condition for stability since the system is assumed to be open-loop stable.

2. Design the auxiliary signal, η, in such a way as to limit performance degradation of the stipulated performance metric. Since this is a linear system, injecting a larger auxiliary signal will always lead to improved AFD performance at the possible expense of additional degradation of the nominal system performance. The AFD system must therefore operate within a given performance degradation envelope.

3. Design the estimator gain, L, and the auxiliary signal, η, in order to minimise the fault detection time. There are two main factors which determine the detection speed - the detector threshold, and the average slope of the detection signal after a failure.

4. Decide whether to optimise for the average- or worst-case. This determines if the control signal must be considered.

3.1 A Setup for Active Fault Detection in General MIMO Systems

The optimisation requirements stated above in point 2, 3 and 4 are now formalized below.

Design goal 2 requires that the impact of the auxiliary signal on the system error output be known and kept within the stipulated design constraint. Now, consider design goal 3. This design goal requires that the impact of the auxiliary signal on the triggering output be known and maximised. Furthermore, this design goal requires that the impact of the estimator gain on the nominal detector noise level be known and minimised. A complying setup is shown in figure 3.1.

With reference to this figure a number of definitions are now made:

- Define Λ_0 and Λ_1 as the nominal and faulty system AFD induced disturbance constraint respectively. Therefore $\| (P_{e\eta}(0,s)\mathcal{H}(s)) \|_\infty \leq \Lambda_0$ and

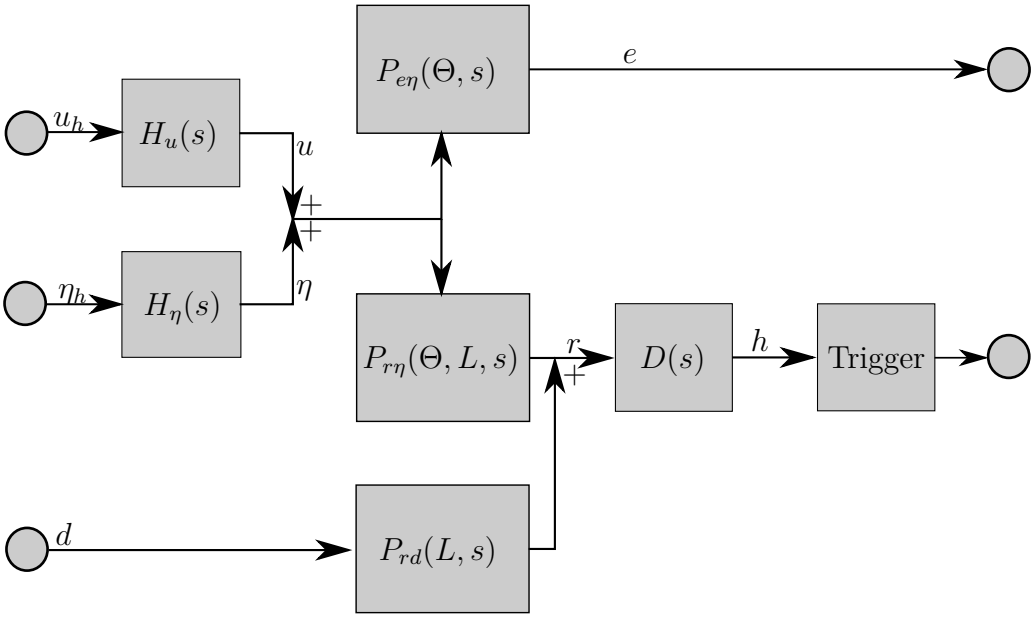

Figure 3.1: Setup used for Active Fault Detection. From left to right the following is shown: input shaping filter; plant excitation dynamics; linearised detector dynamics; and fault trigger. It should be noted that the fault trigger is just a representation of the detection threshold, and not a separate dynamic system.

$\| (P_{e\eta}(\Theta_1, s)\mathcal{H}(s)) \|_\infty \leq \Lambda_1$ must hold for all $t > 0$ and the postulated fault condition Θ_1.

- Standard AFD is defined as an AFD implementation where $\Lambda_0 \neq 0$, while Zero Disturbance AFD is defined as an AFD implementation where it is possible to achieve $\Lambda_0 = 0$.

- The signal η_h is a simple periodic signal of unity amplitude given by, $\eta_h = \sin \omega t$.

- The signal η is the excitation signal used for the purpose of AFD, and is given by, $\mathcal{H}(s) = H_\eta(s)\mathcal{H}_h(s)$ where $H_\eta(s)$ is a filter which transforms η_h into a signal of correct dimension which adheres to the performance degradation constraints Λ_0 and Λ_1.

- The signal d is a zero mean white noise signal. This signal injects noise into the residual signal through the disturbance dynamics, $P_{rd}(L, s)$. The

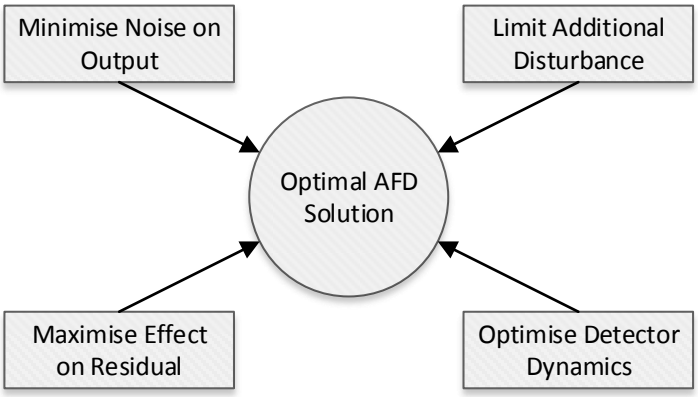

Figure 3.2: Aspects of the Active Fault Detection Optimisation Problem.

noise injected into the residual must be of finite power, in other words the H_2 norm of $P_{rd}(L, s)$ must exist.

- When present, the signal u is an external control signal not under the control of the AFD design, where $\|u\|_2 \gg \|\eta\|_2$ However, for the purpose of AFD modelling the control signal u is given by, $U(s) = H_u(s)U_h(s)$, where u_h is zero mean white noise and the filter $H_u(s)$ transforms the infinite bandwidth input into a signal representative of the power distribution of a practically realisable band-limited system input u.

- The control signal u is summed with the shaped excitation signal η before entering the system.

- h is the signal on which thresholding is performed, and is given by, $H(s) = D_r(s)R(s)$. Where, $D_r(s)$ is a linear approximation of the detector dynamics.

From these definitions and the informal discussion provided earlier, the following optimisation criteria is now formulated:

Criterion 1. *Find the estimator gain L, excitation frequency ω_η, and the admissible shaping filter $H_\eta(s)$, which maximises the average fault signal to nominal noise ratio on $h(t)$ over a fixed time period t_d.*

The basic optimisation strategy is represented by figure 3.2. In the remainder of this section the subsystems making up the optimal AFD setup are considered and combined to arrive at the optimised AFD solution. With

reference to figure 3.1 these subsystems are: the input shaping filter and how it relates to the disturbance constraints; an approximated description of the detector dynamics and how it relates to the excitation frequency; a characterisation of the effect of the auxiliary signal control input on the residual output; and a description of the nominal detection noise.

3.2 Disturbance Constraints and the Auxiliary Signal Input Shaping Filter

Consider the novel AFD input shaping filter $H_\eta(s)$ shown in figure 3.1. This subsystem is responsible for transforming the single periodic signal η_h into an auxiliary signal which complies with the given disturbance constraints. This subsystem is additionally responsible for incorporating the majority of the MIMO complexity.

The input shaping filter $H_\eta(s)$ can be given by the following state space model:

$$\begin{aligned} \dot{x}_\eta &= A_{H_\eta} x_\eta + B_{H_\eta} \eta_h \\ \eta &= C_{H_\eta} x_\eta + D_{H_\eta} \eta_h \end{aligned} \tag{3.2.1}$$

where, x_η is the state vector for the input shaping filter.

3.2.1 Standard AFD

Implementing standard AFD results in a reduction in both the nominal and faulty system performance. It is therefore of primary importance to limit the nominal performance degradation. It is further noted that since the failed system disturbance is simply a function of the nominal system, the failure case as well as the nominal disturbance constraint, only a single constraint is required. Therefore,

$$\Lambda_0 = c_0 \qquad\qquad \Lambda_1 = \infty \tag{3.2.2}$$

where, c_0 is a constant.

The input shaping filter must be designed to satisfy the single constraint Λ_0. This single constraint does not lead to a fully defined $H_\eta(s)$ in the case

of MIMO systems, therefore an additional reasonable design decision must be made. It is suggested that $H_\eta(s)$ is designed such that each actuator is excited to the same degree. Therefore

$$\begin{aligned} \dot{x}_\eta &= 0x_\eta + 0\eta_h \\ \eta &= 0x_\eta + aH_{\eta_0}\eta_h \end{aligned} \tag{3.2.3}$$

where H_{η_0} is chosen so that each actuator gain b is given by $|\eta_i|/\delta_{i_{max}} = b$[1].

Assuming maximum additional system disturbance[2], the maximum auxiliary signal amplitude is given by

$$\begin{aligned} \sigma_{\max}\left(\mathcal{H}(j\omega)\right) &= c_0\sigma_{\max}(P_{e\eta}(0,j\omega))^{-1} \\ &= c_0\sigma_{\max}(G_{eu}(0,j\omega))^{-1} \end{aligned} \tag{3.2.4}$$

where, $(P_{e\eta}(0,j\omega))^{-1}$ and $(G_{eu}(0,j\omega))^{-1}$ are the left inverses of $P_{e\eta}(0,j\omega)$ and $G_{eu}(0,j\omega)$ respectively. As before these left inverses exist if and only if $P_{e\eta}(0,j\omega)$ and $G_{eu}(0,j\omega)$ are of full row-rank.

Now, given that

$$\mathcal{H}(s) = H_\eta(s)\mathcal{H}_h(s) \qquad \text{with} \qquad H_\eta(s) = a\tilde{H}_\eta(s) \tag{3.2.5}$$

using equation 3.2.4 and noting that by definition $\|\mathcal{H}_h(j\omega)\| = 1$, the following holds:

$$a = c_1\sigma_{\max}(G_{eu}(0,j\omega)\tilde{H}_\eta(j\omega))^{-1} \tag{3.2.6}$$

where, $(G_{eu}(0,j\omega)\tilde{H}_\eta(j\omega))^{-1}$ is the left inverse of $G_{eu}(0,j\omega)\tilde{H}_\eta(j\omega)$. The left inverse exists if and only if the number of error outputs do not exceed the number of auxiliary inputs, and the row echelon form of $G_{eu}(0,j\omega)\tilde{H}_\eta(j\omega)$ contains pivot elements on every row. Otherwise stated, $G_{eu}(0,j\omega)\tilde{H}_\eta(j\omega)$ is of full row-rank.

The input shaping filter is now fully defined by equations (3.2.3) and (3.2.6).

[1] $\delta_{i_{max}}$ is the maximum control authority for the specific control actuator, while b is a constant

[2] This implies that the AFD induced disturbance is the maximum allowed by the design constraint.

3.2.2 Zero Disturbance AFD

By definition zero disturbance AFD results in zero nominal system performance degradation, therefore

$$\Lambda_0 = 0 \qquad \Lambda_1 = c_1 \tag{3.2.7}$$

where c_1 is a constant.

The input shaping filter $H_\eta(s)$ must be designed to meet these two disturbance constraints. First consider the constraint $\Lambda_0 = 0$. This implies that

$$P_{e\eta}(s)H_\eta(s) = 0 \tag{3.2.8}$$

Using the theory discussed earlier in this dissertation, $H_\eta(S)$ is now calculated for a few different scenarios.

Input Cancellation: From (2.4.2) and (2.5.3) it is simple to derive a linear state space model to describe the input shaping filter.

$$\begin{aligned} \dot{x}_\eta &= 0x_\eta + 0\eta_h \\ \eta &= 0x_\eta + aH_{\eta_0}\eta_h \end{aligned} \tag{3.2.9}$$

where H_{η_0} is a base matrix for the kernel of B_u as well as of D_{eu}. Therefore, $H_{\eta_0}\eta_h \in \ker B$ and $H_{\eta_0}\eta_h \in \ker D_{eu}$.

Output Cancellation (Proper Systems) : If D_{eu} is a matrix of full row rank [73], then from (2.4.17) and (2.4.18) a linear state space model can be derived to describe the input shaping filter.

$$\begin{aligned} \dot{x}_\eta &= (A - B_u D_{eu}^+ C_e)x_\eta + B_u a H_{\eta_0}\eta_h \\ \eta &= -D_{eu}^+ C_e x_\eta + I a H_{\eta_0}\eta_h \end{aligned} \tag{3.2.10}$$

where H_{η_0} is a base matrix for the kernel of D_{eu}. Therefore, $H_{\eta_0}\eta_h \in \ker D_{eu}$.

In the general case the output zeroing input does not necessarily exist. However, if the set of invariant zeros is non-empty an output-zeroing solution must exist for each of these invariant zeros [73].

Output Cancellation (Strictly Proper Systems) : If $C_e A^k B_u$ is a matrix of full row rank [73], then from equations (2.4.12) and (2.4.13) it is simple to derive a linear state space model to describe the input shaping filter.

$$\begin{aligned} \dot{x}_\eta &= K_k A x_\eta + B_u a H_{\eta_0}\eta_h \\ \eta &= -(C_e A^k B_u)^+ C_e A^{k+1} x_\eta + I a H_{\eta_0}\eta_h \end{aligned} \tag{3.2.11}$$

where $H_{\eta 0}$ is a base matrix for the kernel of $C_e A^k B_u$ Therefore, $H_{\eta 0}\eta_h \in \ker C_e A^k B_u$. The value of k is defined by equation 2.4.7.

Next, consider the second disturbance constraint, $\Lambda_1 = c_1$. Although the injection of the auxiliary signal does not affect nominal system performance, it still causes a reduction in post failure performance. Now, assuming maximum additional system disturbance, the maximum auxiliary signal is given by

$$\begin{aligned}\sigma_{\max}\left(\mathcal{H}(j\omega)\right) &= c_1\sigma_{\max}(P_{e\eta}(\Theta, j\omega))^{-1} \\ &= c_1\sigma_{\max}(G_{eu}(\Theta, j\omega))^{-1}\end{aligned} \tag{3.2.12}$$

where, $(P_{e\eta}(\Theta, j\omega))^{-1}$ and $(G_{eu}(\Theta, j\omega))^{-1}$ are the left inverses of $(P_{e\eta}(\Theta, j\omega))$ and $(G_{eu}(\Theta, j\omega))$ respectively. These left inverses exist if and only if the number of error outputs do not exceed the number of auxiliary inputs, and its row echelon form contains pivot elements on every row. Otherwise stated, $P_{e\eta}(\Theta, j\omega)$ and $G_{eu}(\Theta, j\omega)$ are of full row-rank.

Now, given that

$$\mathcal{H} = H_\eta(s)\mathcal{H}_h \qquad \text{with} \qquad H_\eta(s) = a\tilde{H}_\eta(s) \tag{3.2.13}$$

using equation 3.2.12 and noting that by definition $\|\mathcal{H}_h(j\omega)\| = 1$, the following holds:

$$a = c_1\sigma_{\max}(G_{eu}(\Theta, j\omega)\tilde{H}_\eta(j\omega))^{-1} \tag{3.2.14}$$

where $(G_{eu}(\Theta, j\omega)\tilde{H}_\eta(j\omega))^{-1}$ is the left inverse of $G_{eu}(\Theta, j\omega)\tilde{H}_\eta(j\omega)$. The left inverse exists if and only if the number of error outputs do not exceed the number of auxiliary inputs, and the row echelon form of $G_{eu}(\Theta, j\omega)\tilde{H}_\eta(j\omega)$ contains pivot elements on every row. Otherwise stated, $G_{eu}(\Theta, j\omega)\tilde{H}_\eta(j\omega)$ is of full row-rank.

The input shaping filter is now fully defined by equations (3.2.9), (3.2.10), (3.2.11), and (3.2.14)

3.3 Approximated Detector Dynamics

The aim of this section is to approximately characterise the detector's response in terms of excitation frequency as a linear transfer function. The detector is

responsible for detecting the small change in the residual signal due to a failure. Although not the only possible approach, in this dissertation the focus is on using an integrative change in mean detector. This type of detector is used to detect small changes in the mean value of a signal by means of integration. The other main detector type is called a variance detector, and focuses on detecting changes in the variance of a signal.

The optimisation problem presented in research such as [55] and [54] does not consider the effect of the detector dynamics on the AFD optimisation problem.

As previously stated the auxiliary signal is a filtered single frequency periodic signal of the following form:

$$\mathcal{H} = H_\eta(s)\mathcal{L}(\sin(\omega_\eta t)) \tag{3.3.1}$$

Since all filters as well as the system are linear and stable, and given enough time for transient behaviour to have ceased. The residual output resulting in the largest singular value is of the form

$$r(t) = a\sin(\omega_\eta t + \phi) + \nu(t) \tag{3.3.2}$$

where $\nu(t)$ is a zero mean noise component. It is important to remember that for a linear system a sinusoidal input will result in a sinusoidal output of the same frequency and a zero mean input will result in a zero mean output [57].

To generate a detection signal with a zero mean in the nominal case and a non-zero mean in the faulty case, the residual is multiplied by a single frequency periodic signal of frequency ω_η. This allows the optimisation to be performed at a single frequency point, additionally this method is used extensively in the literature [57]. The detection signal is therefore given by

$$\nu_0(t) = \nu(t)\sin(\omega_\eta t + \phi_0) \tag{3.3.3}$$

in the nominal case, and

$$\nu_1(t) = \nu(t)\sin(\omega_\eta t + \phi_1) + a_1\sin^2(\omega_\eta t + \phi_1) \tag{3.3.4}$$

in the faulty case. Where subscript 0 and 1 are used to indicate the nominal and faulty cases receptively.

Now, consider the second term of equation (3.3.4). This term has a non-zero mean value, and is used for fault detection. Since it is not known at what time a fault will occur it is further assumed that $\phi_1 = 0$ [3].

The detector integrates ν_1, and after a time t_d seconds the output is given by

$$h = a_1 \int_0^{t_d} \sin^2(\omega t) dt \tag{3.3.5}$$

$$= a_1 \left(\frac{t_d}{2} - \frac{\sin(2\omega t_d)}{4\omega} \right) \tag{3.3.6}$$

It can be seen that as ω becomes large, h approaches $a_1 \frac{t_d}{2}$. Furthermore, when ω becomes small, h approaches zero.

It is now shown that the detector's integration action can be closely approximated by a second order transfer function of the form

$$D_r(s) \approx \frac{a_1 t_d s^2}{2\left(s^2 + 2\left(\frac{a}{t_d}\right)s + \left(\frac{a}{t_d}\right)^2\right)} \tag{3.3.7}$$

where a is a constant approximately equal to one.

The value of a for small values of ω is calculated by setting equation (3.3.6) equal to the magnitude of (3.3.7)

$$\frac{t_d}{2} - \frac{\sin(2\omega t_d)}{4\omega} = \left| \frac{t_d (j\omega)^2}{2\left((j\omega)^2 + 2\left(\frac{a}{t_d}\right)(j\omega) + \left(\frac{a}{t_d}\right)^2\right)} \right| \tag{3.3.8}$$

where $s = j\omega$.

The function $\sin(2\omega t_d)$, is approximated by a second order Taylor series expansion.

$$\frac{t_d}{2} - \frac{2\omega t_d - \frac{(2\omega t_d)^3}{3!}}{4\omega} = \left| \frac{t_d (j\omega)^2}{2\left((j\omega)^2 + 2\left(\frac{a}{t_d}\right)(j\omega) + \left(\frac{a}{t_d}\right)^2\right)} \right| \tag{3.3.9}$$

Now, assuming that a, t_d and ω are positive, real numbers, equation (3.3.9) is simplified as

$$\frac{\omega^2 t_d^3}{2(a + t_d\omega)^2} = \frac{\omega^2 t_d^3}{3}$$

$$2(a + t_d\omega)^2 = 3 \tag{3.3.10}$$

[3] Of primary interest is the effect of the excitation frequency on detector performance. This parameter can be designed for, while the phase at which a failure occurs is random.

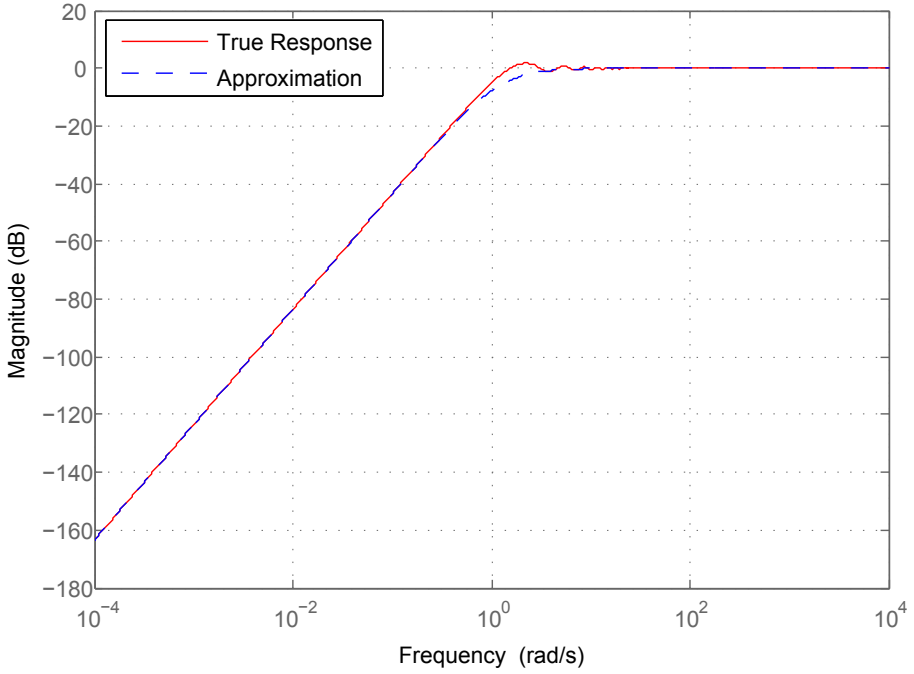

Figure 3.3: True frequency response of detector versus seconded order approximated response. For this plot $t_d = 1$ and the magnitude is normalised so that $\lim_{\omega\to\infty} h(\omega) = 1$.

Therefore, as ω approaches zero,

$$a = \sqrt{\frac{3}{2}} \tag{3.3.11}$$

From figure 3.3, equation (3.3.11) and equation (3.3.7), it can be seen that auxiliary signal frequencies lower than $\frac{1}{t_d}$ are severely penalised by the detector dynamics. It is therefore up to the control engineer to select a reasonable minimum targeted detection time. Please note that it is not suggested that it is impossible to detect a fault in less time than t_d , merely that doing so may[4] require a much larger change in ν.

3.3.1 Using a Leaky Detector

It is rarely possible to know the system model with perfect accuracy, therefore it is often necessary to employ a leaky detector. The detector discussed previously is now modified to introduce a leakiness factor.

[4]The optimal auxiliary signal frequency is not simply a function of the detector dynamics, but is also influenced by other factors, such as $P_{r\eta}(\Theta)$.

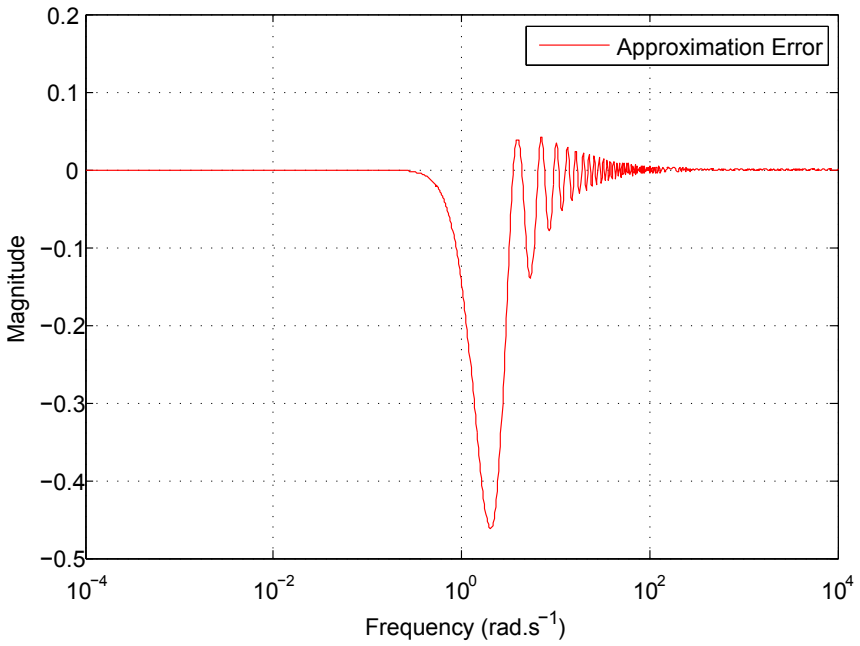

Figure 3.4: True frequency response of detector versus seconded order approximated response approximation induced error. For this plot $t_d = 1$ and the magnitude is normalised so that $\lim_{\omega\to\infty} h(\omega) = 1$.

Over the time period t_d the leaky detector provides a constant reduction to the detector output relative to the extent of the leakiness employed. Using the Taylor series expansion from equation (3.3.9), the leaky detector is approximately given by

$$h \approx \frac{t_d}{2} - \frac{2\omega t_d - \frac{(2\omega t_d)^3}{3!}}{4\omega} - \frac{t_d}{c_l} \tag{3.3.12}$$

where c_l is the chosen leakiness factor.

From figure 3.5 it can be seen that employing a leaky detector causes a severe performance drop in the low cut-off region of the detector dynamics. Furthermore, it can be seen that the leaky detector provides an asymptote in the low frequency region. The position of this asymptote line is given by setting equation (3.3.12) to zero and solving for ω as follows

$$\frac{t_d}{2} - \frac{2\omega_0 t_d - \frac{(2\omega_0 t_d)^3}{3!}}{4\omega_0} - \frac{t_d}{c_l} = 0 \tag{3.3.13}$$

assuming $c_l t_d \neq 0$, $\omega_0 > 0$ and $\frac{t_d}{2} \gg \frac{t_d}{c_l}$,

$$\omega_0 = \frac{\sqrt{3}}{\sqrt{c_l} t_d} \tag{3.3.14}$$

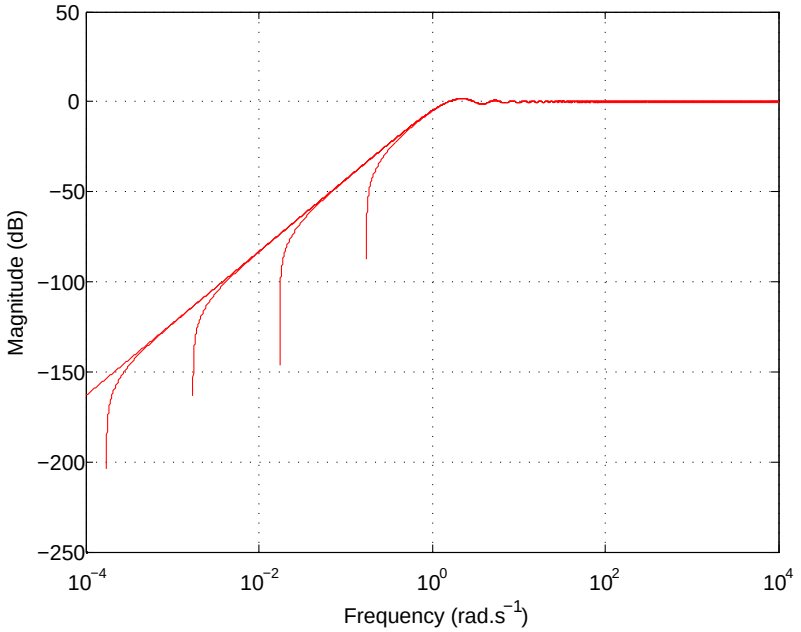

Figure 3.5: Detector response plot showing the effect of using a leaky detector. In this case t_d was chosen as 1 second. As the leakiness increases, the severe performance drop moves closer to $\sqrt{\frac{3}{2}}/t_d$.

Since this area is typically excluded as an optimal solution due to the detector dynamics the extra dynamics, can usually be ignored. However, it is advisable to remain well clear of the ω_0 asymptote.

It is important to take note that the leakiness factor c_l introduces a small additional error into the second order approximation, given by

$$\frac{t_d}{c_l} \quad \textbf{for} \quad \omega \gg \frac{\sqrt{3/2}}{t_d} \tag{3.3.15}$$

3.4 The Auxiliary Input Signal

As previously stated, the transfer function from auxiliary input to residual output is given by the dual Youla parameter. With reference to equation (2.3.21), this parameter is given by

$$P_{r\eta}(\Theta) = \tilde{M}_p G_{yw} \Theta \left(I - G_{zw}\Theta\right)^{-1} G_{zu} \tag{3.4.1}$$

As is evident from (2.3.7), the transfer function $\tilde{M}$ is dependent on L, therefore

$$P_{r\eta}(\Theta, L) = \tilde{M}_p(L) G_{yw} \Theta \left(I - G_{zw}\Theta\right)^{-1} G_{zu} \tag{3.4.2}$$

$P_{r\eta}$ is an indication of the effectiveness of the auxiliary signal in altering the residual, therefore it is advantageous to maximise $P_{r\eta}$.

$$\max_{L} \left(P_{r\eta}(\Theta, L) \right) \tag{3.4.3}$$

The exact norm used to maximise the above will be disused later.

3.5 Noise Covariance on Nominal Residual Signal

From the criterion, it would seem that the noise covariance on h(t) is required. However, if it is assumed that the system has been active for a long time, the dynamic effect of the detector is of minimal importance. Therefore, it is acceptable to consider the noise covariance on the nominal residual instead. This assumption can further be motivated as follows:

- From the detector dynamics it can be seen that the detector cut-off frequency becomes lower as t_d increases. In other words, the effect of the detector becomes smaller as time passes.
- It is reasonable to assume that the detector has been active far longer than what the minimum targeted detection time is. This implies that the detector dynamics will affect the post failure detection signal far more than the disturbance dynamics.
- It is advantageous to remain mostly detector agnostic. Doing this allows the methods presented here to be applicable to a larger number of systems. This was also the case for the underlying theory.

The nominal residual noise power determines the maximum attainable detector sensitivity for a given false detection rate[5]. It is therefore desirable to minimise the residual covariance. It is not suggested that the optimal AFD system simply minimises output noise covariance, but rather that in the final

[5]Calculating statistical metrics, such as the false detection rate, is beyond the scope this dissertation. The interested reader should refer to literature such as [76]. It is assumed that a simple change detector is used. If this is not the case refer to literature on detector theory and the universally most powerful test, such as [77].

optimisation a lower output noise covariance is advantageous, as it leads to a higher signal to noise ratio.

The covariance on the residual prior to a fault occurring can be calculated using the H_2 system norm. The H_2 norm for a stable proper continuous system is given by [78]

$$\|H\|_2 = \sqrt{\frac{1}{2\pi}\int_{-\infty}^{\infty} \text{Trace}\left[H(j\omega)^* H(j\omega)\right] d\omega} \tag{3.5.1}$$

From equations (2.3.19) (with $\Theta = 0$) and (3.5.1), the output noise power is dependant on the estimator gain, and is given by

$$\|P_{rd_0}(L)\|_2 = \sqrt{\frac{1}{2\pi}\int_{-\infty}^{\infty} \text{Trace}\left[P_{rd_0}(j\omega, L)^* P_{rd_0}(j\omega, L)\right] d\omega} \tag{3.5.2}$$

The estimator gain which minimises the nominal residual covariances satisfies

$$\max_L \left(\frac{1}{\|P_{rd_0}(L)\|_2}\right) \tag{3.5.3}$$

3.6 The Control Input and the Control Shaping Filter

Consider the control input u shown in figure 3.1. As previously stated, the control input is not under the control of the AFD system. However, this does not necessary exclude it from the AFD optimisation problem. Its influence may be considered using a novel yet simple approach as described in this section. The influence of the control signal may be described in terms of the following scenarios:

- **The degenerative scenario:** The control signal is exactly given by the negative of the auxiliary signal. In this scenario no AFD or control is performed. However, this case is excluded, since it is given that $u \gg \eta$.
- **The best-case scenario:** The control signal is a simple periodic signal of optimal excitation frequency.
- **The worst-case scenario:** The control signal is equal to zero.

- **The average scenario:** The control signal is given by a band-limited, finite power signal.

In this investigation the worst-case and average scenarios are considered important, as these are related to minimum and average AFD performance parameters.

From the same figure it can be seen that the control input enters the system in the same manner as the auxiliary signal and therefore,

$$P_{ru}(\Theta, L) = P_{r\eta}(\Theta, L) = \tilde{M}_p(L) G_{yw} \Theta \left(I - G_{zw}\Theta\right)^{-1} G_{zu} \tag{3.6.1}$$

P_{ru} is an indication of the effectiveness of the control signal in altering the residual in the faulty system, therefore it is advantageous to maximise P_{ru}.

$$\max_{L} \left(P_{ru}(\Theta, L)\right) \tag{3.6.2}$$

Next, consider the input shaping filter $H_u(s)$ shown in figure 3.1. This subsystem is responsible for transforming the zero-mean white noise signal u_h into a signal representative of the power distribution of a practically realisable band-limited system input u. For the purpose of this investigation a simple low-pass filter of the form

$$H_u(s) = \left(\frac{a}{s+a}\right)^n \tag{3.6.3}$$

is used, where a gives a cut-off frequency much higher than our system dynamics and n is large enough to ensure finite system bandwidth.

3.7 Combining Results

In this chapter, the components of the optimal open-loop AFD setup have been investigated. Firstly, the input shaping filter was introduced and discussed for a number of different scenarios. Next, approximated detector dynamics were derived. Then the noise power on the residual of nominal system was minimised. This allows the sensitivity of the detector to be maximised. Equations were derived which can be used to maximise the effect of η on r. Lastly, equations were derived which can be used to maximise the effect of u on r. This allows the detector threshold to be reached as fast as possible.

From the equations given in 3.2, 3.3, 3.4 and 3.6, the transfer function from input η_h to the thresholding signal h is given by

$$P_{h\eta_h}(\Theta, L, s) = D(s)P_{r\eta}(\Theta, L, s)H_\eta(s) \tag{3.7.1}$$

and the transfer function from input u to the thresholding signal h is given by

$$P_{hu_h}(\Theta, L, s) = D_r(s)P_{ru}(\Theta, L, s)H_u(s) \tag{3.7.2}$$

Worst-Case Scenario: The peak gain in the frequency response of a linear system is given by the H_∞ norm

$$\|H(s)\|_\infty = \max_\omega \sigma_{\max}\left(H(j\omega)\right) \tag{3.7.3}$$

Therefore,

$$\|P_{h\eta_h}(\Theta, L)\|_\infty = \max_\omega \sigma_{\max}\left(D(j\omega)P_{r\eta}(\Theta, L, j\omega)H_\eta(j\omega)\right) \tag{3.7.4}$$

Therefore, the estimator gain which leads to the largest value of h after the time period t_d is given by

$$\max_L \left(\|P_{h\eta_h}(\Theta, L)\|_\infty\right) \tag{3.7.5}$$

Even though $P_{r\eta_h}(\Theta, L, s)$ is a MIMO system in the general case, $\|P_{h\eta_h}(L)\|_\infty$ is always a single norm in terms of L , as it relates the effect of a single periodic signal on the output resulting in the largest singular value.

As was stated in *criterion 1*, the average fault signal to nominal noise ratio on $h(t)$ must be maximised, therefore from (3.5.3) and (3.7.5),

$$\max_L \left(\frac{\|P_{h\eta_h}(\Theta, L)\|_\infty}{\|P_{rd_0}(L)\|_2}\right) \tag{3.7.6}$$

where the optimal estimator gain, L_{opt} satisfies (3.7.6), while the optimal auxiliary signal frequency is the excitation frequency argument maximising $\|P_{h\eta_h}(\Theta, L_{opt})\|_\infty$.

Average Scenario: Since the input is no longer a simple sinusoidal signal, it is more reasonable to maximise the power output of the detector due to the control excitation. The total output power of a linear system is given by the H_2 norm

$$\|H(s)\|_2 = \sqrt{\frac{1}{2\pi}\int_{-\infty}^{\infty} \text{Trace}\left[H(j\omega)^* H(j\omega)\right] d\omega} \tag{3.7.7}$$

Therefore,

$$\|P_{hu_h}(L)\|_2 = \sqrt{\frac{1}{2\pi}\int_{-\infty}^{\infty} \text{Trace}\left[P_{hu_h}(\Theta, L, j\omega)^* P_{hu_h}(\Theta, L, j\omega)\right] d\omega} \tag{3.7.8}$$

Therefore, the estimator gain which leads to the largest h is given by

$$\max_L \left(\|P_{hu_h}(\Theta, L)\|_2\right) \tag{3.7.9}$$

As was stated in *criterion 1* the average fault signal to nominal noise ratio on $h(t)$ must be maximised, therefore from (3.5.3) and (3.7.9),

$$\max_L \left(\frac{\|P_{hu_h}(\Theta, L)\|_2}{\|P_{rd_0}(L)\|_2}\right) \tag{3.7.10}$$

where the optimal estimator gain, L_{opt} satisfies (3.7.10).

Chapter 4

Optimal Open-Loop Active Fault Detection: The Simplified SISO Case

In this chapter optimal open-loop AFD is investigated for the simplified SISO case. The purpose of this chapter is to reduce the full MIMO theory into a far simpler SISO framework. Restricting the investigation to SISO systems leads to significant simplifications highlighting key aspects and properties of the optimisation framework, as well as providing the new reader with an easier to understand starting point.

The focus in this chapter will be on those aspects which are simplified by this SISO system restriction. To further simplify the investigation the control signal is removed from the optimisation problem. This implies that only the worst-case AFD scenario can be considered.

In SISO systems, the injection of the auxiliary signal always results in a reduction of the nominal system performance. Therefore, unlike MIMO systems, the nominal performance degradation is always of concern. Keeping this in mind, the following simplified design goals are considered to be important during the design of the optimal estimator and auxiliary signal pair:

1. Design the estimator gain so that $A + LC_y$ is stable.
2. Design the auxiliary signal, η, in such a way as to limit nominal performance degradation.

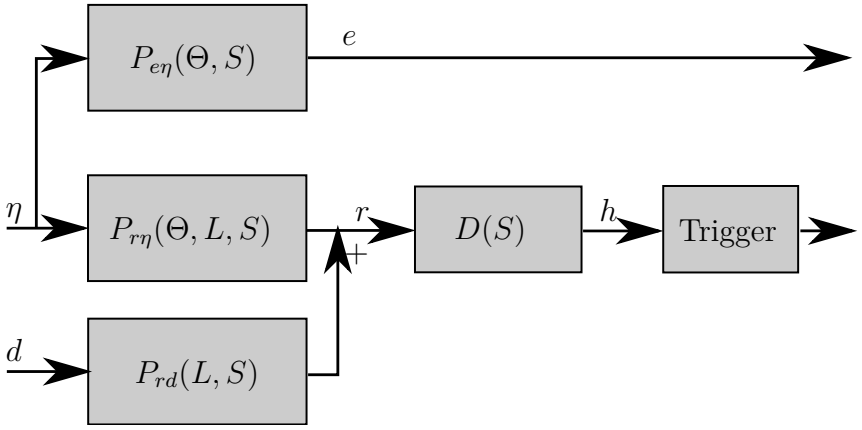

Figure 4.1: Setup used for Active Fault Detection. From left to right the following is shown: plant excitation dynamics; linearised detector dynamics; and fault trigger.

3. Design the estimator gain, L, and the auxiliary signal, η, in order to minimise the fault detection time.

4.1 A Setup for Active Fault Detection in SISO Systems

Design goal 2 requires that the impact of the auxiliary signal on the system error output be known and kept within the stipulated design constraint. Now, consider design goal 3. This design goal requires that the impact of the auxiliary signal on the triggering output be known and maximised. Furthermore, this design goal requires that the impact of the estimator gain on the nominal detector noise level be known and minimised. A complying setup is shown in figure 4.1, noting that the input shaping filter of the MIMO system was replaced by a simple gain α.

With reference to this figure, a number of definitions are now made:

- Define Λ_0 as the nominal system AFD disturbance constraint. Therefore, $\sigma_{\max}\left(P_{e\eta}(0, s)\mathcal{H}\right) \leq \Lambda_0$ must hold for all $t > 0$ and the postulated fault condition Θ_1.

- The signal η is the excitation signal used for the purpose of AFD, and is given by $\eta = a\sin(\omega t)$, where a is a simple gain such that the performance

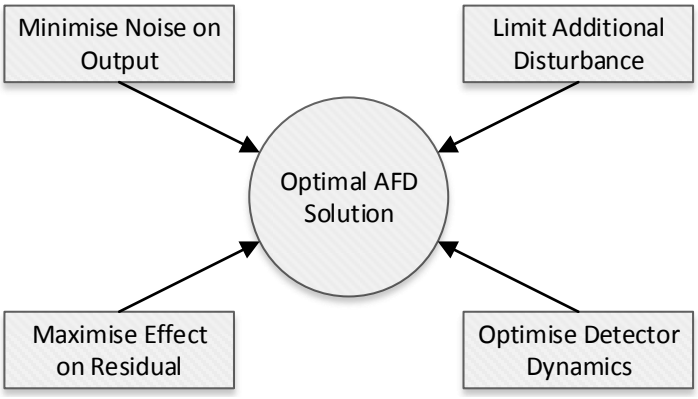

Figure 4.2: Aspects of the Active Fault Detection Optimisation Problem.

degradation constraint Λ_0 is adhered to.

- The signal d is a zero mean white noise signal. This signal injects noise into the residual signal through the disturbance dynamics, $P_{rd}(L, s)$. The noise injected into the residual must be of finite power, in other words the H_2 norm of $P_{rd}(L, s)$ must exist.

- h is the signal on which thresholding is performed, and is given by $H = D_r(s)R$, where $D_r(s)$ is a linear approximation of the detector dynamics.

From these definitions and the informal discussion provided earlier, the following optimisation criteria is now formulated.

Criterion 2. *Find the estimator gain L, excitation frequency ω_η, and the admissible gain which maximises the average fault signal to nominal noise ratio on $h(t)$ over a fixed time period t_d.*

The basic optimisation strategy is again shown graphically by figure 4.2. In the remainder of this section the subsystems making up the optimal AFD setup are considered and combined to arrive at the optimised AFD solution. With reference to figure 4.1, these subsystems are: the auxiliary signal and how it relates to the disturbance constraint; an approximated description of the detector dynamics and how it relates to the excitation frequency; a characterisation of the effect of the auxiliary signal on the residual output; and a description of the nominal detection noise.

4.2 Disturbance Constraint and the Auxiliary Signal

Implementing AFD results in a reduction in nominal system performance. It is therefore of primary importance to limit this performance degradation. Therefore,

$$\Lambda_0 = c_0 \tag{4.2.1}$$

where c_0 is a constant.

The auxiliary signal must be designed to satisfy the single constraint Λ_0. Assuming maximum additional system disturbance, the maximum auxiliary signal amplitude is given by

$$a = c_0 \left| \frac{1}{P_{e\eta}(0, j\omega)} \right| = c_0 \left| \frac{1}{G_{eu}(0, j\omega)} \right| \tag{4.2.2}$$

The Dual Youla Parameter remains unchanged from the MIMO case, and is simply restated here for clarity

$$P_{r\eta}(\Theta, L) = \tilde{M}_p(L) G_{yw} \Theta \left(I - G_{zw}\Theta\right)^{-1} G_{zu} \tag{4.2.3}$$

As before it is advantageous to maximise $P_{r\eta}$.

$$\max_L \left(P_{r\eta}(\Theta, L)\right) \tag{4.2.4}$$

4.3 Approximated Detector Dynamics

The derivation of the approximated detector dynamics remain unchanged from the MIMO case, and is therefore not shown again. However for clarity the result is briefly restated here.

The detector's integration action can be closely approximated by a second order transfer function of the form

$$D_r(s) \approx \frac{t_d s^2}{2\left(s^2 + 2\left(\frac{a}{t_d}\right)s + \left(\frac{a}{t_d}\right)^2\right)} \tag{4.3.1}$$

where a is a constant given by

$$a = \sqrt{\frac{3}{2}} \tag{4.3.2}$$

4.4 Noise Covariance on Nominal Residual Signal

The nominal noise covariance remains unchanged from the MIMO case, and is simply restated here for clarity:

$$\|P_{rd_0}(L)\|_2 = \sqrt{\frac{1}{2\pi}\int_{-\infty}^{\infty} \text{Trace}\left[P_{rd_0}(j\omega, L)^* P_{rd_0}(j\omega, L)\right] d\omega} \tag{4.4.1}$$

The estimator gain which minimises the nominal residual covariances satisfies

$$\max_L \left(\frac{1}{\|P_{rd_0}(L)\|_2}\right) \tag{4.4.2}$$

4.5 Combining Results

In this section the components of the simplified optimal open-loop SISO AFD setup is investigated. Of primary importance is the simplification of the input shaping filter into a simple gain. From the equations given in 4.2 and 4.3, the transfer function from input η_h to the thresholding signal h is given by

$$P_{h\eta_h}(\Theta, L, s) = aD_r(s)P_{r\eta}(\Theta, L, s) \tag{4.5.1}$$

The peak gain in the frequency response of a linear SISO system is given by the H_∞ norm

$$\|H(s)\|_\infty = \max_\omega |H(j\omega)| \tag{4.5.2}$$

Therefore,

$$\|P_{h\eta_h}(\Theta, L)\|_\infty = \max_\omega |aD_r(j\omega)P_{r\eta}(\Theta, L, j\omega)| \tag{4.5.3}$$

Therefore, the estimator gain which leads to the largest h is given by

$$\max_L \left(\|P_{h\eta_h}(\Theta, L)\|_\infty\right) \tag{4.5.4}$$

As was stated in *criterion 2*, the average fault signal to nominal noise ratio on $h(t)$ must be maximised. Therefore from (4.4.2) and (4.5.4),

$$\max_L \left(\frac{\|P_{h\eta_h}(\Theta, L)\|_\infty}{\|P_{rd_0}(L)\|_2}\right) \tag{4.5.5}$$

where the optimal estimator gain, L_{opt} satisfies (4.5.5), while the optimal auxiliary signal frequency is the excitation frequency argument maximising $\|P_{h\eta_h}(\Theta, L_{opt})\|_\infty$.

Chapter 5

Optimal Open-Loop Active Fault Detection: Discussion

In this chapter the novel theoretical framework developed in the previous chapters is discussed. This includes choosing the appropriate optimisation scheme, selecting a reasonable targeted detection time, and solving the optimisation problem. Additionally, a brief summary of the active fault detection framework is provided.

5.1 Selecting the AFD Implementation

In the previous chapters a number of different AFD methods are introduced. These methods range from simple SISO methods to far more complex zero-disturbance MIMO methods. From these chapters it can be seen that the main AFD implementations are:

- **Standard SISO AFD**: This is by far the simplest of the proposed AFD implementations. This method can only be applied to open-loop stable LTI SISO systems.
- **Standard MIMO AFD**: This is an extension of the SISO theory to MIMO systems. This method can be applied to any open-loop stable LTI MIMO system.

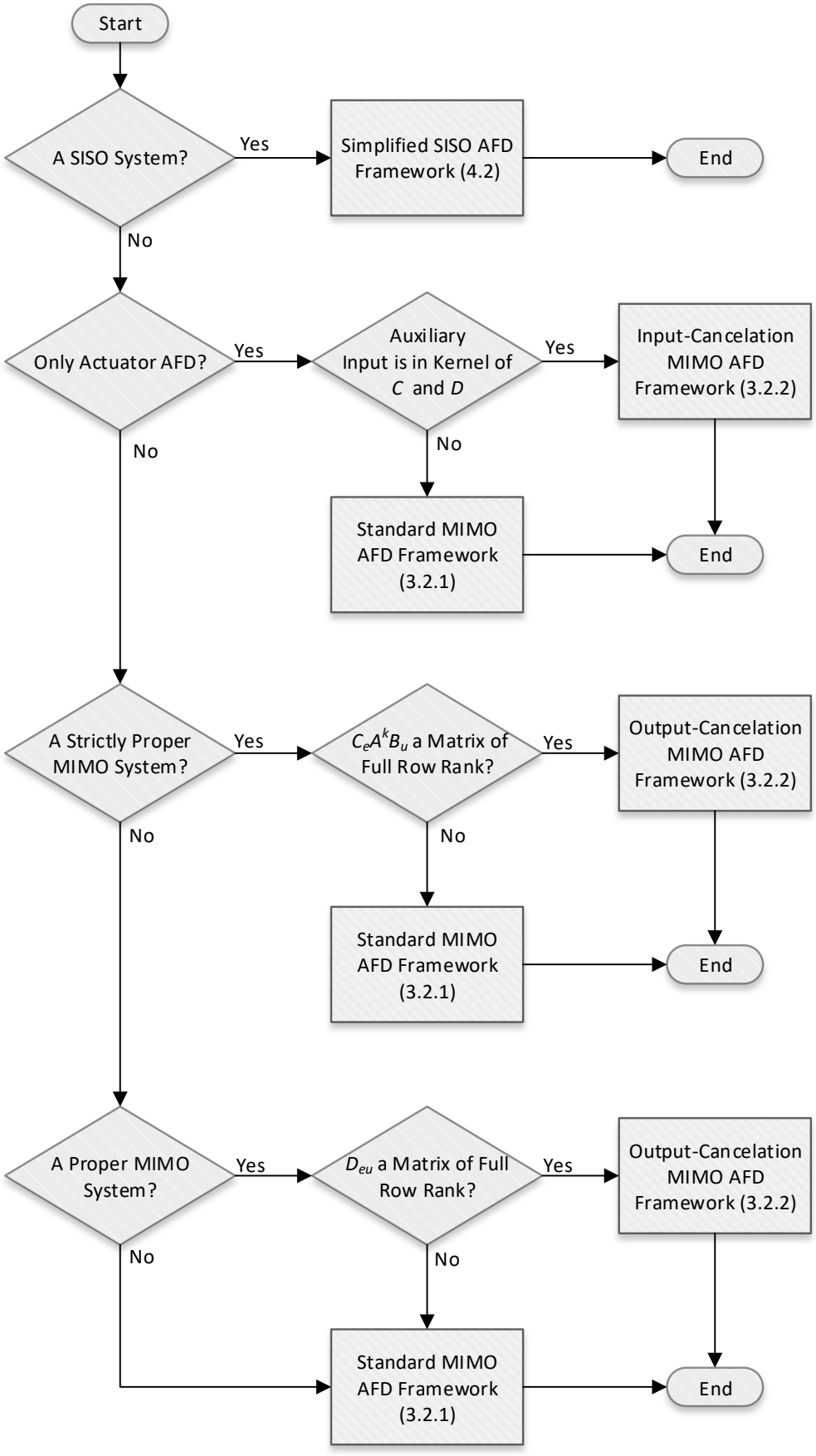

Figure 5.1: Active Fault Detection Framework Selection Proses. The section or subsection related to the auxiliary input design for each framework is shown in brackets.

- **MIMO AFD with input zeroing**: This is an extension of the standard MIMO AFD method which decouples the auxiliary excitation from the system state dynamics in the nominal case. This is done by injecting the excitation signal into the input null-space. Therefore, only actuator faults are detectable when using input cancellation. This method can be applied to open-loop stable LTI MIMO systems with a non-empty input null-space.

- **MIMO AFD with output zeroing**: This is an alternative extension of the standard MIMO AFD method which decouples the auxiliary excitation from the system output dynamics in the nominal case. This is performed by designing the input shaping filter in such a way that the excitation is cancelled in the measurement equation. This method can be applied to proper open-loop stable LTI MIMO systems when D_{eu} is a matrix of full row rank or to strictly proper open-loop stable LTI MIMO systems when $C_e A^k B_u$ is a matrix of full row rank. Furthermore, care should be taken that the excitation injected into the individual actuators and states are within acceptable limits. This is especially of concern when one or more of the system outputs are strongly correlated to only a subset of the system states. Stated differently, this method is most suited to systems where the output is strongly correlated to all system states and inputs.

5.2 Average or Worst-Case Optimisations

As is discussed in chapter 3, the optimisation can either be performed for the average or worst-case performance scenarios. Both of these approaches have advantages and disadvantages, which are now briefly discussed:

- In general, the worst-case optimisation is simpler to perform. It avoids having to model the power spectrum of the control input.

- It is true that the average-case optimisation will, in most cases, lead to superior detection performance. However, it should be noted that the

effect of this is relatively limited since the excitation provided by the control signal far outweighs that of the auxiliary signal.

- In most cases the results obtained will be very similar, with just a small shift in the excitation frequency and filter bandwidth.

5.3 Choosing the Targeted Detection Time

One of the parameters required by the optimisation problem presented is the targeted detection time. This parameter places a soft lower bound on the optimal excitation frequency, estimator bandwidth, as well as the fault detection time. When selecting this design parameter the following criteria should be considered:

- Changing t_d provides a mechanism for exchanging small error detection performance (sensitivity) for detection speed and vice versa. A longer t_d provides more sensitivity but slower detection speed for larger errors while a shorter t_d provides less sensitivity but faster detection speed for larger errors.
- The shortest reasonable t_d is determined by the inverse of the system bandwidth. As the minimum excitation frequency is pushed beyond the system bandwidth, the efficacy of the excitation signal starts to diminish.
- The longest reasonable t_d is determined by the fault detection specification.

Figure 5.2 shows the effect of varying the targeted detection time. It can be seen from the figure that as t_d is shortened the detection gain is reduced and vice versa.

5.4 Using the Open-Loop AFD Optimisation in a Closed-Loop system

Solving the optimisation problem in the open-loop case is substantially simplified when compared to solving the closed-loop problem directly. Therefore

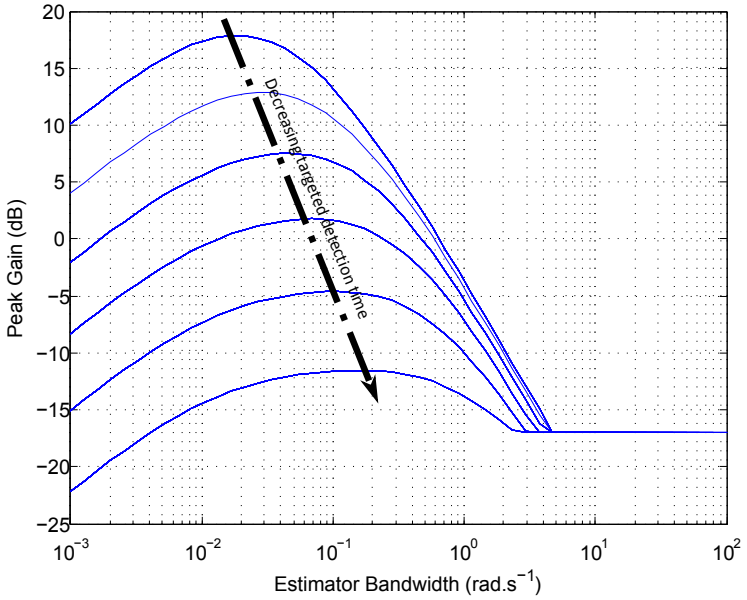

Figure 5.2: Peak gain plot showing the effect of the targeted detection time. As t_d becomes shorter the optimal estimator bandwidth increases, while the peak gain is significantly reduced. This is indicated by the arrow in the figure.

it is of particular interest to investigate the effect of using such a simplified optimisation for closed-loop systems.

The following must be considered when applying the AFD system to closed-loop systems:

- The auxiliary signal must ideally become part of the reference input in order to avoid being rejected as a disturbance by the control system. The auxiliary signal is therefore not an unknown disturbance to the closed-loop controller.

- When injecting the auxiliary signal in this manner, the controller bandwidth must be substantially larger than the auxiliary excitation frequency. This prevents the controller from rejecting the desired excitation signal.

- The magnitude of the auxiliary input signal must be adjusted in order to compensate for the effect of the control system. This adjustment compensates for the fact that the auxiliary signal now forms part of

the reference input and must ensure that the desired output disturbance constraint is met.

- A stable control loop changes the post fault system behaviour by partially or completely rejecting the change in the system behaviour. Therefore, the output of the post fault system might be unchanged from the nominal system.

The first three points mentioned above are self explanatory, therefore further details are not provided. The final point is now analysed in more detail.

When analysing the effect of closing a control loop on the post fault system a simple, practical approach is needed in order to maintain the simplicity of using the open-loop optimisation. The following approach is taken:

- It is assumed that the closed-loop system remains stable.
- The control system will at most completely reject the change in the system.
- The completely rejected case therefore represents the largest performance change from the faulty open-loop to faulty closed-loop system.
- Only the maximum change is analysed, with partially rejected faults experiencing AFD performance changes somewhere between this maximum and the open-loop performance.

Denote the maximum change in post failure error signal amplitude as,

$$\Delta_{max} = \frac{|P(\Theta_1)_{e\eta_{cl}}\mathcal{H}_{cl}|}{|P(\Theta_1)_{e\eta_{ol}}\mathcal{H}_{ol}|} \tag{5.4.1}$$

where, Θ_1 denotes the postulated fault case. As stated above, the largest change scenario is when the fault is completely rejected. Additionally, the closed-loop excitation signal has been adjusted so that

$$|P(0)_{e\eta_{cl}}\mathcal{H}_{cl}| = |P(0)_{e\eta_{ol}}\mathcal{H}_{ol}| \tag{5.4.2}$$

holds. For equation (5.4.2) it is assumed that the nominal disturbance is non-zero, therefore it is not suitable for the output and input cancellation schemes.

From equation (5.4.1), (5.4.2), and the details noted above the maximum change in post failure error signal amplitude is given by

$$\Delta_{max} = \frac{|P(0)_{e\eta_{cl}}\mathcal{H}_{cl}|}{|P(\Theta_1)_{e\eta_{ol}}\mathcal{H}_{ol}|} \tag{5.4.3}$$

Therefore, the change in post failure error signal is given by the ratio of the nominal closed loop output disturbance and the post-failure open-loop disturbance output. This result implies the following:

- If the failure results in a reduction to the excitation, the controller will increase the system input thereby improving the fault detection performance versus the open-loop case.
- However, if the failure results in an increase to the excitation, the controller will reduce the system input thereby reducing the fault detection performance versus the open-loop case.

Please refer to section 6.7 for a detailed example.

5.5 Solving the Optimisation Problem

For simple first and second order problems the optimisation problem can easily be solved by simple numerical methods, and can be visualised using simple plots. A basic solver is shown in figure 5.3. The solver starts at a frequency far below what would be reasonable for the giving value of t_d. It then simply solves for a number of frequency points until it reaches a value far above the system bandwidth. The largest value is then selected, and used to calculate the optimal estimator gain as well as excitation frequency.

However, for more complex problems drawing simple plots becomes impractical. In these cases the optimisation problem can be solved using a number of standard advanced numerical techniques. For a detailed discussion of these and other techniques please refer to [79] and [80]. Ultimately even the most efficient algorithm will be undone by the exponential time complexity of the optimisation problem as the number of states increase.

If, however, a slightly suboptimal solution is acceptable, the time complexity problem can be easily overcome by restricting the estimator error dynamics

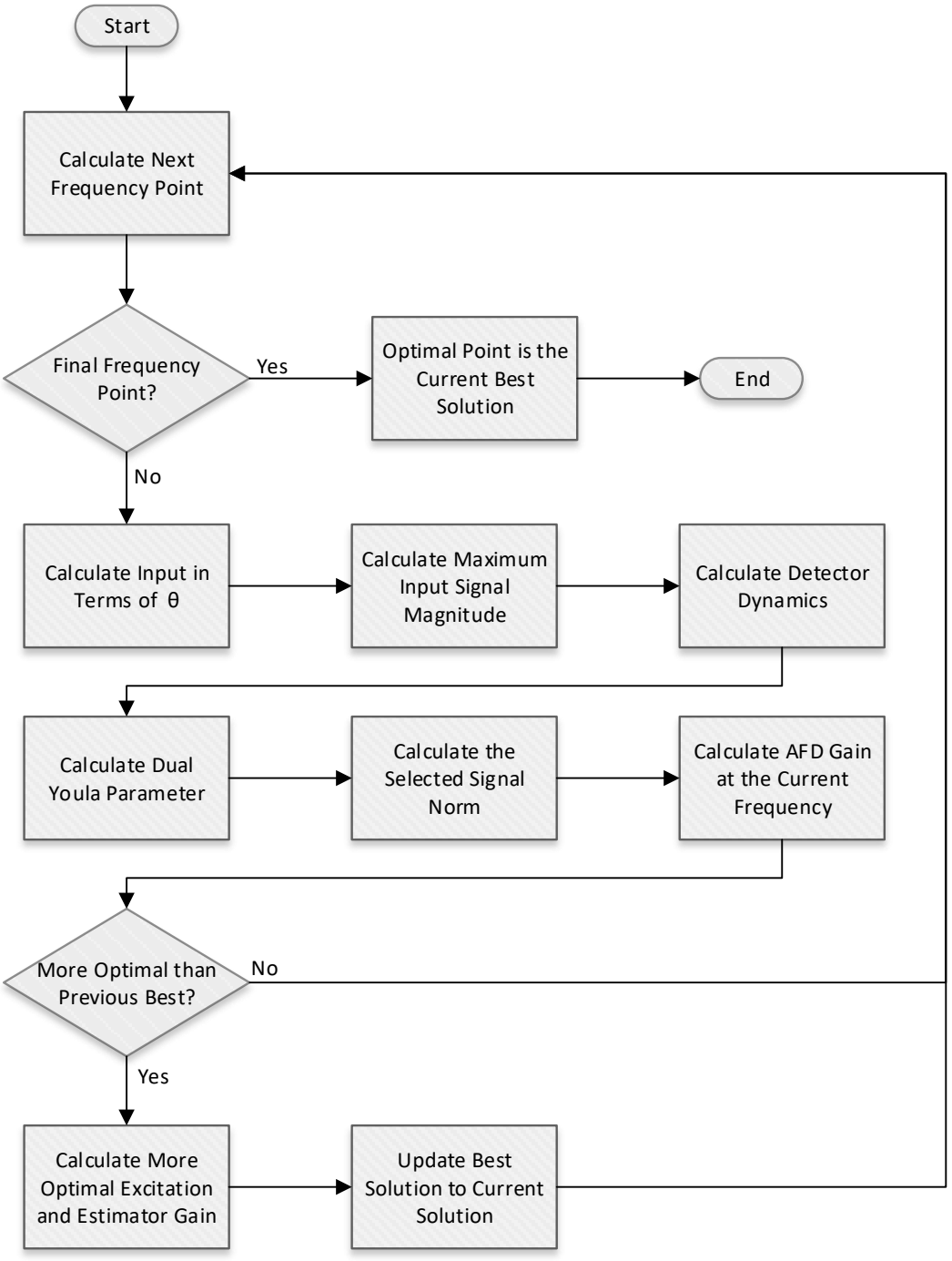

Figure 5.3: A simple algorithm for solving the AFD optimisation problem.

to that of a simple low-pass filter. This modified problem leads to the following optimisation criteria in the general case:

Criterion 3. *Find the estimator bandwidth ω_L, excitation frequency ω_η, and the admissible shaping filter $H_\eta(s)$ which maximises the average fault signal to nominal noise ratio on $h(t)$ over a fixed time period t_d.*

Or in the simplified SISO case:

Criterion 4. *Find the estimator bandwidth ω_L, excitation frequency ω_η, and admissible gain a which maximises the average fault signal to nominal noise ratio on $h(t)$ over a fixed time period t_d.*

When using this modified criterion the estimator gain in equation (3.7.6) is determined via the optimal bandwidth and the chosen filter topology, therefore the time complexity of the numerical solution is now independent of the number of states. Furthermore, using this problem setup allows the use of the same simple numerical methods to solve higher order problems, as was suggested previously for first order problems.

Finally, it is important to note that even though the equations contain a number of linear system inversions it is not necessary to solve these explicitly. For SISO and single output MIMO systems the inversion can be performed easily enough. However, for more complex MIMO problems the system inverse might not even exist. In these cases it is easily solved by performing the inversion numerically at the points of interest, rather than attempting to derive an analytic solution.

5.6 Summary of Theoretical Development

Optimal open-loop active fault detection is investigated for stable systems. The design of the estimator is considered an integral part of the AFD optimisation process instead of being a fixed controller attribute. The research presented in [69], [71], [54] and [55] is simplified for the open-loop case considered. Equations are derived to minimise the noise covariance on the nominal residual output as well as to maximise the detection signal. In order to realise a non-trivial solution, the theory is extended to include dynamical effects of the detector. It is found that this effect can be closely approximated by a second order transfer function, with a low-pass cut-off frequency determined by the minimum targeted detection time design parameter.

When optimising for the worst-case AFD scenario, the resulting optimal estimator and auxiliary signal pair is found to be given by

$$\max_{L} \left(\frac{\|P_{h\eta_h}(\Theta, L)\|_\infty}{\|P_{rd_0}(L)\|_2} \right) \tag{5.6.1}$$

where the optimal estimator gain, L_{opt}, satisfies (5.6.1), while the optimal auxiliary signal frequency is the excitation frequency argument maximising $\|P_{h\eta_h}(\Theta, L_{opt})\|_\infty$.

However, when optimising for the average-case AFD scenario, the resulting optimal estimator and auxiliary signal pair is given by

$$\max_{L} \left(\frac{\|P_{hu_h}(\Theta, L)\|_2}{\|P_{rd_0}(L)\|_2} \right) \tag{5.6.2}$$

where the optimal estimator gain, L_{opt} satisfies (5.6.2), while the optimal auxiliary signal frequency is the excitation frequency argument maximising $\|P_{h\eta_h}(\Theta, L_{opt})\|_\infty$.

$\|P_{rd_0}(L)\|_2$ gives the noise covariance on the nominal residual signal, and is given by

$$\|P_{rd_0}(L)\|_2 = \sqrt{\frac{1}{2\pi} \int_{-\infty}^{\infty} \text{Trace}\left[P_{rd_0}(j\omega, L)^* P_{rd_0}(j\omega, L)\right] d\omega} \tag{5.6.3}$$

$\|P_{h\eta_h}(L)\|_\infty$ describes the effectiveness of the auxiliary signal in altering the detector output, and is given by,

$$\|P_{h\eta_h}(\Theta, L)\|_\infty = \max_{\omega} \sigma_{\max}\left(D_r(j\omega) P_{r\eta}(\Theta, L, j\omega) H_\eta(j\omega)\right) \tag{5.6.4}$$

where, $H_\eta(s)$ captures the input shaping filter dynamics, $P_{r\eta}(\Theta, L, s)$ the system dynamics from the auxiliary input to residual output, and $D_r(s)$ the detector dynamics.

Alternatively, $\|P_{h\eta_h}(\Theta, L)\|_2$ describes the effectiveness of the control signal in altering the detector output and is given by

$$\|P_{hu_h}(\Theta, L)\|_2 = \sqrt{\frac{1}{2\pi}\int_{-\infty}^{\infty} \text{Trace}\left[P_{hu_h}(\Theta, L, j\omega)^* P_{hu_h}(\Theta, L, j\omega)\right] d\omega} \quad (5.6.5)$$

for the average-case optimisation.

Together these three equations form the basis of the signal to noise ratio based optimisation presented here.

Part II

Theoretical Application

Chapter 6

Illustrative Examples

In the previous chapters a number of Active Fault Detection concepts are introduced and explored. These concepts are then used to derive an estimator-based theoretical AFD optimisation framework. In this chapter this theoretical framework is applied to a number of simple illustrative examples. These examples are purposefully designed to provide insight into the chosen theory or concept, and are not meant to be exhaustive, practical or entirely realistic.

6.1 General Problem Setup

The examples given in this chapter all follow the same basic problem setup, which is now briefly introduced.

For nearly all the problems considered the following procedure is followed:

1. First, the generic system model used for the example is introduced.
2. Next, the fault model is introduced and added to the system model. The fault dynamics are placed in a feedback path by using a linear fractional transform.
3. Following this, the system is augmented with a basic disturbance or noise model.
4. Next, the specific numeric values are provided and the optimisation is performed to find the optimal estimator bandwidth.

5. With the estimator bandwidth known, the optimal estimator gain and auxiliary excitation frequency can be determined.

The disturbance model used throughout this and the next chapter is now briefly introduced.

6.1.1 The Disturbance Model

For the examples in this chapter the following simple noise model is used.

- Zero mean white process noise which enters the system in the same manner as the control input
- Bandwidth limited zero mean white measurement noise
- The error signal is equal to the plant output

This disturbance model can be described by the following state space model:

$$\begin{bmatrix} \dot{x} \\ \dot{x_n} \end{bmatrix} = \begin{bmatrix} A & 0 \\ 0 & c \end{bmatrix} \begin{bmatrix} x \\ x_n \end{bmatrix} + \begin{bmatrix} k_P \\ -c \end{bmatrix} d \tag{6.1.1}$$

$$e = \begin{bmatrix} C & k_m \end{bmatrix} \begin{bmatrix} x \\ x_n \end{bmatrix} \tag{6.1.2}$$

where A and C are system matrices, k_P and k_m are the process and measurement noise gains, and $-c$ is the measurement noise bandwidth.

6.2 Example 1: Limitations of The Existing Theory

This simple example will demonstrate the problem with simply applying the previously existing theory to the open loop optimal AFD problem. It will be shown that using the existing Dual Youla based theory in this manner leads to a trivial solution, because the existing theory was intended to be used with a pre-existing estimator, and not to be used in designing an estimator for optimal AFD.

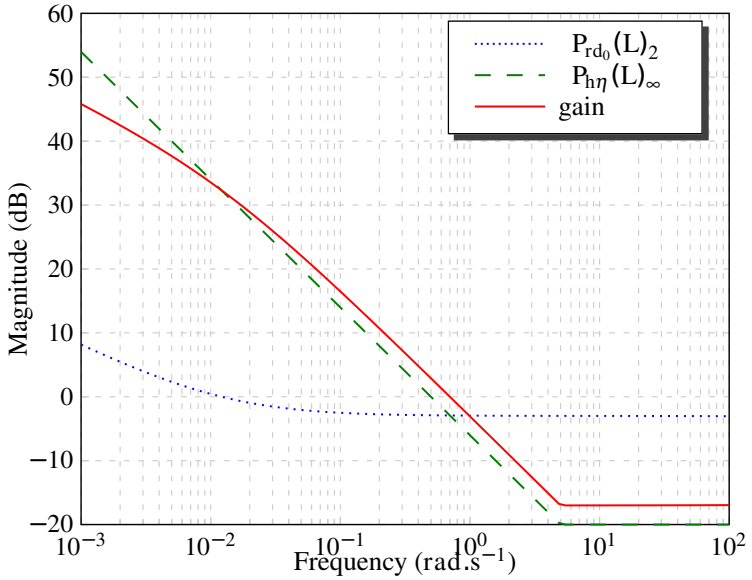

Figure 6.1: AFD performance as a function of estimator bandwidth. $\omega_{L_{opt}}$ is given by peak of $\frac{\|P_{h\eta}(\Theta,L)\|_\infty}{\|P_{rd_0}(L)\|_2}$.

In general, a first order linear differential equation is given by the following equation:

$$\dot{x} = ax + bu \tag{6.2.1}$$

This can be represented by the following state space representation.

$$\dot{x} = \begin{bmatrix} a \end{bmatrix} x + \begin{bmatrix} b \end{bmatrix} u \tag{6.2.2}$$

$$y = \begin{bmatrix} 1 \end{bmatrix} x \tag{6.2.3}$$

Consider the following fault model:

$$a = a_0 \left(1 + \theta_a\right) \tag{6.2.4}$$

$$b = b_0 \left(1 + \theta_b\right) \tag{6.2.5}$$

where, θ_a and θ_b are zero in the nominal case.

Using an upper linear fractional transform the system can be written as

$$\dot{x} = \begin{bmatrix} a_0 \end{bmatrix} x + \begin{bmatrix} a_0 & b_0 \end{bmatrix} w + \begin{bmatrix} b_0 \end{bmatrix} u \tag{6.2.6}$$

$$z = \begin{bmatrix} 1 \\ 0 \end{bmatrix} x + \begin{bmatrix} 0 \\ 1 \end{bmatrix} u \tag{6.2.7}$$

$$y = [1]x \tag{6.2.8}$$

with,

$$w = \begin{bmatrix} \theta_a & 0 \\ 0 & \theta_b \end{bmatrix} z \tag{6.2.9}$$

Next, the disturbance model is introduced. In this example, the model introduced at the start of this chapter will be used.

Adding the disturbance model results in the following three port model:

$$\begin{bmatrix} \dot{x} \\ \dot{x_n} \end{bmatrix} = \begin{bmatrix} a_0 & 0 \\ 0 & c \end{bmatrix} \begin{bmatrix} x \\ x_n \end{bmatrix} + \begin{bmatrix} a_0 & b_0 \\ 0 & 0 \end{bmatrix} w + \begin{bmatrix} b \\ 0 \end{bmatrix} u + \begin{bmatrix} k_P \\ -c \end{bmatrix} d \tag{6.2.10}$$

$$z = \begin{bmatrix} 1 & 0 \\ 0 & 0 \end{bmatrix} \begin{bmatrix} x \\ x_n \end{bmatrix} + \begin{bmatrix} 0 \\ 1 \end{bmatrix} u \tag{6.2.11}$$

$$y = \begin{bmatrix} 1 & k_m \end{bmatrix} \begin{bmatrix} x \\ x_n \end{bmatrix} \tag{6.2.12}$$

$$e = \begin{bmatrix} 1 & k_m \end{bmatrix} \begin{bmatrix} x \\ x_n \end{bmatrix} \tag{6.2.13}$$

The values for a_0, b_0, c, k_m and k_p are now chosen as, -1, -5, -10000, 0.01, 0.1 respectively.

Suppose that the plant suffers damage which results in

$$\Theta = \begin{bmatrix} -0.4 & 0 \\ 0 & -0.1 \end{bmatrix} \tag{6.2.14}$$

Therefore, there is a 40% reduction in damping and a 10% reduction in control authority.

From figure 6.1 it can be seen that simply applying the theory from [54] when the estimator is not a fixed entity leads to incomplete results. In [54] the estimator is considered fixed, and the detector dynamics is amused to be unity. It should be noted that when referring to gain in terms of an optimisation plot, this document is referring to $\max_L \left(\frac{\|P_{h\eta_h}(\Theta, L)\|_\infty}{\|P_{rd_0}(L)\|_2} \right)$. The results obtained suggest that the best estimator is the open-loop case, and that the optimal excitation frequency is $0\ rad.s^{-1}$. This would lead to an infinite detection time, which is most certainly not optimal. Furthermore, this shows that ignoring the

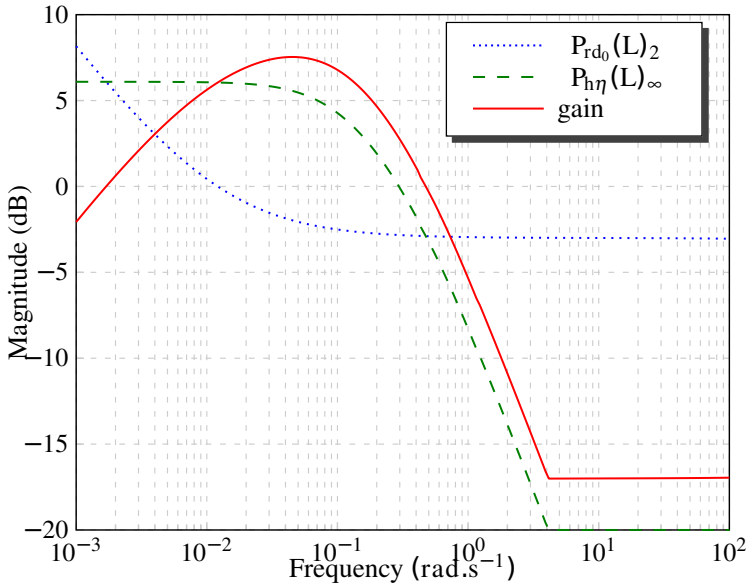

Figure 6.2: AFD performance as a function of estimator bandwidth. $\omega_{L_{opt}}$ is given by peak of $\frac{\|P_{h\eta}(\Theta,L)\|_\infty}{\|P_{rd_0}(L)\|_2}$.

detector dynamics may potentially lead to unexceptionably large optimisation errors.

6.3 Example 2: Basic SISO Application

Example 1 is now repeated for the Optimal AFD problem, using the augmented theory described in this dissertation where detector dynamics are also taken into consideration.

This example uses the same model as in example 1, and the model is therefore not restated here.

Now, using the equations derived in this work, a frequency plot can be easily produced showing the AFD performance as a function of the estimator bandwidth. The results are shown in figure 6.2. From this figure it is easy to determine the optimal estimator bandwidth as

$$\omega_{L_{opt}} = 0.0455 \text{ rad.s}^{-1} \tag{6.3.1}$$

when a targeted detection time of $10s$ is used.

Finally, with $\omega_{L_{opt}}$ known, a plot of $P_{h\eta}(L_{opt})$ can be produced. The result

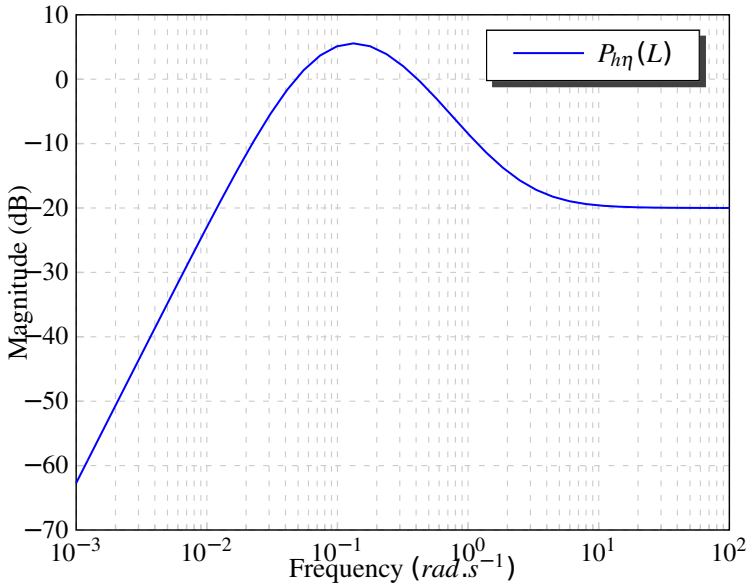

Figure 6.3: Magnitude response of $P_{h\eta}(L_{opt})$. The optimal excitation frequency ($\omega_{\eta_{opt}}$) is given by the peak of the magnitude response.

is shown in figure 6.3. From the figure the optimal excitation frequency is

$$\omega_{\eta_{opt}} = 0.1365 \text{ rad.s}^{-1} \tag{6.3.2}$$

When compared with the results in the first example, it can be seen that a non-trivial solution is realised. The resulting estimator is no longer open-loop, and the excitation is not a constant input.

These results are used to set up a simulation of the optimal AFD system. The simulation results are shown in Figure 6.4 for moderate levels of white noise and in Figure 6.5 for high levels of white noise. Note that the setup proves robust against white noise, while providing a substantial gain from error signal to residual output. As can be seen the detection time is above the minimum targeted detection time, and would not be adversely affected by the detector dynamics.

It is important to note that model inaccuracies are a major hurdle to effective fault detection. Parametric uncertainties are mathematically identical to faulty parameters, and therefore much effort should be spent in determining accurate system models. Notwithstanding this, there are a number of steps that can be taken in order to deal with parameter uncertainties. These include employing the system as part of an active fault tolerant control system and/or using a leaky detector.

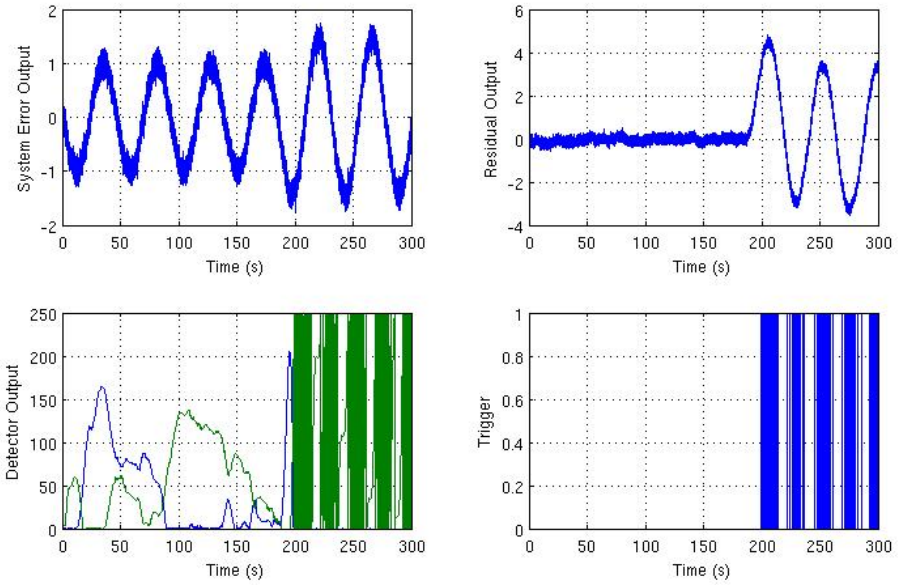

Figure 6.4: Simulation results with a moderate amount of noise in the correct ratio. Failure occurs at 186 seconds and is detected 13 seconds later. In the detector output both the positive and negative part of the two-sided CUSUM detector is shown. Note that each time the threshold is reached the detector is reset, and the trigger value is set to one for a single sample period.

6.4 Example 3: Zero-Disturbance AFD Using Input Cancellation

This simple example demonstrates using control cancellation to achieve zero-disturbance AFD. Since the auxiliary signal is within the kernel of the system input, only actuator fault detection can be performed.

A simple first order MIMO system can be captured by the following state space representation:

$$\dot{x} = \begin{bmatrix} a \end{bmatrix} x + \begin{bmatrix} b_1 & b_2 \end{bmatrix} u \qquad\qquad y = \begin{bmatrix} 1 \end{bmatrix} x \tag{6.4.1}$$

Consider the following fault model

$$b_1 = b_{1_0} \left(1 + \theta_{b_1}\right) \qquad\qquad b_2 = b_{2_0} \left(1 + \theta_{b_2}\right) \tag{6.4.2}$$

where θ_{b_1} and θ_{b_2} are zero in the nominal case.

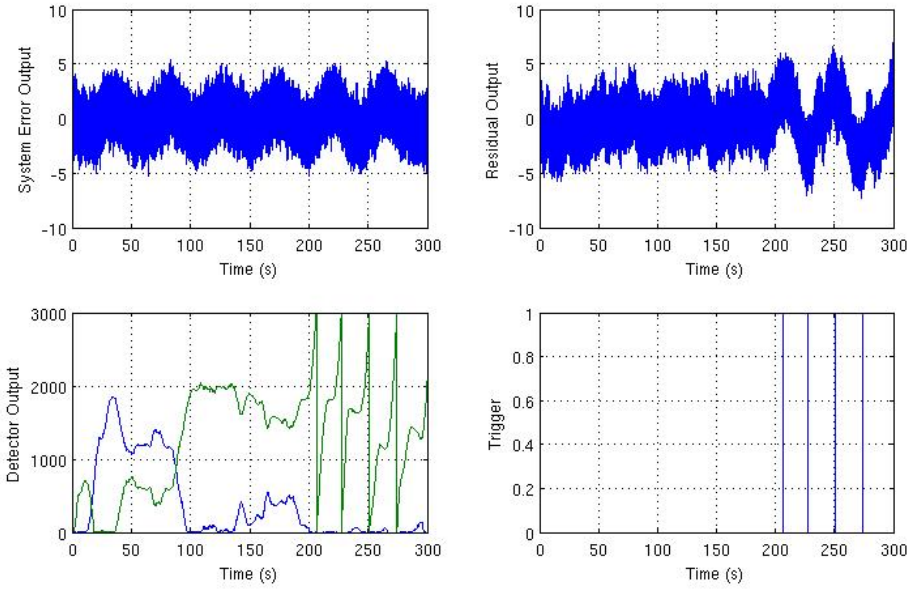

Figure 6.5: Simulation results with a large amount of noise in the correct ratio. Failure occurs at 186 seconds and is detected 20 seconds later. Note that each time the threshold is reached the detector is reset, and the trigger value is set to one for a single sample period.

Using an upper linear fractional transform, the system can be written as

$$\dot{x} = \begin{bmatrix} a \end{bmatrix} x + \begin{bmatrix} b_{1_0} & b_{2_0} \end{bmatrix} w + \begin{bmatrix} b_{1_0} & b_{2_0} \end{bmatrix} u \tag{6.4.3}$$

$$z = \begin{bmatrix} 0 \end{bmatrix} x + \begin{bmatrix} 1 \\ 1 \end{bmatrix} u \tag{6.4.4}$$

$$y = [1]x \tag{6.4.5}$$

with

$$w = \begin{bmatrix} \theta_{b_1} & 0 \\ 0 & \theta_{b_2} \end{bmatrix} z \tag{6.4.6}$$

Next, the disturbance model is introduced. Again, the model introduced at the start of this chapter will be used.

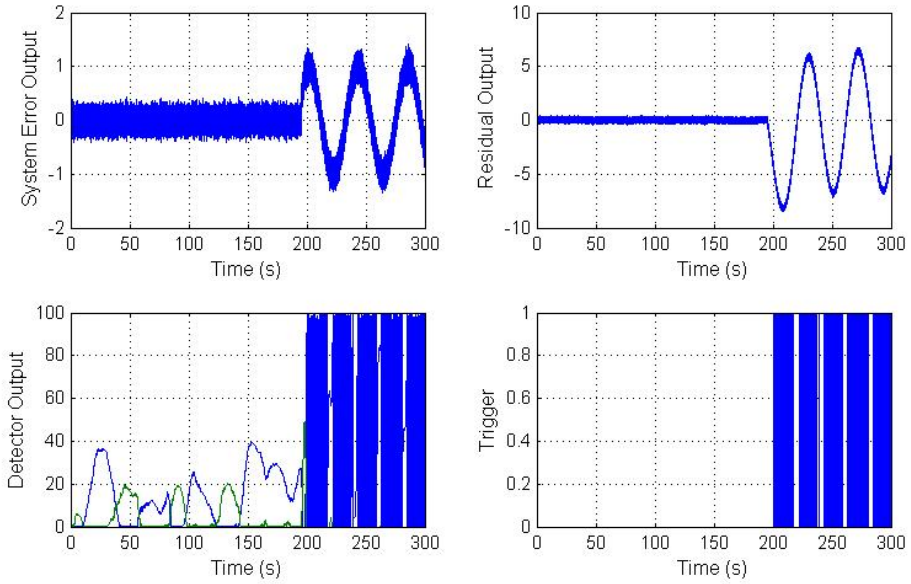

Figure 6.6: Simulation results with a moderate amount of noise in the correct ratio. Failure occurs at 195 seconds and is detected 5 seconds later. Note that each time the threshold is reached the detector is reset, and the trigger value is set to one for a single sample period.

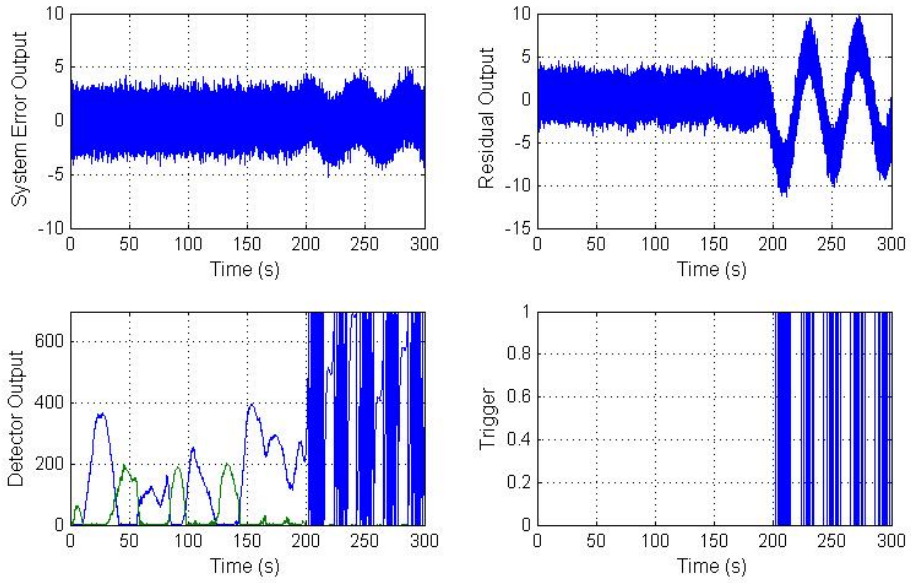

Figure 6.7: Simulation results with a large amount of noise in the correct ratio. Failure occurs at 186 seconds and is detected 7 seconds later. Note that each time the threshold is reached the detector is reset, and the trigger value is set to one for a single sample period.

Adding the disturbance model results in the following three port model:

$$\begin{bmatrix} \dot{x} \\ \dot{x_n} \end{bmatrix} = \begin{bmatrix} a & 0 \\ 0 & c \end{bmatrix} \begin{bmatrix} x \\ x_n \end{bmatrix} + \begin{bmatrix} b_{1_0} & b_{2_0} \\ 0 & 0 \end{bmatrix} w + \begin{bmatrix} b_{1_0} & b_{2_0} \\ 0 & 0 \end{bmatrix} u + \begin{bmatrix} k_P \\ -c \end{bmatrix} d \tag{6.4.7}$$

$$z = \begin{bmatrix} 0 & 0 \\ 0 & 0 \end{bmatrix} \begin{bmatrix} x \\ x_n \end{bmatrix} + \begin{bmatrix} 1 & 0 \\ 0 & 1 \end{bmatrix} u \tag{6.4.8}$$

$$y = \begin{bmatrix} 1 & k_m \end{bmatrix} \begin{bmatrix} x \\ x_n \end{bmatrix} \tag{6.4.9}$$

$$e = \begin{bmatrix} 1 & k_m \end{bmatrix} \begin{bmatrix} x \\ x_n \end{bmatrix} \tag{6.4.10}$$

The values for a, b_{1_0}, b_{2_0}, c, k_m, and k_p are now chosen as, -1, -5, -2, -10000, 0.01, 0.1 respectively.

Suppose that the plant suffers damage which results in

$$\Theta = \begin{bmatrix} -0.4 & 0 \\ 0 & -0.1 \end{bmatrix} \tag{6.4.11}$$

Therefore, there is a 40% reduction in b_1 and 10% reduction in b_2 control authority.

Now, using a similar process as in [81] and example 2 and a targeted detection time of $10s$, it is found that the optimal estimator bandwidth is $0.0464\ rad.s^{-1}$, while the optimal excitation frequency is $0.1489\ rad.s^{-1}$.

The simulation results are shown in Figure 6.6 for moderate levels of white noise and in Figure 6.7 for high levels of white noise. From this simulation it can be seen that no additional disturbance is visible in the nominal system, while a large residual is generated in the faulty system.

Note that the setup proves robust against white noise, while providing a substantial gain from error signal to residual output. It is also noted that since the detection time falls below the targeted minimum, the detector dynamics may have adversely affected performance. Therefore, the detection could be performed faster when a smaller t_d is used. This would however reduce detection performance for small faults.

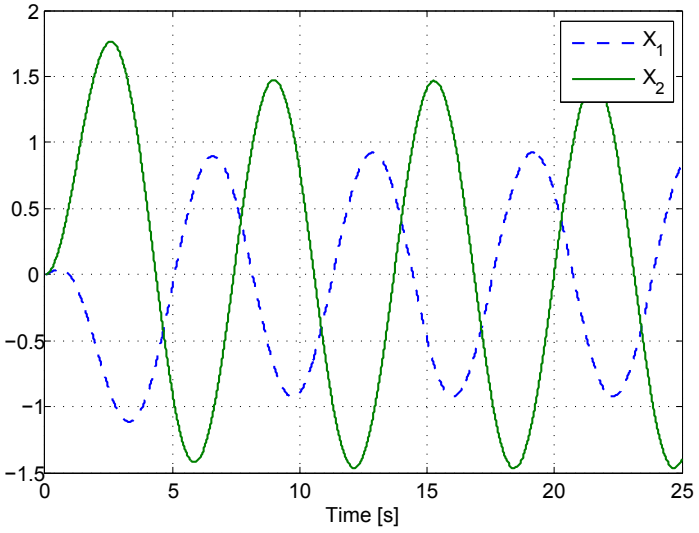

Figure 6.8: The output zeroing states. Note that both the system states are non-zero.

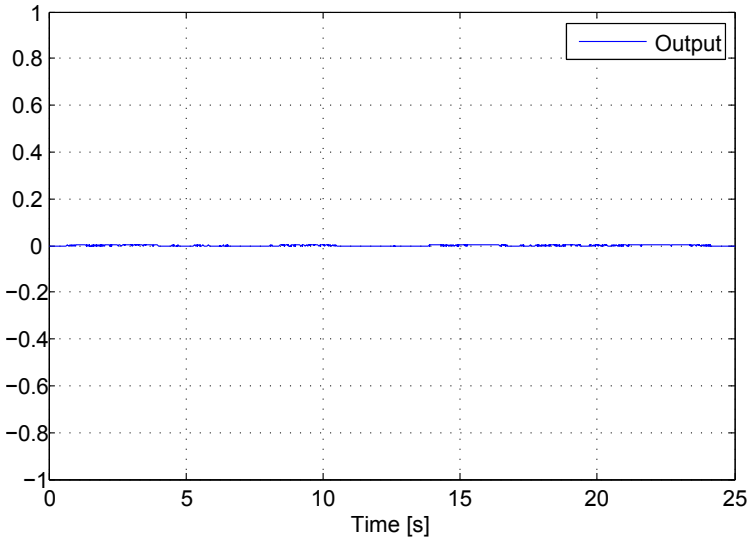

Figure 6.9: Although there is a non-zero input and non-zero states, the resulting output is zero.

6.5 Example 4: Zero-Disturbance AFD Using Output Cancellation

This simple example demonstrates using the output cancellation theory to design an appropriate input shaping filter.

A simple generic second order system can be represented by the following

state-space model:

$$\dot{x} = \begin{bmatrix} a_{11} & a_{12} \\ a_{21} & a_{22} \end{bmatrix} x + \begin{bmatrix} b_{11} & b_{12} \\ b_{21} & b_{22} \end{bmatrix} u \tag{6.5.1}$$

$$y = \begin{bmatrix} c_{11} & c_{12} \end{bmatrix} x + \begin{bmatrix} d_{11} & d_{12} \end{bmatrix} u \tag{6.5.2}$$

The values for a_{11}, a_{12}, a_{21}, a_{22}, b_{11}, b_{12}, b_{21}, b_{22}, c_{11}, c_{12}, d_{11}, d_{12} are chosen as 2, -1, 0, -1, 1, 0, 1, 1, 1, 2, 0.5, -1 respectively.

The system given above is proper with D of full row rank, therefore equation 3.2.10 applies. Now, assuming that the error output is equal to the system output, the input shaping filter is given by,

$$\begin{aligned} \dot{x}_\eta &= \begin{bmatrix} -2.4 & -1.8 \\ 0.4 & -0.2 \end{bmatrix} x_\eta + \begin{bmatrix} 1 & 0 \\ 1 & 1 \end{bmatrix} aH_0\eta_h \\ \eta &= \begin{bmatrix} -0.4 & -0.8 \\ 0.8 & 1.6 \end{bmatrix} x_\eta + \begin{bmatrix} 1 & 0 \\ 0 & 1 \end{bmatrix} aH_0\eta_h \end{aligned} \tag{6.5.3}$$

where H_0 is a base matrix for the kernel of the system matrix D_{eu}, given that $e = y$. Therefore, $H_0\eta_h \in \begin{bmatrix} 0.8944 & 0.4472 \end{bmatrix}^T$.

With reference to figure 6.8 and 6.9, it can be seen that the auxiliary input excites both system states, but has no impact on the system output. In the case of a faulty system the provided excitation is no longer contained within the kernel of D_{eu}, providing a residual signal for fault detection. This input shaping filter forms the basis of the MIMO output cancellation scheme.

From this point onwards, the design procedure to follow is identical to that of example 3, and is therefore not restated here.

6.6 Example 5: Worst-Case vs Average-Case Optimisation

This simple example demonstrates the difference between using a worst-case or average-case optimisation. It is specifically designed to illustrate the loss of detection performance when the latter is selected while no control input is present.

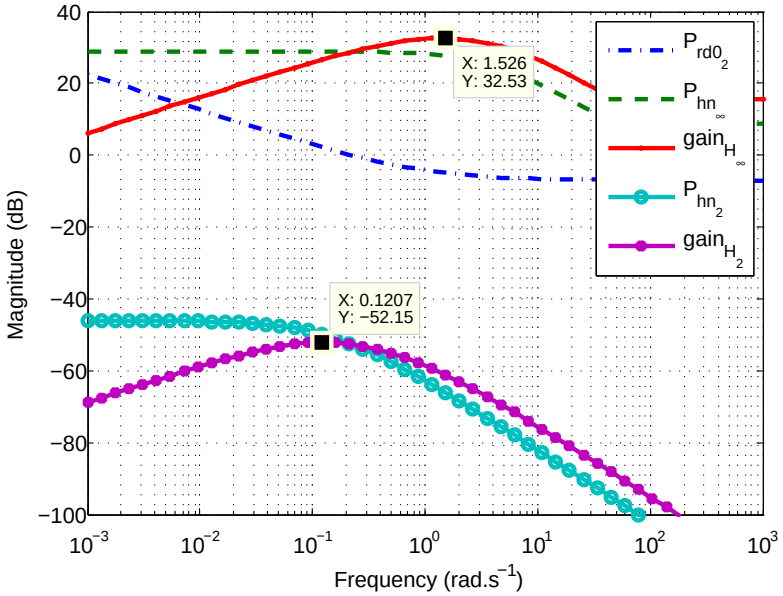

Figure 6.10: AFD performance as a function of estimator bandwidth. The optimisation is performed for the H_∞ as well H_2 optimisation criteria from the auxiliary input and control input respectively.

A simple first order MIMO system can be captured by the following state space representation:

$$\dot{x} = \begin{bmatrix} a \end{bmatrix} x + \begin{bmatrix} b_1 & b_2 \end{bmatrix} u \qquad y = \begin{bmatrix} 1 \end{bmatrix} x \tag{6.6.1}$$

Consider the following fault model:

$$b_1 = b_{1_0}\left(1 + \theta_{b_1}\right) \qquad b_2 = b_{2_0}\left(1 + \theta_{b_2}\right) \tag{6.6.2}$$

where θ_{b_1} and θ_{b_2} are zero in the nominal case.

Using an upper linear fractional transform, the system can be written as:

$$\dot{x} = \begin{bmatrix} a \end{bmatrix} x + \begin{bmatrix} b_{1_0} & b_{2_0} \end{bmatrix} w + \begin{bmatrix} b_{1_0} & b_{2_0} \end{bmatrix} u \tag{6.6.3}$$

$$z = \begin{bmatrix} 0 \end{bmatrix} x + \begin{bmatrix} 1 \\ 1 \end{bmatrix} u \tag{6.6.4}$$

$$y = [1]x \tag{6.6.5}$$

with

$$w = \begin{bmatrix} \theta_{b_1} & 0 \\ 0 & \theta_{b_2} \end{bmatrix} z \tag{6.6.6}$$

Next, the disturbance model is introduced. As before, the model introduced at the start of this chapter will be used.

Adding the disturbance model results in the following three port model:

$$\begin{bmatrix} \dot{x} \\ \dot{x_n} \end{bmatrix} = \begin{bmatrix} a & 0 \\ 0 & c \end{bmatrix} \begin{bmatrix} x \\ x_n \end{bmatrix} + \begin{bmatrix} b_{1_0} & b_{2_0} \\ 0 & 0 \end{bmatrix} w + \begin{bmatrix} b_{1_0} & b_{2_0} \\ 0 & 0 \end{bmatrix} u + \begin{bmatrix} k_P \\ -c \end{bmatrix} d \tag{6.6.7}$$

$$z = \begin{bmatrix} 0 & 0 \\ 0 & 0 \end{bmatrix} \begin{bmatrix} x \\ x_n \end{bmatrix} + \begin{bmatrix} 1 & 0 \\ 0 & 1 \end{bmatrix} u \tag{6.6.8}$$

$$y = \begin{bmatrix} 1 & k_m \end{bmatrix} \begin{bmatrix} x \\ x_n \end{bmatrix} \tag{6.6.9}$$

$$e = \begin{bmatrix} 1 & k_m \end{bmatrix} \begin{bmatrix} x \\ x_n \end{bmatrix} \tag{6.6.10}$$

The parameters given above are now chosen as follows: $a = -50$, $b_{1_0} = -5$, $b_{2_0} = -2$, $c = -100000$, $k_m = 0.002$, and $k_p = 0.5$.

Assume that the plant is typically controlled by relatively low bandwidth control inputs. The control power may be modelled as a simple low-pass filter given by

$$H_u = \begin{bmatrix} a_u^3 / (s + a_u)^3 \\ a_u^3 / (s + a_u)^3 \end{bmatrix} \tag{6.6.11}$$

with $a_u = 0.1$.

The plant fault dynamics are excited by an auxiliary signal injected into the system control null-space

$$\eta = aH_{\eta_0}\eta_h = 0.1 \begin{bmatrix} -0.3714 \\ 0.9285 \end{bmatrix} \eta_h \tag{6.6.12}$$

Now, suppose that the plant suffers damage which results in

$$\Theta = \begin{bmatrix} -0.75 & 0 \\ 0 & 0 \end{bmatrix} \tag{6.6.13}$$

Therefore, there is a 75% reduction in the b_1 control authority.

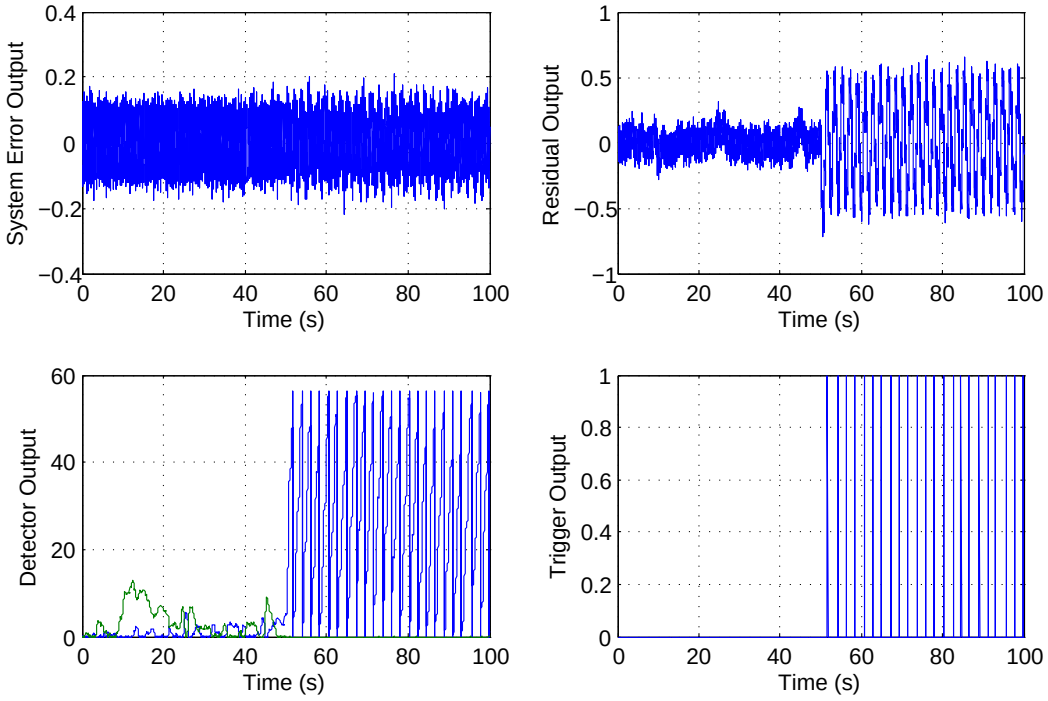

Figure 6.11: Simulation results for the H_∞ case with a large amount of noise in the correct ratio. Failure occurs at 186 seconds and is detected 1.7 seconds later. Note that each time the threshold is reached the detector is reset, and the trigger value is set to one for a single sample period.

Using the equations derived in this work, the AFD performance as a function of the estimator bandwidth can be determined. The optimisation is performed for both the worst-case (H_∞ optimisation), as well as the average-case (H_2 optimisation). The results are shown in figure 6.10. From this figure it is easy to determine the optimal estimator bandwidth and gain as

$$\omega_{L_{opt}} = 1.526 \text{ rad.s}^{-1} \qquad L_{opt} = 48.474 \tag{6.6.14}$$

for the H_∞ optimisation, and

$$\omega_{L_{opt}} = 0.1207 \text{ rad.s}^{-1} \qquad L_{opt} = 49.879 \tag{6.6.15}$$

for the H_2 optimisation.

With L_{opt} known, $P_{h\eta}(L_{opt})$ can be can be determined, as

$$\omega_{\eta_{opt}} = 3.3419 \text{ rad.s}^{-1} \qquad \eta_{max} = 2.389 \tag{6.6.16}$$

for the H_∞ optimisation, and

$$\omega_{\eta_{opt}} = 2.4683 \text{ rad.s}^{-1} \qquad \eta_{max} = 2.748 \tag{6.6.17}$$

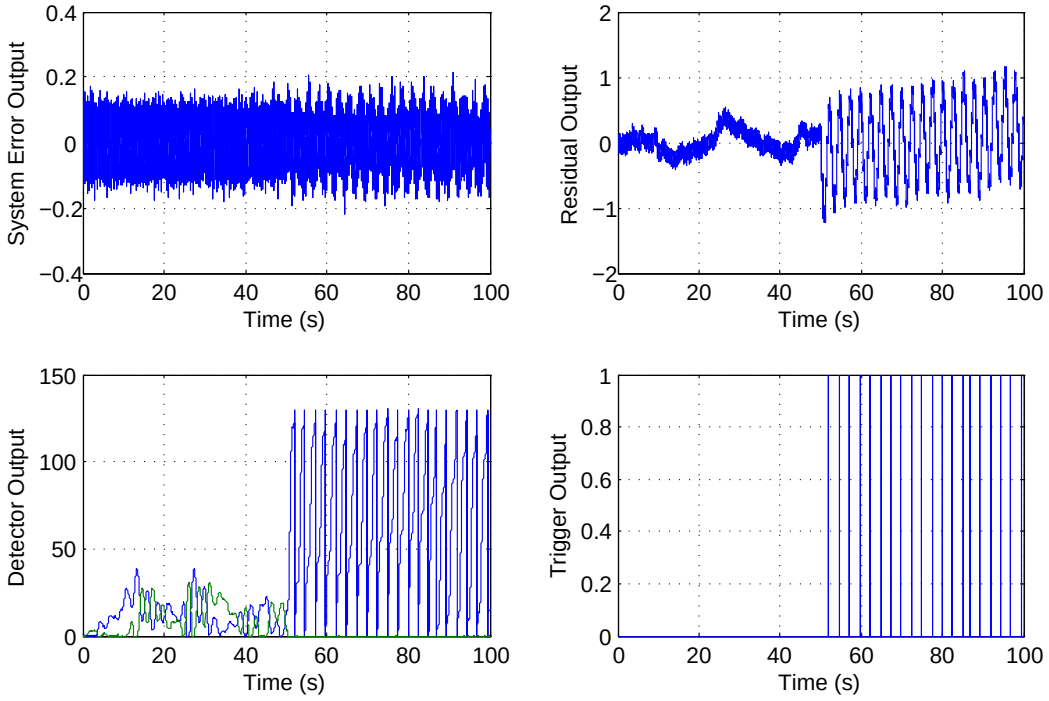

Figure 6.12: Simulation results for the H_2 with a large amount of noise in the correct ratio. Failure occurs at 50 seconds and is detected 2 seconds later. Note that each time the threshold is reached the detector is reset, and the trigger value is set to one for a single sample period.

for the H_2 optimisation, where the maximum excitation induced disturbance is taken as 0.1.

It is now possible to determine a reasonable trip threshold for the detector. From the calculations above, the noise power as a function of the estimator bandwidth is known. For simplicity the detector threshold (h_T) is simply selected as 100 times the noise power prior to a failure, and is given by

$$P_{rd_0} = 0.5647 \qquad h_T = 56.47 \tag{6.6.18}$$

for the H_∞ optimisation, and

$$P_{rd_0} = 1.301 \qquad h_T = 130.1 \tag{6.6.19}$$

for the H_2 optimisation.

These results are used to set up a simulation of both optimal AFD system. The simulation results for the worst-case as well as for the average-case optimisations are shown in Figure 6.11 and Figure 6.12 respectively. Note

that in both cases it can be seen that the H_2 optimisation results in a small reduction in the worst-case detection performance when compared to the H_∞ optimisation.

6.7 Example 6: Basic SISO Closed Loop Application

This example will demonstrate the application of the proposed AFD framework to a simple closed-loop SISO system using the technique proposed in section 5.4. It is shown that the open-loop framework can easily be adapted for use in closed-loop systems. The open-loop case is first considered, and then a simple control loop is closed around the system.

In general, a first order linear differential equation is given by the following equation:

$$\dot{x} = ax + bu \tag{6.7.1}$$

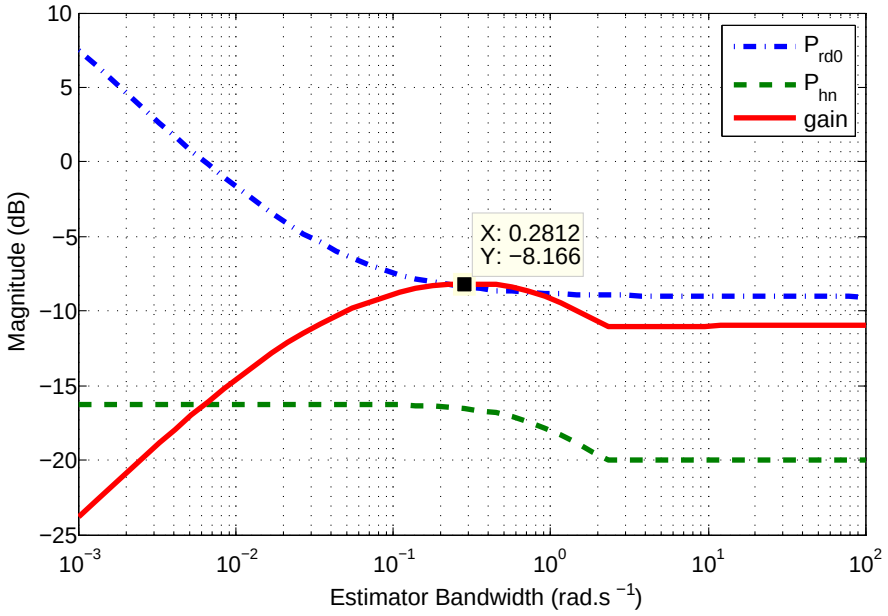

Figure 6.13: AFD performance as a function of estimator bandwidth. $\omega_{L_{opt}}$ is given by peak of $\frac{\|P_{h\eta}(\Theta,L)\|_\infty}{\|P_{rd_0}(L)\|_2}$.

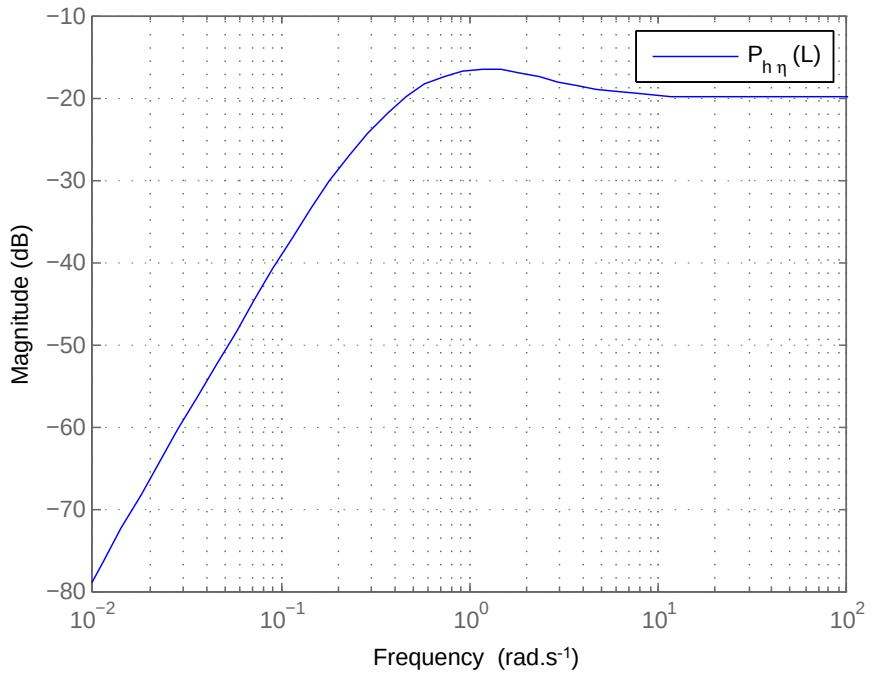

Figure 6.14: Magnitude response of $P_{h\eta}(L_{opt})$. The optimal excitation frequency ($\omega_{\eta_{opt}}$) is given by the peak of the magnitude response.

This can be represented by the following state space representation.

$$\dot{x} = \begin{bmatrix} a \end{bmatrix} x + \begin{bmatrix} b \end{bmatrix} u \tag{6.7.2}$$

$$y = \begin{bmatrix} 1 \end{bmatrix} x \tag{6.7.3}$$

Consider the following fault model:

$$a = a_0 \left(1 + \theta_a\right) \tag{6.7.4}$$

$$b = b_0 \left(1 + \theta_b\right) \tag{6.7.5}$$

where θ_a and θ_b are zero in the nominal case.

Using an upper linear fractional transform, the system can be written as

$$\dot{x} = \begin{bmatrix} a_0 \end{bmatrix} x + \begin{bmatrix} a_0 & b_0 \end{bmatrix} w + \begin{bmatrix} b_0 \end{bmatrix} u \tag{6.7.6}$$

$$z = \begin{bmatrix} 1 \\ 0 \end{bmatrix} x + \begin{bmatrix} 0 \\ 1 \end{bmatrix} u \tag{6.7.7}$$

$$y = [1]x \tag{6.7.8}$$

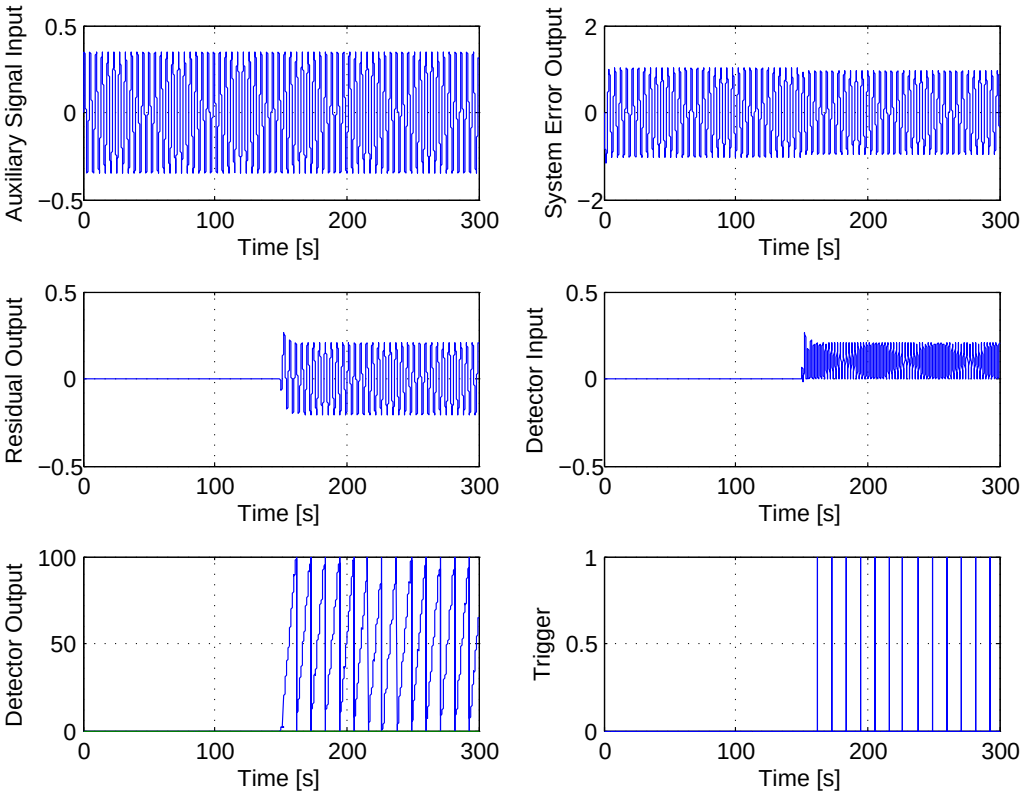

Figure 6.15: Simulation results of the open-loop system without any added noise. Failure occurs at 150 seconds and is detected 12 seconds later. Note that each time the threshold is reached the detector is reset, and the trigger value is set to one for a single sample period.

with

$$w = \begin{bmatrix} \theta_a & 0 \\ 0 & \theta_b \end{bmatrix} z \tag{6.7.9}$$

Next, the disturbance model is introduced. In this example, the model introduced at the start of this chapter will be used.

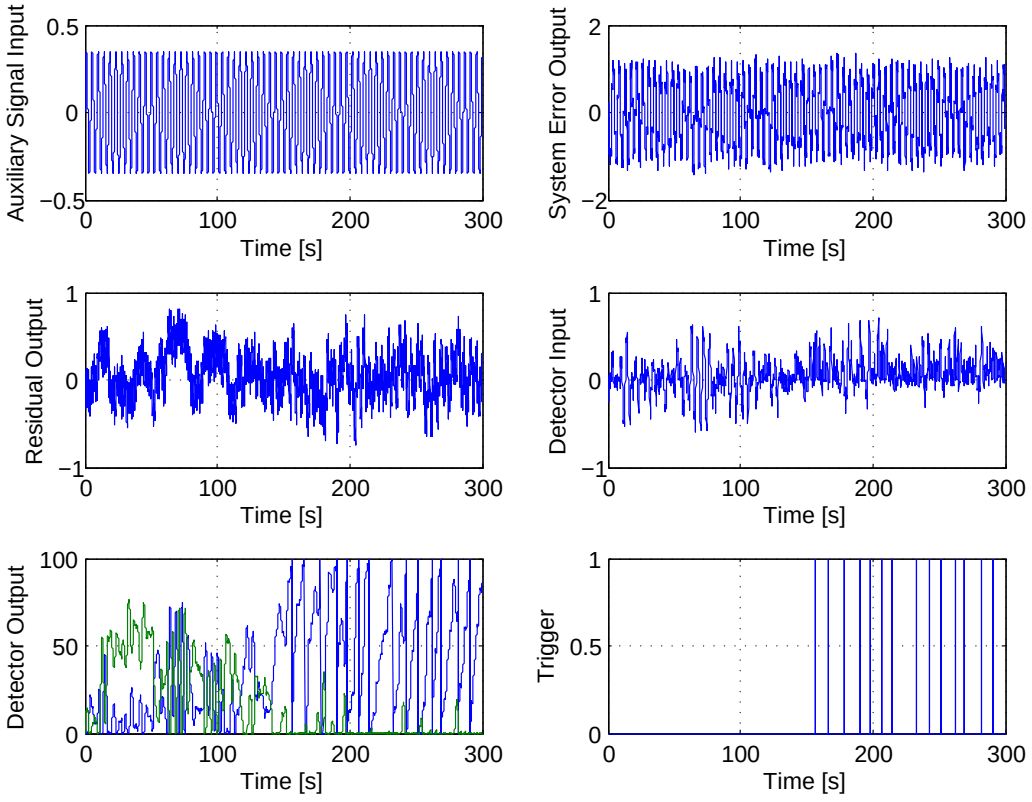

Figure 6.16: Simulation results of the open-loop system with added noise. Failure occurs at 150 seconds and is detected 8 seconds later. Note that each time the threshold is reached the detector is reset, and the trigger value is set to one for a single sample period.

Adding the disturbance model results in the following three port model:

$$\begin{bmatrix} \dot{x} \\ \dot{x_n} \end{bmatrix} = \begin{bmatrix} a_0 & 0 \\ 0 & c \end{bmatrix} \begin{bmatrix} x \\ x_n \end{bmatrix} + \begin{bmatrix} a_0 & b_0 \\ 0 & 0 \end{bmatrix} w + \begin{bmatrix} b \\ 0 \end{bmatrix} u + \begin{bmatrix} k_P \\ -c \end{bmatrix} d \tag{6.7.10}$$

$$z = \begin{bmatrix} 1 & 0 \\ 0 & 0 \end{bmatrix} \begin{bmatrix} x \\ x_n \end{bmatrix} + \begin{bmatrix} 0 \\ 1 \end{bmatrix} u \tag{6.7.11}$$

$$y = \begin{bmatrix} 1 & k_m \end{bmatrix} \begin{bmatrix} x \\ x_n \end{bmatrix} \tag{6.7.12}$$

$$e = \begin{bmatrix} 1 & k_m \end{bmatrix} \begin{bmatrix} x \\ x_n \end{bmatrix} \tag{6.7.13}$$

The values for a_0, b_0, c, k_m and k_p are now chosen as -1, -5, -10000,

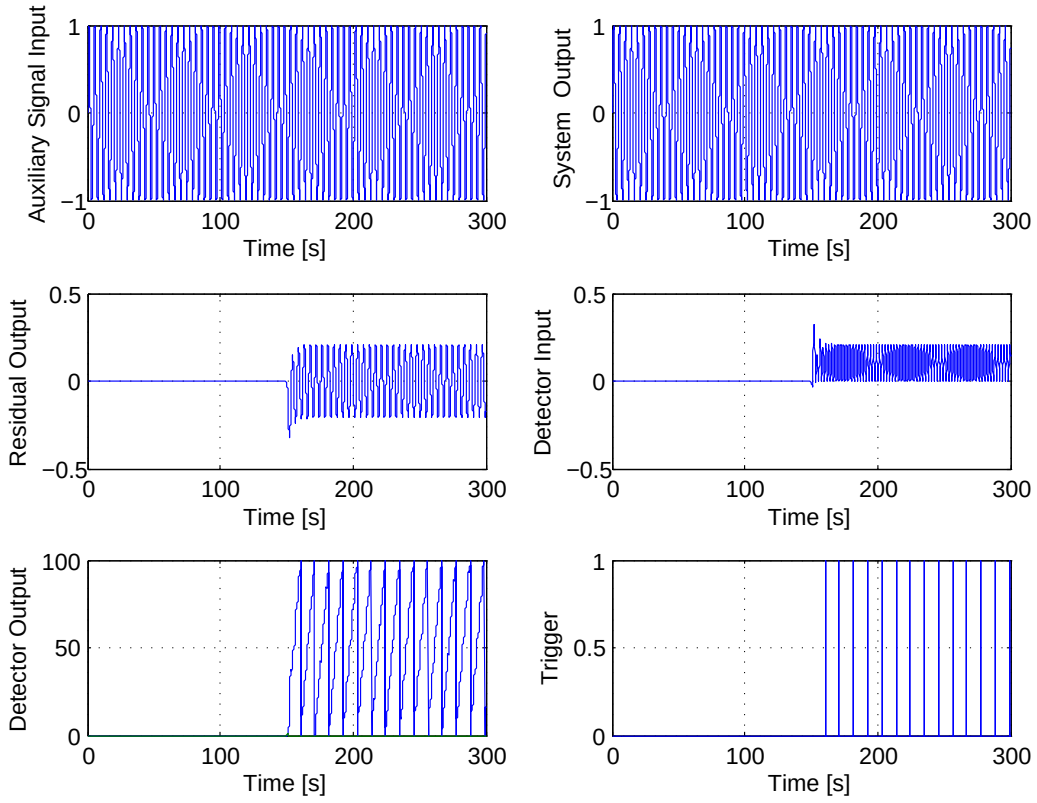

Figure 6.17: Simulation results of the closed-loop system without any added noise. Failure occurs at 150 seconds and is detected 11 seconds later. Note that each time the threshold is reached the detector is reset, and the trigger value is set to one for a single sample period.

0.005 and 0.1 respectively.

Suppose that the plant suffers damage which results in

$$\Theta = \begin{bmatrix} -0.4 & 0 \\ 0 & -0.1 \end{bmatrix} \tag{6.7.14}$$

Therefore, there is a 40% reduction in damping and a 10% reduction in control authority.

Now, using the equations derived in this work, a frequency plot can easily be produced showing the AFD performance as a function of the estimator bandwidth. The results are shown in figure 6.13. From this figure it is easy to determine the optimal estimator bandwidth as

$$\omega_{L_{opt}} = 0.2812 \text{ rad.s}^{-1} \tag{6.7.15}$$

when a targeted detection time of $1s$ is used.

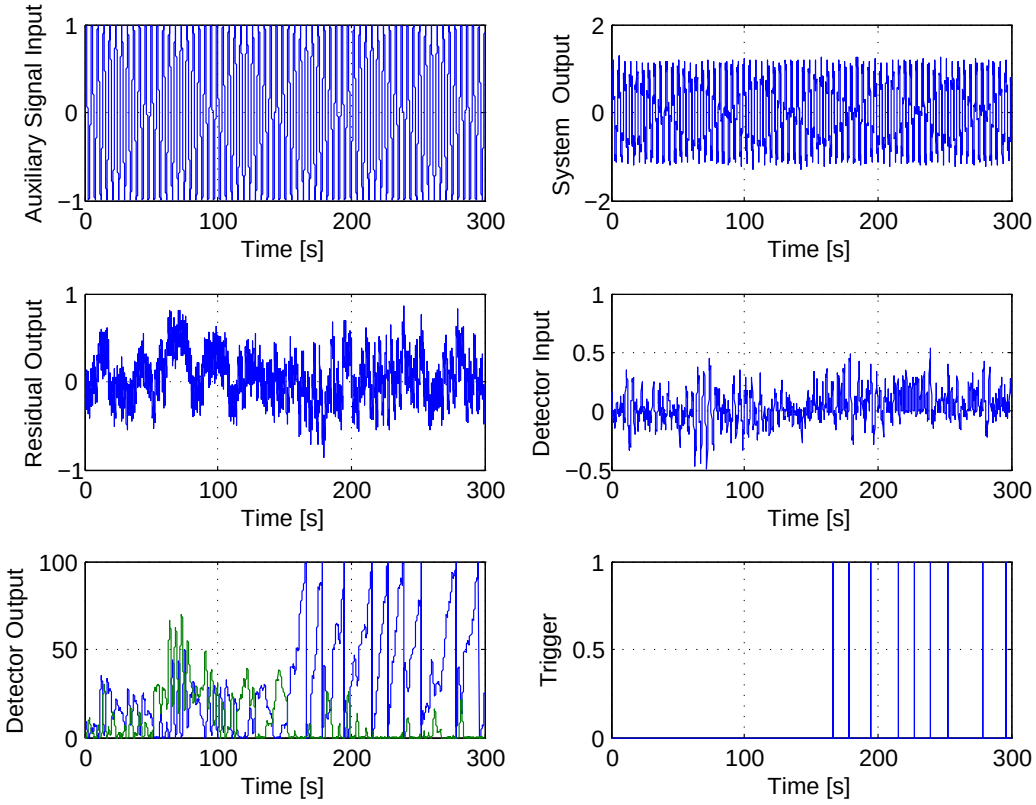

Figure 6.18: Simulation results of the closed-loop system with added noise. Failure occurs at 150 seconds and is detected 16 seconds later. Note that each time the threshold is reached the detector is reset, and the trigger value is set to one for a single sample period.

Finally, with $\omega_{L_{opt}}$ known, a plot of $P_{h\eta}(L_{opt})$ can be produced. The result is shown in figure 6.14. From the figure the optimal excitation frequency is

$$\omega_{\eta_{opt}} = 1.3518 \text{ rad.s}^{-1} \tag{6.7.16}$$

These results are used to set up a simulation of the optimal open-loop AFD system. The simulation results are shown in Figure 6.15 without added white noise and in Figure 6.16 with white noise added.

Now, a full state feedback controller is added by applying the following control law,

$$u = -kx + k_i x_i \tag{6.7.17}$$

where the system state vector is augmented with an integrator state x_i.

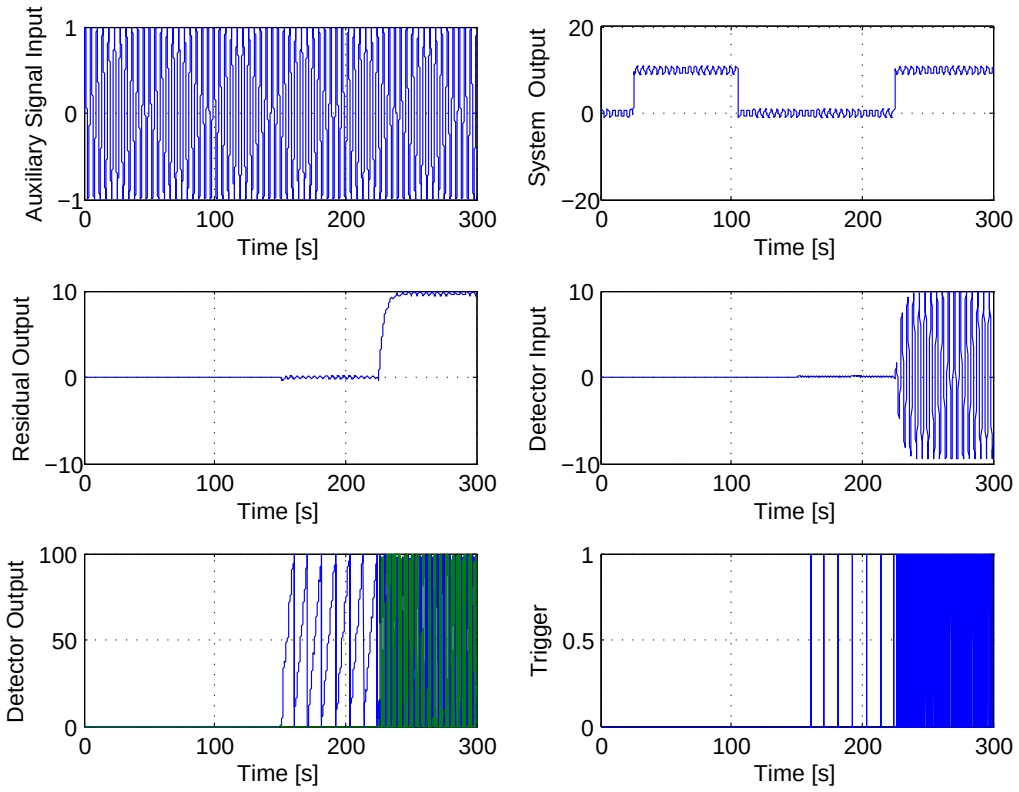

Figure 6.19: Simulation results of the closed-loop system without any added noise, while a reference input is provided. Failure occurs at 150 seconds and is detected 11 seconds later. Note that each time the threshold is reached the detector is reset, and the trigger value is set to one for a single sample period.

Therefore, the closed-loop system is given by

$$\begin{bmatrix} \dot{x} \\ \dot{x}_i \end{bmatrix} = \begin{bmatrix} a - bk & bk_i \\ -c & 0 \end{bmatrix} \begin{bmatrix} x \\ x_i \end{bmatrix} + \begin{bmatrix} 0 \\ 1 \end{bmatrix} r \tag{6.7.18}$$

Now, design the gain $\hat{K} = [k \;\; k_i]$ so that the closed loop poles of equation (6.7.18) are at $[-5 \pm 5j]$. Using standard pole placement techniques, the associated gain is calculated as

$$\hat{K} = [-1.8 \;\; 10] \tag{6.7.19}$$

Now, from equation 5.4.3

$$\Delta_{max} = \frac{|P(0)_{e\eta_{cl}}\eta_{cl}|}{|P(\Theta_1)_{e\eta_{ol}}\eta_{ol}|} = \frac{1}{0.96} = 1.04 \tag{6.7.20}$$

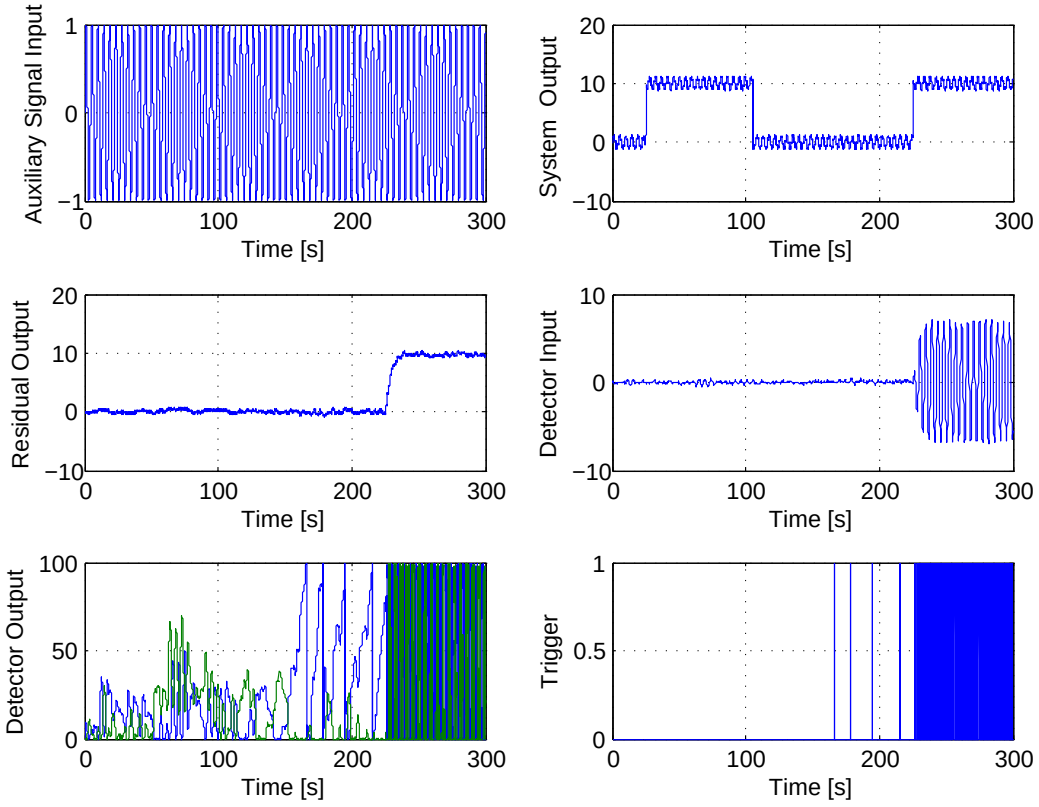

Figure 6.20: Simulation results of the closed-loop system with added noise, while a reference input is provided. Failure occurs at 150 seconds and is detected 16 seconds later. Note that each time the threshold is reached the detector is reset, and the trigger value is set to one for a single sample period.

it can be seen that a small 4% increase in detection signal is expected.

These results are used to repeat the previously performed simulation for the closed-loop AFD system. The simulation results are shown in Figure 6.17 without added white noise and in Figure 6.18 with white noise added.

When comparing Figures 6.15 and 6.17 the following is noted:

- The closed-loop detection time has improved slightly from the open-loop case.
- This slight increase in performance is due to the slight increase in the post-failure excitation signal due to the controller rejecting the system fault.

Finally, the closed-loop is repeated while providing a reference input to

the controller. The simulation results are shown in Figure 6.19 without added white noise and in Figure 6.20 with white noise added.

From Figure 6.19 and 6.20 it is clearly visible the the system is still effectively tracing the reference input. Furthermore, it can be clearly seen that the fault is detected nearly instantly as soon as a control input is provided.

6.8 Summary

In this chapter a number of examples are used to demonstrate the various aspects of the proposed AFD framework. The following was demonstrated:

- Example 1: This is a open-loop SISO example without considering the effect of the detector dynamics. The results show that doing this causes the result to be unreasonably inaccurate, or that the optimisation often degrades to the trivial case.

- Example 2: This is a open-loop SISO example using the same model as example 1. In this case the detector dynamics are also considered, avoiding the trivial solution and resulting in a far more realistic optimisation solution. It further shows that the targeted detection time places a soft lower bound on the optimisation result.

- Example 3: In the example the application of the zero-disturbance AFD framework using the input cancellation technique is demonstrated. It is shown how to design the input shaping filter, thereby injecting the excitation into the system null-space. It is shown that no disturbance in the nominal system is present, while still providing fast post-failure actuator fault detection.

- Example 4: This example demonstrates the application of the zero-disturbance AFD framework using the output cancellation technique. The example focuses on the design of the required input shaping filter.

- Example 5: In this example the worst-case versus the average-case optimisation is demonstrated. The same example is performed for both optimisation goals, and the performance differences illustrated. It is found

that when no control input is present, a small performance reduction is visible when optimising for the average-case.

- Example 6: This is a closed-loop SISO example using the same model as example 1 and 2. This example demonstrates the application of the open-loop AFD framework to closed loop systems. It is shown how to adapt the open-loop solution to the closed-loop system. Furthermore, it is demonstrated that effective AFD can be achieved in closed-loop systems.

Part III

Practical Application: The Modular UAV

Chapter 7

Active Fault Detection for a Small Unmanned Aerial Vehicle

In this chapter, the theory developed in the previous chapters is applied to a larger, more realistic problem. As a case study an active fault detection system is developed for a small unmanned aerial vehicle. It is, however, important to bear in mind that this case study is still treated in an abstract manner. Several assumptions will be made in order to keep the problem informative and concise. However, these assumptions may not necessarily be practical. It is for this reason that the physical parameters and units are not discussed.

Before developing the AFD system, the vehicle dynamics are briefly introduced. The AFD system is then first designed around a simplified decoupled dynamics model, and then redesigned for the full lateral dynamics model.

7.1 Architecture for Active Fault Tolerant Control of an UAV

In this section, a simple yet flexible control system architecture is proposed. This architectural design is done at an abstract level, and therefore the developed architecture is not aircraft or implementation specific.

This section starts by introducing a number of important design considerations which are to be addressed by the proposed architecture. Following this, the controller architecture is discussed in abstract terms. It is important

to note that this section is included only to provide some context, and that the controller architecture is not a focus of this research. Furthermore, if the reader is well versed in the topics discussed here, this section may be skipped.

7.1.1 Background

During the early days of aviation, aircraft required constant input from the pilot in order to maintain stability. As the range of aircraft increased over the years, pilots started to suffer from severe fatigue. Early autopilots were therefore developed in order to lighten the workload on pilots during longer flights. The first of these early autopilots was demonstrated during the 1914 Paris aircraft safety competition [82]. This simple mechanical autopilot was able to keep the aircraft flying straight and level without constant pilot input, therefore significantly reducing the pilot's workload.

With the advent of small yet powerful digital computers, autopilot technology started to progress rapidly. Today we have autopilot systems which are able to take off, navigate an assigned course, and then land at the end of the flight.

There s however a difference between a human pilot and a classical flight control system. When a survivable fault or failure occurs on a piloted aircraft, the experienced pilot requires only a few moments in order to adjust his or her inputs to the aircraft's now reduced capabilities. On the other hand, a classical autopilot makes no adjustments to the control law it is using. This rigid approach can lead to severe performance reductions, or even the complete loss of the vehicle.

One way to increase the reliability of a control system is by employing Active Fault Tolerant Control (AFTC). The basic idea is to develop an autopilot which is able to handle failures in a similar or superior manner to the human pilot. This type of autopilot is considerably more complex than a standard one, as it requires a number of complex subsystems to work together in a coherent manner. These subsystems include: a robust, yet fast, fault detection and diagnosis (FDD) algorithm; a reconfigurable inner-loop controller; a reconfigurable guidance system; as well as a reconfigurable navigation system.

AFTC involves the control system responding to faults by actively altering

the control law. To be able to do this efficiently, faults must be detected in a reliable and timely manner. Fault detection schemes can be classified as either passive or active fault detection. For a brief discussion of many AFTC related topics please refer to [34] and [83]. AFTC has been applied to a number of practical problems, for example, a detailed study on applying AFTC to small unmanned aerial vehicles was conducted in [84].

7.1.2 Important Design Considerations

The following important considerations must be suitably addressed by the controller architecture:

- The design must be flexible enough to deal with conventional as well as unconventional flight controllers.
- The ability to accommodate unconventional controllers should not substantially complicate the implementation of conventional controllers.
- It is advantageous to allow for a step-wise or partial implementation. For example, all subsystems up to the level of the inner-loop controller is reconfigurable, while guidance and navigation is not.

7.1.3 Conceptual System Overview

Figure 7.1 provides a high level overview of the proposed architecture.

With reference to this figure, the AFTC system is composed of a supervisor, a human operator interface, and four controller nodes. The controller nodes include a reconfigurable navigation system; a reconfigurable guidance system; a reconfigurable inner-loop controller; and finally, a virtual aircraft.

This architecture provides each controller node with two communication paths. These are:

- Simple direct communication with the nodes directly adjacent to it in the controller loop. This is equivalent to what is found in most non-reconfigurable flight control systems.

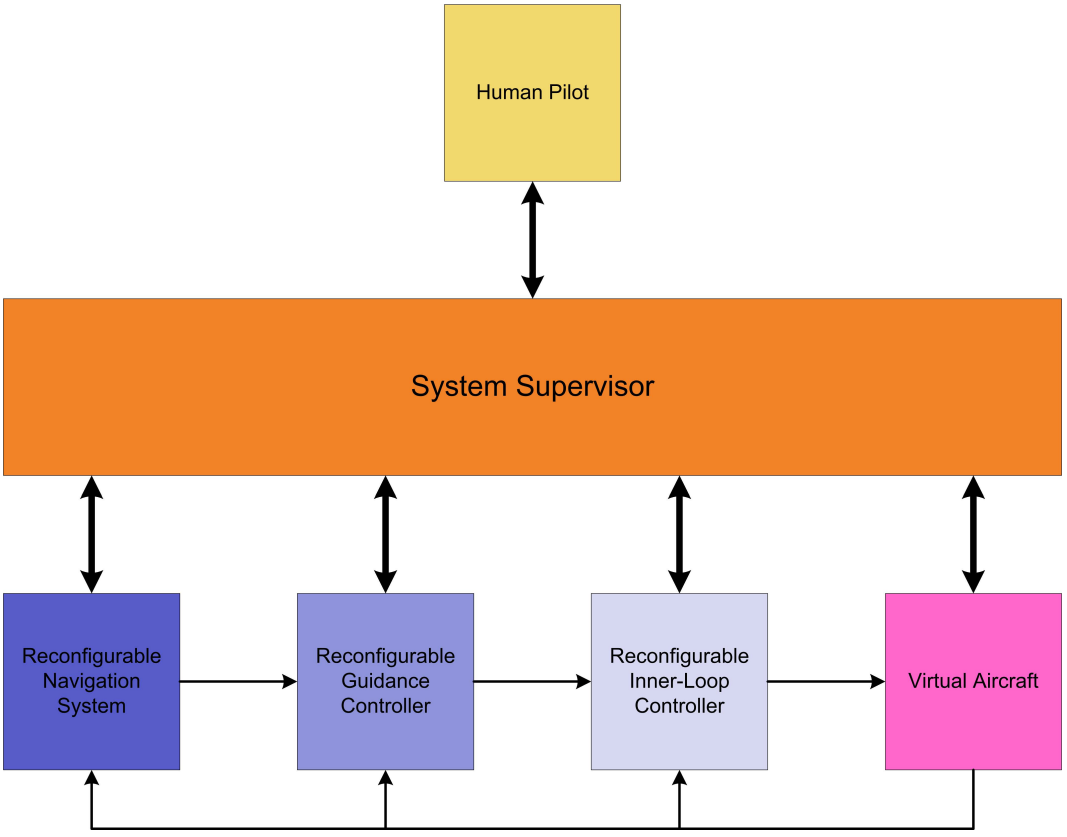

Figure 7.1: System Overview

- Advanced communication via a supervisor request system. This allows for signal injection at any point in the control loop. This route is used to perform all reconfiguration management.

7.1.4 Supervisor

The supervisor is primarily responsible for managing the AFTC system. Some of this subsystem's responsibilities include:

- Making system-wide decisions.
- Providing a system for control and diagnostic signal injection.
- Managing the post fault reconfiguration process.
- Monitoring the health of the various subsystems.
- Providing the operator with easily understandable information.

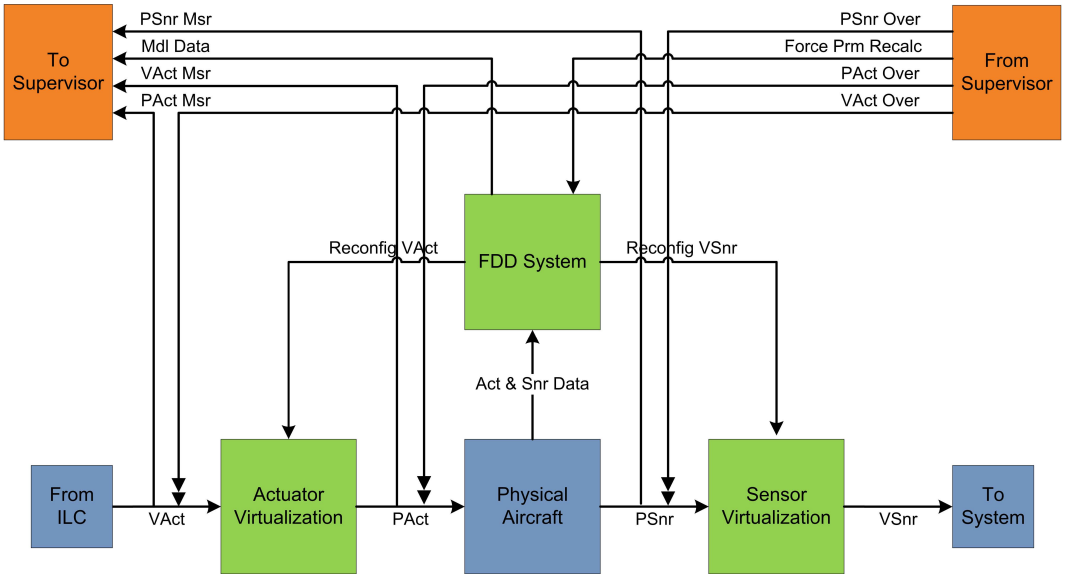

Figure 7.2: Virtual Aircraft

Finally, it is important to note that the supervisor is the only node with the ability to monitor as well as override all major signals and parameters within the system.

7.1.5 Virtual Aircraft

The virtual aircraft encapsulates the physical aircraft under control of the AFT control system. The primary purpose of this block is to provide the best possible, idealised aircraft to the rest of the system. It receives virtual actuator commands from the inner loop controller and provides the rest of the system with virtual sensor readings (aircraft state estimates).

With reference to figure 7.2, this subsystem consists out of four blocks. They are: an FDD system; an actuator virtualisation block; a sensor virtualisation block; and the physical aircraft. Each of these are now discussed in more detail.

7.1.5.1 Fault Detection and Diagnosis System

The FDD system is responsible for detecting and diagnosing aircraft failures. These failures may include control surface, structural damage, or sensor faults. When a fault occurs, the FDD system performs the following functions:

- Detecting that a fault has occurred in the minimum possible time. This is the primary focus of the research presented in this dissertation.
- Calculation of a new physical aircraft model.
- Triggering the reconfiguration of the virtual aircraft.
- Calculation of a new virtual aircraft model if the pre-fault virtual aircraft model could not be maintained.
- Informing the supervisor about the fault, as well as providing the new virtual aircraft model if applicable.

7.1.5.2 Actuator Virtualisation

This block is responsible for mapping the virtual actuator commands to suitable physical commands. When an actuator fault occurs, this block is informed about it by the FDD system, and provided with new physical aircraft data. The mapping is then recalculated in order to provide the best possible virtual aircraft model.

7.1.5.3 Sensor Virtualisation

This block is responsible for producing the vehicle state estimates. When a sensor fault occurs, this block is responsible for managing this in an effective manner[1].

7.1.5.4 Physical Aircraft

This block represents the actual aircraft or aircraft model under control. This block receives physical actuator commands from the actuator virtualisation block and provides the sensor virtualisation block with raw sensor readings.

[1] As it is in general far easier to provide hardware sensor redundancy, this is currently not a research priority.

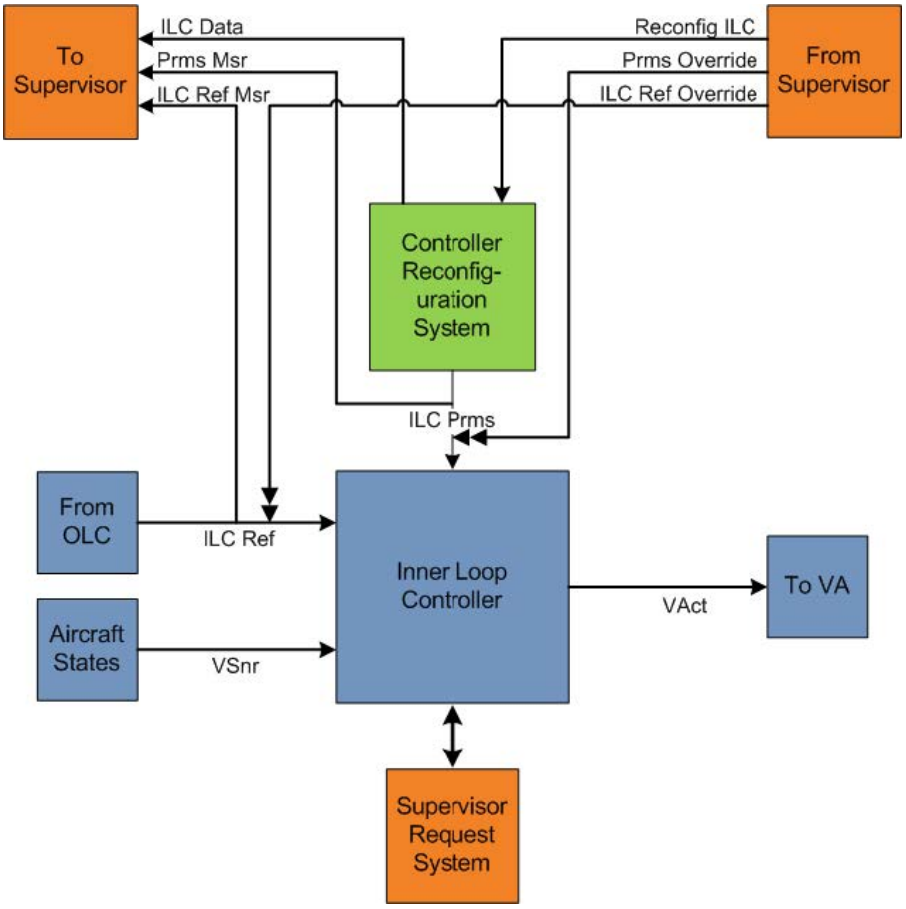

Figure 7.3: Reconfigurable Inner-Loop Controller

7.1.6 Reconfigurable Control System

The reconfigurable inner-loop controller is responsible for generating the virtual actuator commands from reference commands received from the guidance controller. Figure 7.4 depicts this system schematically.

With reference to figure 7.3, this system consists of two subsystems: an inner-loop controller reconfiguration system; and a parameterised inner-loop controller.

7.1.7 Reconfigurable Guidance System

The reconfigurable guidance system or outer-loop controller is responsible for providing the control system with achievable reference commands from reference commands provided by the navigation system. Figure 7.4 depicts this system schematically.

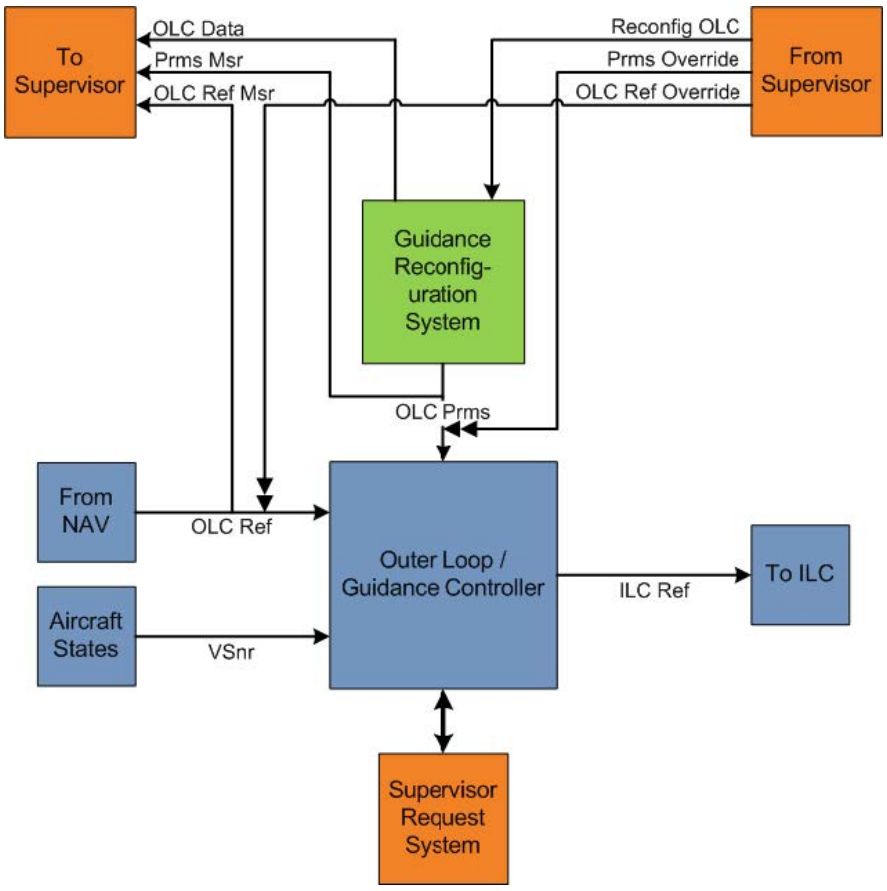

Figure 7.4: Reconfigurable Outer-Loop or Guidance Controller

With reference to figure 7.4, this system consists out of two subsystems: an outer-loop controller reconfiguration system; and a parameterised outer-loop controller.

7.1.8 Reconfigurable Navigation System

The reconfigurable navigation system is responsible for providing the guidance system with appropriate reference commands in order to follow the desired flight plan. In other words, the navigation system provides the guidance system with, for example, the required altitude and heading. Figure 7.5 depicts this system schematically.

With reference to figure 7.5, this system consists out of two subsystems: a navigation reconfiguration system; and a parameterised navigation system.

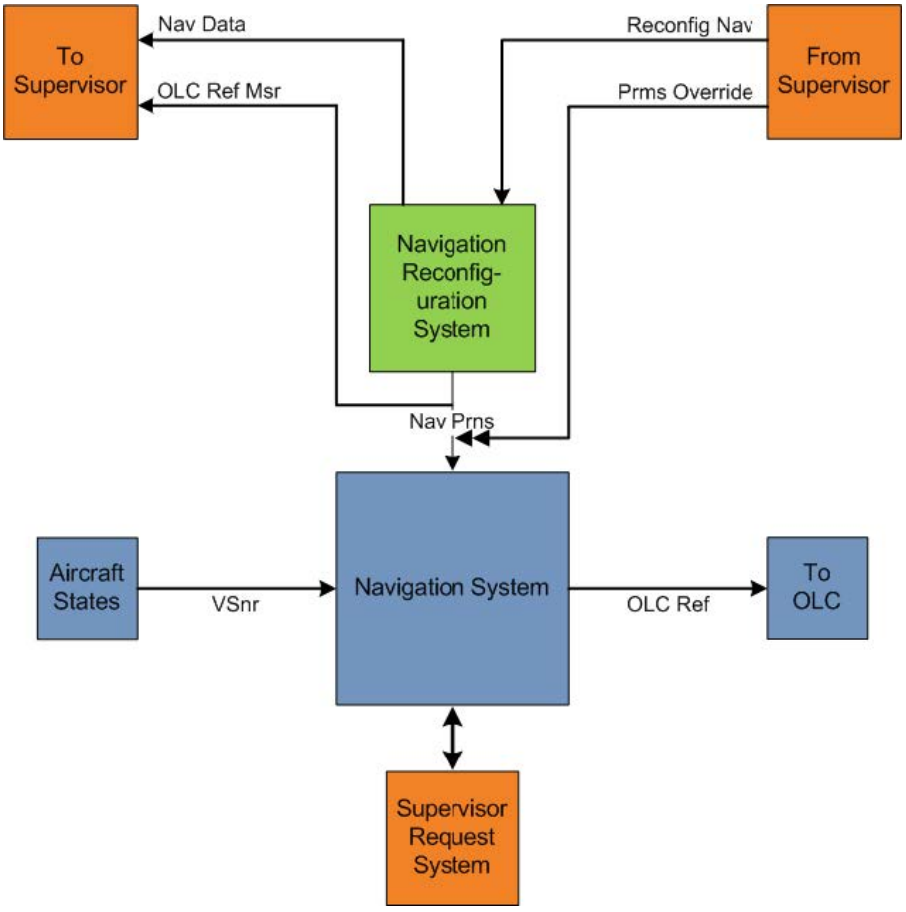

Figure 7.5: Reconfigurable Navigation System

7.2 Vehicle and Operational Definitions

In this section the vehicle parameters as well as the vehicle operating conditions are defined.

7.2.1 Operating Condition

The vehicle operating condition is given by:

$$\rho = 1.2 \tag{7.2.1}$$

where ρ is the air density,

$$\bar{V_0} = 22 \tag{7.2.2}$$

is the vehicle trim velocity, and

$$q = \frac{1}{2}\rho \bar{V_0}^2 \tag{7.2.3}$$

is the dynamic pressure.

7.2.2 Vehicle Actuator Definition

The Modular UAV has a large number of independent aerodynamic actuators. These are defined as follows:

- One aileron is mounted on each of the wings. Define the left and right aileron deflection angles, δ_{A_l} and δ_{A_r} respectively, such that a positive deflection induces a negative rolling moment.
- One flap is mounted on each of the wings. Define the left and right flap deflection angles, δ_{F_l} and δ_{F_r} respectively, such that a positive deflection induces an increase in lift.
- A split elevator is mounted at the rear of the UAV. Define the left and right elevator deflection angles, δ_{E_l} and δ_{E_r} respectively, such that a positive deflection induces a negative pitching moment.
- One rudder is mounted on each of the two vertical tails. Define the left and right rudder deflection angles, δ_{R_l} and δ_{R_r} respectively, such that a positive deflection induces a negative yawing moment.

Now, define the aerodynamic control vector as,

$$c_A = [\delta_{A_l}\ \delta_{A_r}\ \delta_{F_l}\ \delta_{F_r}\ \delta_{E_l}\ \delta_{E_r}\ \delta_{R_l}\ \delta_{R_r}]^T \tag{7.2.4}$$

Alternatively, the control vector can be defined in terms of lumped actuators as,

$$c_A = [\delta_A\ \delta_F\ \delta_E\ \delta_R]^T \tag{7.2.5}$$

where $\delta_X = \delta_{X_l} = \delta_{X_r}$.

7.3 AFD Based on Simplified Dynamics

In this section, active fault detection is applied to simplified decoupled aircraft dynamics models. These models are based on the research presented in [18] and [22]. These models are further simplified by removing the effect of weak secondary control surfaces.

7.3.1 Roll Dynamics AFD

An AFD system is derived for the decoupled roll dynamics.

7.3.1.1 Linear Roll Dynamics

The roll dynamics is given by the following state space representation [22].

$$\dot{P} = \left[\frac{\bar{L}_p}{I_{xx}}\right] P + \left[\frac{\bar{L}_{\delta_A}}{I_{xx}}\right] \delta_A \tag{7.3.1}$$

$$P_w = \left[1\right] P \tag{7.3.2}$$

where,

$$L_P = qSC_{\bar{L}_P}\frac{b}{2\bar{V}_0} \qquad \bar{L}_{\delta_A} = qSbC_{l_{\delta_A}} \tag{7.3.3}$$

7.3.1.2 Scheme Selection

The simplified roll dynamics are governed by a SISO model. Following the selection process shown in Figure 5.1, the simplified SISO framework must be selected. This further implies that the solution will impose an additional nominal performance and disturbance penalty. Since aeronautical applications are in general safety critical, the worst-case optimisation will be performed.

7.3.1.3 The Fault Model

Consider the following fault model:

$$\bar{L}_P = \bar{L}_{P_0}\left(1 + \theta_{\bar{L}_P}\right) \qquad \bar{L}_{\delta_A} = \bar{L}_{\delta_{A_0}}\left(1 + \theta_{\bar{L}_{\delta_A}}\right) \tag{7.3.4}$$

where, $\theta_{\bar{L}_P}$ and $\theta_{\bar{L}_{\delta_A}}$ are zero in the nominal case.

Using an upper linear fractional transform the system can be written as

$$\dot{P} = \left[\frac{\bar{L}_{P_0}}{I_{xx}}\right] P + \begin{bmatrix}\frac{\bar{L}_{P_0}}{I_{xx}} & \frac{\bar{L}_{\delta_{A_0}}}{I_{xx}}\end{bmatrix} w + \left[\frac{\bar{L}_{\delta_{A_0}}}{I_{xx}}\right] \delta_A \tag{7.3.5}$$

$$z = \begin{bmatrix}1\\0\end{bmatrix} P + \begin{bmatrix}0\\1\end{bmatrix} \delta_A \tag{7.3.6}$$

$$P_w = [1]P \tag{7.3.7}$$

with,

$$w = \begin{bmatrix}\theta_{\bar{L}_P} & 0\\ 0 & \theta_{\bar{L}_{\delta_A}}\end{bmatrix} z \tag{7.3.8}$$

7.3.1.4 The Disturbance Model

Next, the disturbance model is introduced. In this example the disturbance model from chapter 6 is again used. It is briefly restated here.

- Zero mean white process noise which enters the system in the same manner as the control input
- Bandwidth limited zero mean white measurement noise
- The error signal is equal to the plant output

Adding the disturbance model results in the following three port model:

$$\begin{bmatrix} \dot{P} \\ \dot{x_n} \end{bmatrix} = \begin{bmatrix} \frac{\bar{L}_{P_0}}{I_{xx}} & 0 \\ 0 & c \end{bmatrix} \begin{bmatrix} P \\ x_n \end{bmatrix} + \begin{bmatrix} \frac{\bar{L}_{P_0}}{I_{xx}} & \frac{\bar{L}_{\delta_{A_0}}}{I_{xx}} \\ 0 & 0 \end{bmatrix} \begin{bmatrix} w_1 \\ w_2 \end{bmatrix} + \begin{bmatrix} \frac{\bar{L}_{\delta_{A_0}}}{I_{xx}} \\ 0 \end{bmatrix} \delta_A + \begin{bmatrix} k_P \\ -c \end{bmatrix} d \tag{7.3.9}$$

$$\begin{bmatrix} z_1 \\ z_2 \end{bmatrix} = \begin{bmatrix} 1 & 0 \\ 0 & 0 \end{bmatrix} \begin{bmatrix} P \\ x_n \end{bmatrix} + \begin{bmatrix} 0 \\ 1 \end{bmatrix} \delta_A \tag{7.3.10}$$

$$P_w = \begin{bmatrix} 1 & k_m \end{bmatrix} \begin{bmatrix} P \\ x_n \end{bmatrix} \tag{7.3.11}$$

$$e = \begin{bmatrix} 1 & k_m \end{bmatrix} \begin{bmatrix} P \\ x_n \end{bmatrix} \tag{7.3.12}$$

The values for vehicle parameters are provided in Appendix A.

7.3.1.5 Solution Synthesis and Results

Suppose that the UAV suffers damage to a wing, resulting in the following fault case

$$\Theta = \begin{bmatrix} -0.1 & 0 \\ 0 & -0.5 \end{bmatrix} \tag{7.3.13}$$

Therefore, the damage results in a 10% reduction in damping and a 50% reduction in roll control authority.

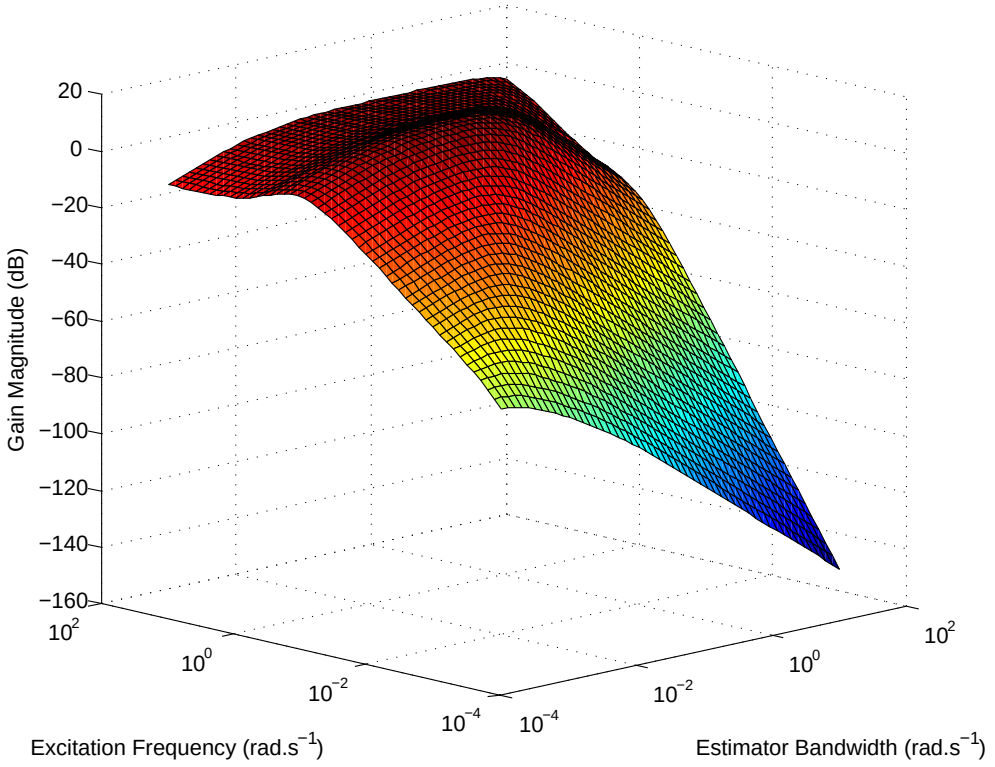

Figure 7.6: Roll AFD performance as a function of estimator bandwidth as well as excitation frequency. As before, the optimisation is performed for a targeted detection time of 1s.

It is considered acceptable to penalise fault detection times of below one second. Therefore, the targeted detection time as chosen as

$$t_d = 1s \tag{7.3.14}$$

Furthermore, the following noise model parameters are used,

$$c = -10000 \qquad k_m = 0.01 \qquad k_p = 0.1 \tag{7.3.15}$$

Using the equations derived in this work, a frequency plot can be easily produced showing the AFD performance as a function of the estimator bandwidth and auxiliary excitation frequency. The results are shown in Figure 7.6. Alternatively, the optimal solution can be represented using separate estimator bandwidth and auxiliary excitation frequency related plots. The results are shown in Figures 7.7 and 7.8.

From these figures or using the solution method shown in Figure 5.3 it is possible to determine the optimal estimator bandwidth and estimator gain as

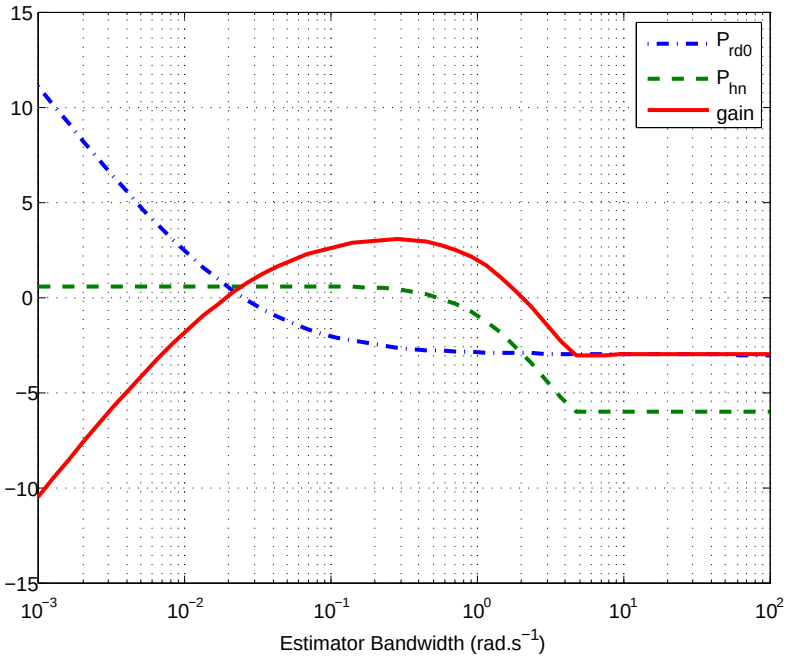

Figure 7.7: Roll AFD performance as a function of estimator bandwidth for a targeted detection time of 1s.

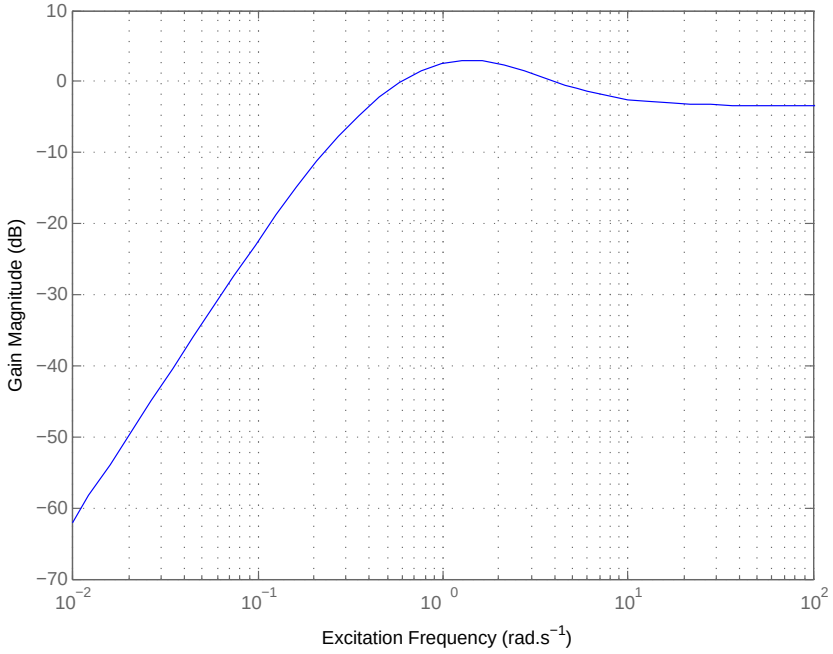

Figure 7.8: Roll AFD performance as a function of excitation frequency for a targeted detection time of 1s and at the optimal estimator bandwidth.

$$\omega_{L_{opt}} = 0.2812 \text{ rad.s}^{-1} \qquad L_{opt} = \begin{bmatrix} 5.4393 & 0 \end{bmatrix}^T \tag{7.3.16}$$

and, the optimal excitation frequency as

$$\omega_{\eta_{opt}} = 1.4204 \text{ rad.s}^{-1} \tag{7.3.17}$$

7.3.2 Lateral Acceleration AFD

Next, an AFD system is derived for the decoupled lateral aircraft dynamics.

7.3.2.1 Linear Lateral Acceleration Dynamics

The directional dynamics are given by the following state space representation [22].

$$\begin{bmatrix} \dot{\beta} \\ \dot{R} \end{bmatrix} = \begin{bmatrix} \frac{Y_\beta}{m\bar{V}_0} & -1 \\ \frac{\bar{N}_\beta}{I_{zz}} & \frac{\bar{N}_R}{I_{zz}} \end{bmatrix} \begin{bmatrix} \beta \\ R \end{bmatrix} + \begin{bmatrix} \frac{Y_{\delta_R}}{m\bar{V}_0} & \frac{Y_{\delta_A}}{m\bar{V}_0} \\ \frac{\bar{N}_{\delta_R}}{I_{zz}} & \frac{\bar{N}_{\delta_A}}{I_{zz}} \end{bmatrix} \begin{bmatrix} \delta_R \\ \delta_A \end{bmatrix} \tag{7.3.18}$$

$$B_W = \begin{bmatrix} \frac{Y_\beta}{m} & \frac{Y_R}{m} \end{bmatrix} \begin{bmatrix} \beta \\ R \end{bmatrix} + \begin{bmatrix} \frac{Y_{\delta_R}}{m} & \frac{Y_{\delta_A}}{m} \end{bmatrix} \begin{bmatrix} \delta_R \\ \delta_A \end{bmatrix} \tag{7.3.19}$$

where,

$$\begin{aligned} Y_\beta &= qSC_{Y_\beta} & Y_R &= qS\frac{b}{2\bar{V}_0}C_{Y_r} \\ \bar{N}_\beta &= qSbC_{N_\beta} & \bar{N}_R &= qSb\frac{b}{2\bar{V}_0}C_{N_r} \\ Y_{\delta_R} &= qSC_{Y_{\delta_R}} & Y_{\delta_A} &= qSC_{Y_{\delta_A}} \\ \bar{N}_{\delta_R} &= qSbC_{\bar{N}_{\delta_R}} & \bar{N}_{\delta_A} &= qSbC_{\bar{N}_{\delta_A}} \end{aligned} \tag{7.3.20}$$

For best results, each control surface should be considered independently rather than lumped units. However, this is not done here in order to keep the model as simple and concise as possible.

7.3.2.2 Scheme Selection

The lateral dynamics are given by a proper MIMO system, were D_{eu} is a matrix of full row-rank. Following the selection process shown in Figure 5.1, the

output-cancellation MIMO framework may be selected. This further implies that the solution will not impose an additional nominal performance and disturbance penalty. As was stated previously the worst-case optimisation will be performed.

7.3.2.3 The Fault Model

At first glance it would seem that a seven parameter fault model is required. However, considering that Y_β, Y_R, and Y_{δ_R} are physically related to $\bar{N}_\beta$, $\bar{N}_R$, and $\bar{N_{\delta_R}}$ any change in the one parameter will also be visible in the other parameter. Therefore, consider the following four parameter fault model:

$$\bar{N}_\beta = \bar{N_{\beta_0}}\left(1+\theta_{\bar{N}_\beta}\right) \qquad \bar{N}_R = \bar{N_{R_0}}\left(1+\theta_{\bar{N}_R}\right)$$
$$\bar{N_{\delta_R}} = \bar{N_{\delta_{R_0}}}\left(1+\theta_{\bar{N_{\delta_R}}}\right) \qquad \bar{N_{\delta_A}} = \bar{N_{\delta_{A_0}}}\left(1+\theta_{\bar{N_{\delta_A}}}\right)$$

where, $\theta_{\bar{N}_\beta}$, $\theta_{\bar{N}_R}$, $\theta_{\bar{N_{\delta_R}}}$, and $\theta_{\bar{N_{\delta_A}}}$ are all zero in the nominal case.

It should be noted that a change will also occur here in the parameters that are being ignored. Therefore, the exact fault condition modelled here is not physically attainable. Real faults will however be detected.

Using an upper linear fractional transform the system can be written as

$$\begin{bmatrix}\dot{\beta}\\ \dot{R}\end{bmatrix} = \begin{bmatrix}\frac{Y_\beta}{m\bar{V}_0} & -1\\ \frac{\bar{N_{\beta_0}}}{I_{zz}} & \frac{\bar{N_{R_0}}}{I_{zz}}\end{bmatrix}\begin{bmatrix}\beta\\ R\end{bmatrix} + \begin{bmatrix}0 & 0 & 0 & 0\\ \frac{\bar{N_{\beta_0}}}{I_{zz}} & \frac{\bar{N_{R_0}}}{I_{zz}} & \frac{\bar{N_{\delta_{R_0}}}}{I_{zz}} & \frac{\bar{N_{\delta_{A_0}}}}{I_{zz}}\end{bmatrix} w + \begin{bmatrix}\frac{Y_{\delta_R}}{m\bar{V}_0} & \frac{Y_{\delta_A}}{m\bar{V}_0}\\ \frac{\bar{N_{\delta_{R_0}}}}{I_{zz}} & \frac{\bar{N_{\delta_{A_0}}}}{I_{zz}}\end{bmatrix}\begin{bmatrix}\delta_R\\ \delta_A\end{bmatrix} \tag{7.3.21}$$

$$z = \begin{bmatrix}1 & 0\\ 0 & 1\\ 0 & 0\\ 0 & 0\end{bmatrix}\begin{bmatrix}\beta\\ R\end{bmatrix} + \begin{bmatrix}0 & 0\\ 0 & 0\\ 1 & 0\\ 0 & 1\end{bmatrix}\begin{bmatrix}\delta_R\\ \delta_A\end{bmatrix} \tag{7.3.22}$$

$$B_W = \begin{bmatrix}\frac{Y_\beta}{m} & \frac{Y_R}{m}\end{bmatrix}\begin{bmatrix}\beta\\ R\end{bmatrix} + \begin{bmatrix}\frac{Y_{\delta_R}}{m} & \frac{Y_{\delta_A}}{m}\end{bmatrix}\begin{bmatrix}\delta_R\\ \delta_A\end{bmatrix} \tag{7.3.23}$$

with,

$$w = \begin{bmatrix} \theta_{\bar{N_\beta}} & 0 & 0 & 0 \\ 0 & \theta_{\bar{N_R}} & 0 & 0 \\ 0 & 0 & \theta_{\bar{N_{\delta_R}}} & 0 \\ 0 & 0 & 0 & \theta_{\bar{N_{\delta_A}}} \end{bmatrix} z \tag{7.3.24}$$

7.3.2.4 The Disturbance Model

Next, the disturbance model is introduced. The same fault model used previously is again assumed here.

Adding the disturbance model results in the following three port model:

$$\begin{bmatrix} \dot{\beta} \\ \dot{R} \\ \dot{x_n} \end{bmatrix} = \begin{bmatrix} \frac{Y_\beta}{m\bar{V}_0} & -1 & 0 \\ \frac{\bar{N_{\beta_0}}}{I_{zz}} & \frac{\bar{N_{R_0}}}{I_{zz}} & 0 \\ 0 & 0 & c \end{bmatrix} \begin{bmatrix} \beta \\ R \\ x_n \end{bmatrix} + \begin{bmatrix} 0 & 0 & 0 & 0 \\ \frac{\bar{N_{\beta_0}}}{I_{zz}} & \frac{\bar{N_{R_0}}}{I_{zz}} & \frac{\bar{N_{\delta_{R_0}}}}{I_{zz}} & \frac{\bar{N_{\delta_{A_0}}}}{I_{zz}} \\ 0 & 0 & 0 & 0 \end{bmatrix} w$$
$$+ \begin{bmatrix} \frac{Y_{\delta_R}}{m\bar{V}_0} & \frac{Y_{\delta_A}}{m\bar{V}_0} \\ \frac{\bar{N_{\delta_{R_0}}}}{I_{zz}} & \frac{\bar{N_{\delta_{A_0}}}}{I_{zz}} \\ 0 & 0 \end{bmatrix} \begin{bmatrix} \delta_R \\ \delta_A \end{bmatrix} + \begin{bmatrix} 0 \\ k_P \\ -c \end{bmatrix} d \tag{7.3.25}$$

$$z = \begin{bmatrix} 1 & 0 & 0 \\ 0 & 1 & 0 \\ 0 & 0 & 0 \\ 0 & 0 & 0 \end{bmatrix} \begin{bmatrix} \beta \\ R \\ x_n \end{bmatrix} + \begin{bmatrix} 0 & 0 \\ 0 & 0 \\ 1 & 0 \\ 0 & 1 \end{bmatrix} \begin{bmatrix} \delta_R \\ \delta_A \end{bmatrix} \tag{7.3.26}$$

$$B_W = \begin{bmatrix} \frac{Y_\beta}{m} & \frac{Y_R}{m} & k_m \end{bmatrix} \begin{bmatrix} \beta \\ R \\ x_n \end{bmatrix} + \begin{bmatrix} \frac{Y_{\delta_R}}{m} & \frac{Y_{\delta_A}}{m} \end{bmatrix} \begin{bmatrix} \delta_R \\ \delta_A \end{bmatrix} \tag{7.3.27}$$

$$e = \begin{bmatrix} \frac{Y_\beta}{m} & \frac{Y_R}{m} & k_m \end{bmatrix} \begin{bmatrix} \beta \\ R \\ x_n \end{bmatrix} + \begin{bmatrix} \frac{Y_{\delta_R}}{m} & \frac{Y_{\delta_A}}{m} \end{bmatrix} \begin{bmatrix} \delta_R \\ \delta_A \end{bmatrix} \tag{7.3.28}$$

The values for the model parameters are provided in Appendix A.

7.3.2.5 Solution Synthesis and Results

Since the lateral acceleration model given is proper with D_{eu} of full row rank, equation 3.2.10 applies. Now, given that the error output is equal to the system

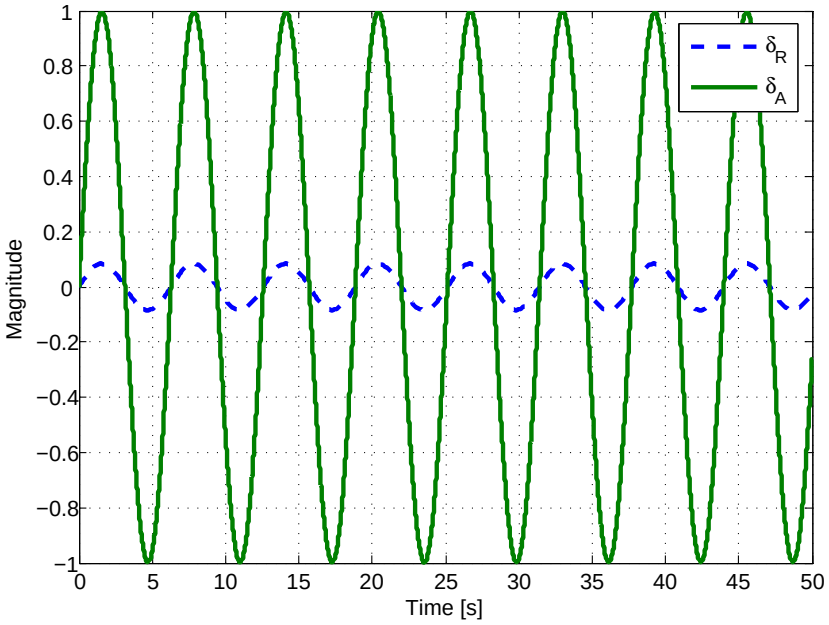

Figure 7.9: The auxiliary excitation signal. Note that both the ailerons and rudders are excited.

output, the input shaping filter is given by,

$$\begin{aligned}
\dot{x_\eta} &= (A - B_u D_{eu}^{+} C_e) x_\eta + B_u a H_{\eta_0} \eta_h \\
&= \begin{bmatrix} -0.1281 & -1 \\ 101.1 & -0.9454 \end{bmatrix} x_\eta + \begin{bmatrix} 0.1579 & -0.01433 \\ -8.809 & 1.468 \end{bmatrix} a H_0 \eta_h \\
\eta &= -D_{eu}^{+} C_e x_\eta + I a H_{\eta_0} \eta_h \\
&= \begin{bmatrix} 0.9816 & 0 \\ -0.08907 & 0 \end{bmatrix} x_\eta + \begin{bmatrix} 1 & 0 \\ 0 & 1 \end{bmatrix} a H_0 \eta_h
\end{aligned} \tag{7.3.29}$$

where H_0 is a base matrix for the kernel of D_{eu}. Therefore, $H_0\eta_h \in \begin{bmatrix} 0.0904 & 0.9959 \end{bmatrix}^T$. From this input shaping filter it can be seen that due to the large variation in lateral actuator effectiveness, the required excitation mix is likely not practical. This problem will be addressed when implementing AFD for the full combined lateral acceleration and roll model.

With reference to figures 7.9, 7.10, and 7.11 it can be seen that the auxiliary input excites both actuators and system states, but has no meaningful impact on the system output.

Suppose that the UAV suffers damage to its tail section, resulting in the

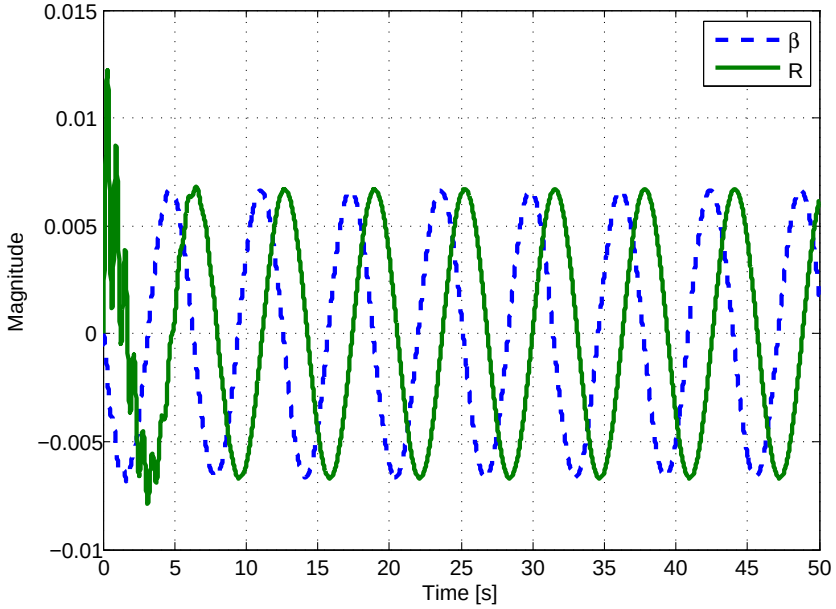

Figure 7.10: The output zeroing states. Note that both the yaw rate and side-slip angle are non-zero.

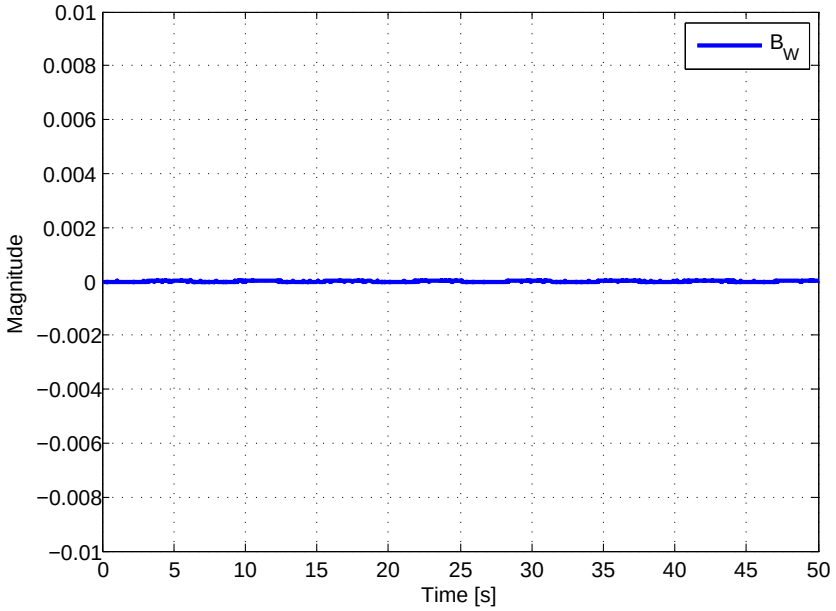

Figure 7.11: Although there is a non-zero input and non-zero states, the resulting output is zero.

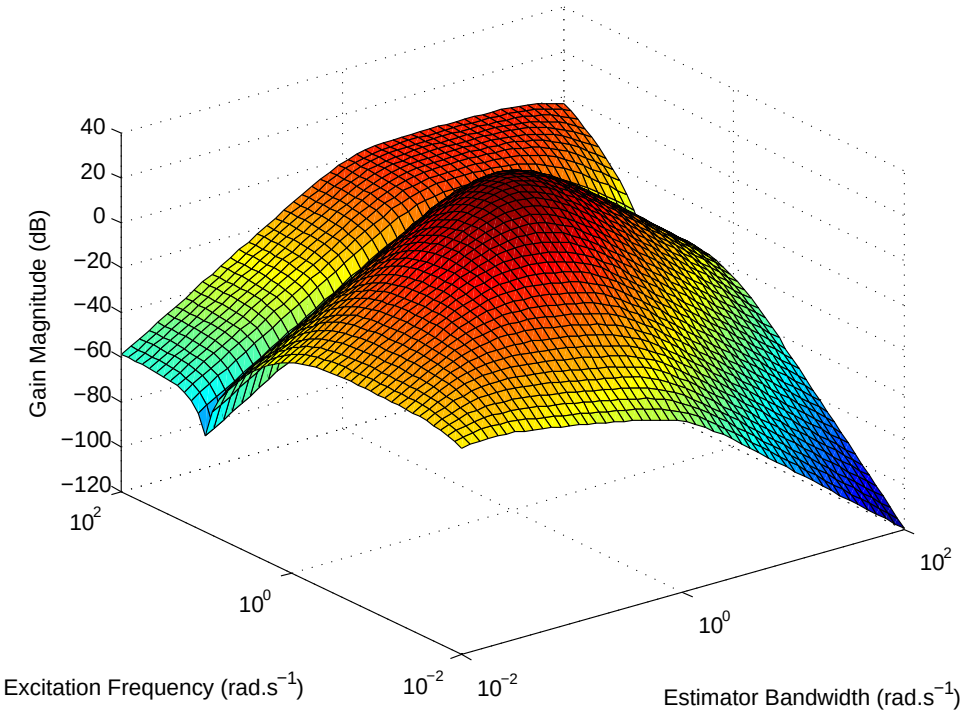

Figure 7.12: Lateral Acceleration AFD performance as a function of estimator bandwidth as well as excitation frequency. As before, the optimisation is performed for a targeted detection time of 1s.

following fault case

$$\Theta = \begin{bmatrix} 0 & 0 & 0 & 0 \\ 0 & -0.2 & 0 & 0 \\ 0 & 0 & -0.1 & 0 \\ 0 & 0 & 0 & 0 \end{bmatrix} \tag{7.3.30}$$

Therefore, the damage results in a 20% reduction in yaw rate damping and a 10% reduction in the rudder's yaw control authority.

It is considered acceptable to penalise fault detection times of below one second. Therefore, the targeted detection time is chosen as

$$t_d = 1s \tag{7.3.31}$$

Furthermore, the following noise model parameters are used,

$$c = -10000 \qquad k_m = 0.01 \qquad k_p = 0.1 \tag{7.3.32}$$

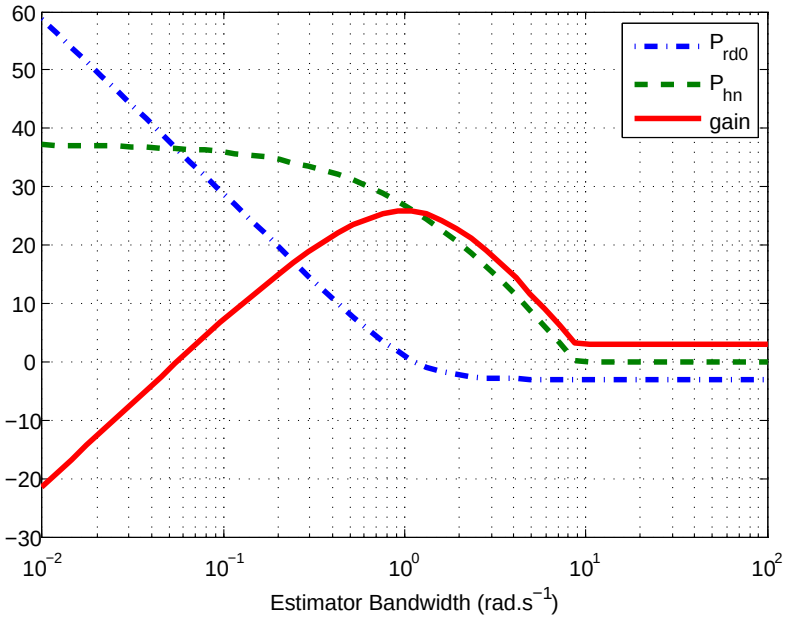

Figure 7.13: Lateral Acceleration AFD performance as a function of estimator bandwidth for a targeted detection time of 1s.

Using the equations derived in this work, a frequency plot can be easily produced showing the AFD performance as a function of the estimator bandwidth and auxiliary excitation frequency. The results are shown in figure 7.12. Alternatively, the optimal solution can be represented using separate estimator bandwidth and auxiliary excitation frequency related plots. The results are shown in Figure 7.13 and 7.14.

From these figures or using the solution method shown in Figure 5.3 it is possible to determine the optimal estimator bandwidth and gain as

$$\omega_{L_{opt}} = 0.9103 \text{ rad.s}^{-1} \qquad L_{opt} = \begin{bmatrix} 0.8277 & 2.8593 & 0 \end{bmatrix}^T \tag{7.3.33}$$

and, the optimal excitation frequency as

$$\omega_{\eta_{opt}} = 1.0422 \text{ rad.s}^{-1} \tag{7.3.34}$$

7.3.3 Normal Acceleration AFD

Finally, an AFD system is now derived for the decoupled normal acceleration aircraft dynamics.

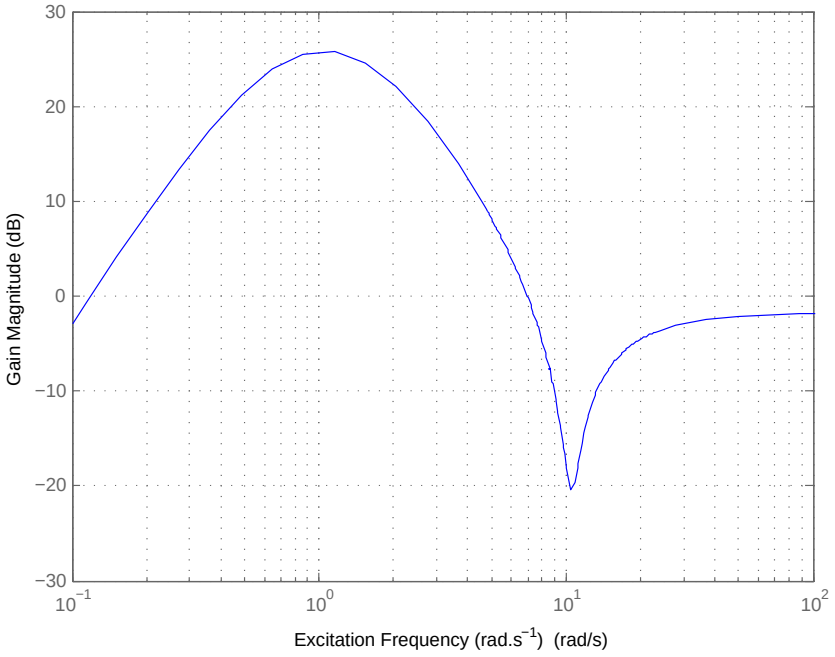

Figure 7.14: Lateral Acceleration AFD performance as a function of excitation frequency for a targeted detection time of 1s and at the optimal estimator bandwidth.

7.3.3.1 Linearised Normal Acceleration Dynamics

The longitudinal dynamics can be given by the following state space representation [22].

$$\begin{bmatrix} \dot{\alpha} \\ \dot{Q} \end{bmatrix} = \begin{bmatrix} \frac{-L_\alpha}{m\bar{V}} & \frac{1-L_Q}{m\bar{V}_0} \\ \frac{M_\alpha}{I_{yy}} & \frac{M_Q}{I_{yy}} \end{bmatrix} \begin{bmatrix} \alpha \\ Q \end{bmatrix} + \begin{bmatrix} 0 \\ \frac{M_{\delta_E}}{I_{yy}} \end{bmatrix} \delta_E \tag{7.3.35}$$

$$C_W = \begin{bmatrix} \frac{-L_\alpha}{m} & 0 \end{bmatrix} \begin{bmatrix} \alpha \\ Q \end{bmatrix} \tag{7.3.36}$$

where,

$$\begin{aligned} L_\alpha &= qSC_{L_\alpha} & L_Q &= qSC_{L_q}\frac{\bar{c}}{2\bar{V}_0} \\ M_\alpha &= qS\bar{c}C_{M_\alpha} & M_Q &= qS\bar{c}C_{M_q}\frac{\bar{c}}{2\bar{V}_0} \\ M_{\delta_E} &= qS\bar{c}C_{M_{\delta_E}} \end{aligned} \tag{7.3.37}$$

For best results, each control surface should be considered independently. However, this is not done here in order to keep the model as simple and concise as possible.

7.3.3.2 Scheme Selection

The normal acceleration dynamics are governed by a SISO model. Following the selection process shown in Figure 5.1, the simplified SISO framework must be selected. This further implies that the solution will impose an additional nominal performance and disturbance penalty. As was stated previously the worst-case optimisation will be performed.

7.3.3.3 The Fault Model

At first glance it would seem that a five parameter fault model is required. However, considering that L_α and L_Q are physically related to M_α and M_Q, any change in the one parameter will also be visible in the other parameter. Therefore, consider the following three parameter fault model:

$$\begin{aligned} M_\alpha &= M_{\alpha_0}\left(1+\theta_{M_\alpha}\right) & M_Q &= M_{Q_0}\left(1+\theta_{M_Q}\right) \\ M_{\delta_E} &= M_{\delta_{E_0}}\left(1+\theta_{M_{\delta_E}}\right) \end{aligned} \tag{7.3.38}$$

where, θ_{M_α}, θ_{M_Q} and $\theta_{M_{\delta_E}}$ are zero in the nominal case.

As before this assumption is made to keep the example informative. Again, it should be noted that a change will also occur here in the parameters that are being ignored.

Using an upper linear fractional transform the system can be written as

$$\begin{bmatrix}\dot{\alpha}\\ \dot{Q}\end{bmatrix} = \begin{bmatrix}\frac{-L_\alpha}{m\bar{V}} & \frac{1-L_Q}{m\bar{V}_0}\\ \frac{M_{\alpha_0}}{I_{yy}} & \frac{M_{Q_0}}{I_{yy}}\end{bmatrix}\begin{bmatrix}\alpha\\ Q\end{bmatrix} + \begin{bmatrix}0 & 0 & 0\\ \frac{M_{\alpha_0}}{I_{yy}} & \frac{M_{Q_0}}{I_{yy}} & \frac{M_{\delta_{E_0}}}{I_{yy}}\end{bmatrix} w + \begin{bmatrix}0\\ \frac{M_{\delta_{E_0}}}{I_{yy}}\end{bmatrix}\delta_E \tag{7.3.39}$$

$$z = \begin{bmatrix}1 & 0\\ 0 & 1\\ 0 & 0\end{bmatrix}\begin{bmatrix}\alpha\\ Q\end{bmatrix} + \begin{bmatrix}0\\ 0\\ 1\end{bmatrix}\delta_E \tag{7.3.40}$$

$$C_W = \begin{bmatrix}\frac{-L_\alpha}{m} & 0\end{bmatrix}\begin{bmatrix}\alpha\\ Q\end{bmatrix} \tag{7.3.41}$$

with,

$$w = \begin{bmatrix}\theta_{M_\alpha} & 0 & 0\\ 0 & \theta_{M_Q} & 0\\ 0 & 0 & \theta_{M_{\delta_E}}\end{bmatrix} z \tag{7.3.42}$$

7.3.3.4 The Disturbance Model

Next, the disturbance model is introduced. In this example the following properties will be assumed:

- Zero mean white process noise which enters the system in the same manner as the control input
- Bandwidth limited zero mean white measurement noise
- The error signal is equal to the plant output

Adding the disturbance model results in the following three port model:

$$\begin{bmatrix} \dot{\alpha} \\ \dot{Q} \\ \dot{x_n} \end{bmatrix} = \begin{bmatrix} \frac{-L_\alpha}{m\bar{V}} & \frac{1-L_Q}{m\bar{V}_0} & 0 \\ \frac{M_{\alpha_0}}{I_{yy}} & \frac{M_{Q_0}}{I_{yy}} & 0 \\ 0 & 0 & c \end{bmatrix} \begin{bmatrix} \alpha \\ Q \\ x_n \end{bmatrix} + \begin{bmatrix} 0 & 0 & 0 \\ \frac{M_{\alpha_0}}{I_{yy}} & \frac{M_{Q_0}}{I_{yy}} & \frac{M_{\delta_{E_0}}}{I_{yy}} \\ 0 & 0 & 0 \end{bmatrix} w + \begin{bmatrix} 0 \\ \frac{M_{\delta_{E_0}}}{I_{yy}} \\ 0 \end{bmatrix} \delta_E + \begin{bmatrix} 0 \\ k_P \\ -c \end{bmatrix} d \tag{7.3.43}$$

$$z = \begin{bmatrix} 1 & 0 & 0 \\ 0 & 1 & 0 \\ 0 & 0 & 0 \end{bmatrix} \begin{bmatrix} \alpha \\ Q \\ x_n \end{bmatrix} + \begin{bmatrix} 0 \\ 0 \\ 1 \end{bmatrix} \delta_E \tag{7.3.44}$$

$$C_W = \begin{bmatrix} \frac{-L_\alpha}{m} & 0 & k_m \end{bmatrix} \begin{bmatrix} \alpha \\ Q \\ x_n \end{bmatrix} \tag{7.3.45}$$

$$e = \begin{bmatrix} \frac{-L_\alpha}{m} & 0 & k_m \end{bmatrix} \begin{bmatrix} \alpha \\ Q \\ x_n \end{bmatrix} \tag{7.3.46}$$

The values for the model parameters are provided in Appendix A.

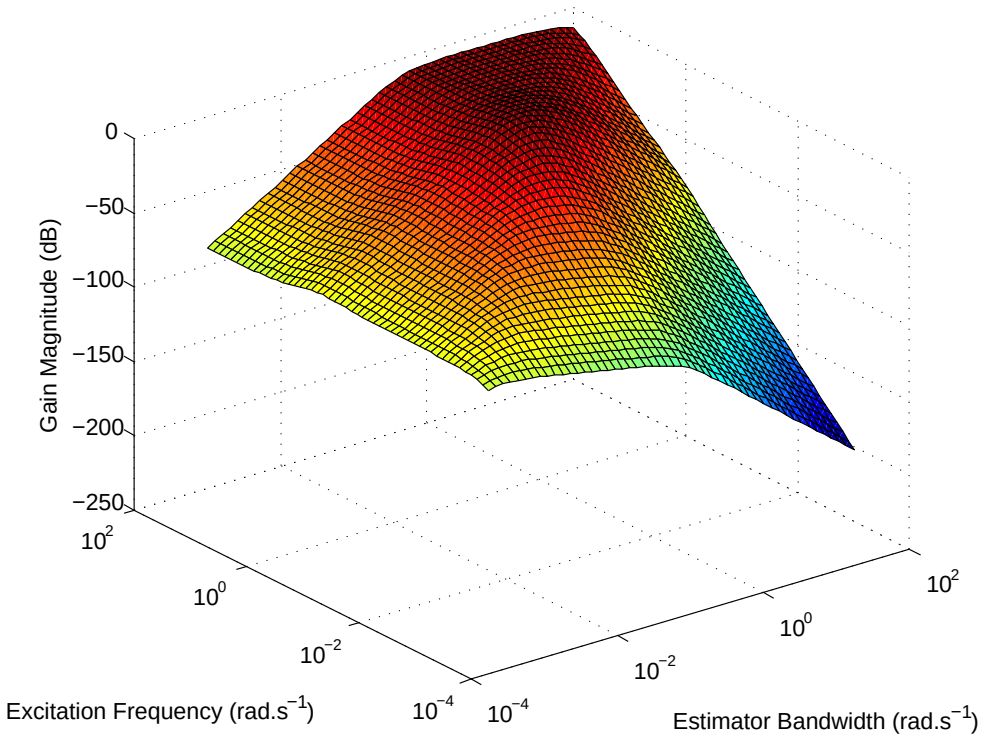

Figure 7.15: Normal Acceleration AFD performance as a function of estimator bandwidth as well as excitation frequency. As before, the optimisation is performed for a targeted detection time of 1s.

7.3.3.5 Solution Synthesis and Results

Suppose that the UAV suffers damage to its tail section, resulting in the following fault case:

$$\Theta = \begin{bmatrix} -0.1 & 0 & 0 \\ 0 & -0.2 & 0 \\ 0 & 0 & -0.3 \end{bmatrix} \tag{7.3.47}$$

Therefore, the damage results in a 10% reduction in the pitching moment due to angle of attack, a 20% reduction in pitch damping, and a 30% reduction in pitch control authority.

It is considered acceptable to penalise fault detection times of below one second. Therefore, the targeted detection time as chosen as

$$t_d = 1s \tag{7.3.48}$$

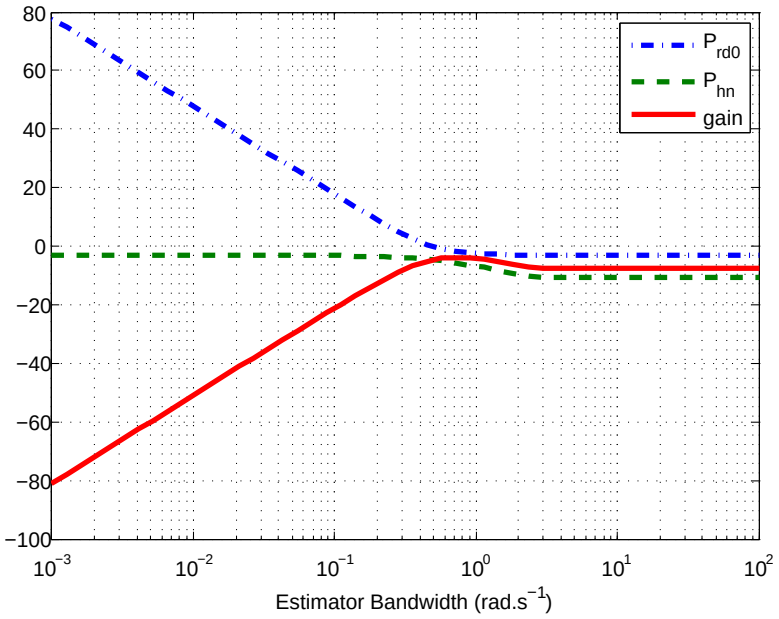

Figure 7.16: Normal Acceleration AFD performance as a function of estimator bandwidth for a targeted detection time of 1s.

Furthermore, the following noise model parameters are used,

$$c = -10000 \qquad k_m = 0.01 \qquad k_p = 0.1 \tag{7.3.49}$$

Using the equations derived in this work, a frequency plot can be easily produced showing the AFD performance as a function of the estimator bandwidth and auxiliary excitation frequency. The results are shown in figure 7.15. Alternatively, the optimal solution can be represented using separate estimator bandwidth and auxiliary excitation frequency related plots. The results are shown in Figure 7.16 and 7.17.

From these figures or using the solution method shown in Figure 5.3 it is possible to determine the optimal estimator bandwidth and gain as

$$\omega_{L_{opt}} = 0.7197 \text{ rad.s}^{-1} \qquad L_{opt} = \begin{bmatrix} -0.0513 & -0.5272 & 0 \end{bmatrix}^T \tag{7.3.50}$$

and the optimal excitation frequency as

$$\omega_{\eta_{opt}} = 1.6882 \text{ rad.s}^{-1} \tag{7.3.51}$$

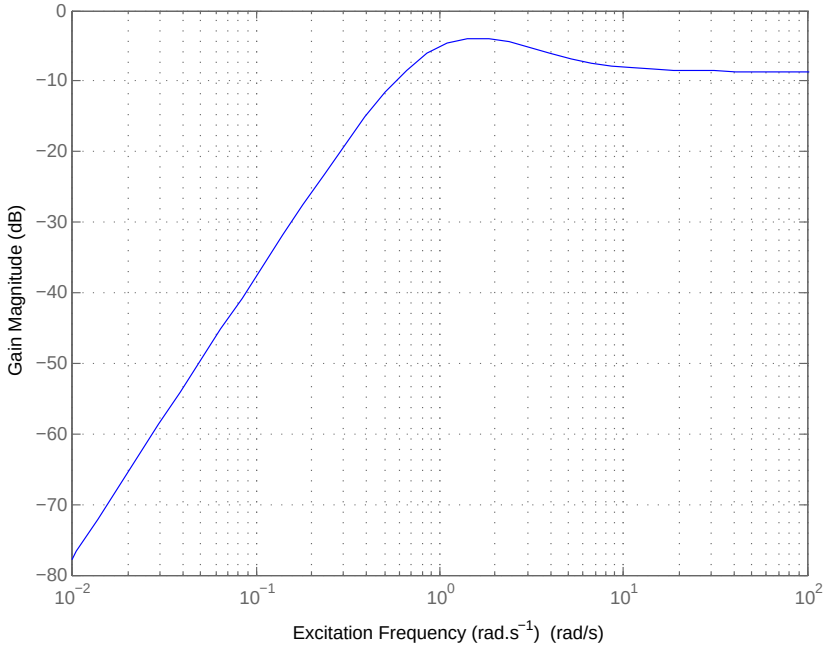

Figure 7.17: Normal Acceleration AFD performance as a function of excitation frequency for a targeted detection time of 1s and at the optimal estimator bandwidth.

7.4 Full Lateral Acceleration-Roll Dynamics AFD

In this section, active fault detection is applied to the full lateral acceleration and roll aircraft dynamics model. This model is based on the research presented in [18] and [22]. These models are further refined by considering each control surface independently as defined in subsection 7.2.2, thereby enabling improved actuator cancellation.

7.4.1 Full Lateral Acceleration-Roll Dynamics

The full lateral acceleration dynamics are given by the following state space representation [22].

$$\begin{bmatrix}\dot{\beta}\\ \dot{R}\\ \dot{P}\end{bmatrix} = \begin{bmatrix}\frac{Y_\beta}{m\bar{V}_0} & -1 & \frac{Y_P}{m\bar{V}_0}\\ \frac{\bar{N}_\beta}{I_{zz}} & \frac{\bar{N}_R}{I_{zz}} & \frac{\bar{N}_P}{I_{zz}}\\ \frac{\bar{L}_\beta}{I_{xx}} & \frac{\bar{L}_R}{I_{xx}} & \frac{\bar{L}_P}{I_{xx}}\end{bmatrix}\begin{bmatrix}\beta\\ R\\ P\end{bmatrix} + \begin{bmatrix}\frac{Y_{\delta_{R_l}}}{m\bar{V}_0} & \frac{Y_{\delta_{R_r}}}{m\bar{V}_0} & \frac{Y_{\delta_{A_l}}}{m\bar{V}_0} & \frac{Y_{\delta_{A_r}}}{m\bar{V}_0}\\ \frac{\bar{N}_{\delta_{R_l}}}{I_{zz}} & \frac{\bar{N}_{\delta_{R_r}}}{I_{zz}} & \frac{\bar{N}_{\delta_{A_l}}}{I_{zz}} & \frac{\bar{N}_{\delta_{A_r}}}{I_{zz}}\\ \frac{\bar{L}_{\delta_{R_l}}}{I_{xx}} & \frac{\bar{L}_{\delta_{R_r}}}{I_{xx}} & \frac{\bar{L}_{\delta_{E_l}}}{I_{xx}} & \frac{\bar{L}_{\delta_{E_r}}}{I_{xx}}\end{bmatrix}\begin{bmatrix}\delta_{R_l}\\ \delta_{R_r}\\ \delta_{A_l}\\ \delta_{A_r}\end{bmatrix} \tag{7.4.1}$$

$$B_W = \begin{bmatrix}\frac{Y_\beta}{m} & \frac{Y_R}{m} & \frac{Y_P}{m}\end{bmatrix}\begin{bmatrix}\beta\\ R\\ P\end{bmatrix} + \begin{bmatrix}\frac{Y_{\delta_{R_l}}}{m} & \frac{Y_{\delta_{R_r}}}{m} & \frac{Y_{\delta_{A_l}}}{m} & \frac{Y_{\delta_{A_r}}}{m}\end{bmatrix}\begin{bmatrix}\delta_{R_l}\\ \delta_{R_r}\\ \delta_{A_l}\\ \delta_{A_r}\end{bmatrix} \tag{7.4.2}$$

7.4.2 Scheme Selection

The full lateral-roll dynamics are given by a proper MIMO system, where D_{eu} is a matrix of full-row rank. Following the selection process shown in Figure 5.1, the output-cancellation MIMO framework may be selected. This further implies that the solution will not impose an additional nominal performance and disturbance penalty. As was stated previously, the worst-case optimisation will be performed.

7.4.3 The Fault Model

At first glance it would seem that a twenty-one parameter fault model is required. However, considering that many parameters are physically related to other parameters, any change in the one parameter will also be visible in the other parameter. Therefore, consider the following seven parameter fault model:

$$\begin{aligned}
\bar{N_\beta} &= \bar{N_{\beta_0}}\left(1+\theta_{\bar{N_\beta}}\right) & \bar{N_R} &= \bar{N_{R_0}}\left(1+\theta_{\bar{N_R}}\right)\\
\bar{N_{\delta_{R_l}}} &= \bar{N_{\delta_{R_{l_0}}}}\left(1+\theta_{\bar{N_{\delta_{R_l}}}}\right) & \bar{N_{\delta_{R_r}}} &= \bar{N_{\delta_{R_{r_0}}}}\left(1+\theta_{\bar{N_{\delta_{R_r}}}}\right)\\
\bar{L_P} &= \bar{L_{P_0}}\left(1+\theta_{\bar{L_P}}\right) & \bar{L_{\delta_{A_l}}} &= \bar{L_{\delta_{A_{l_0}}}}\left(1+\theta_{\bar{L_{\delta_{A_l}}}}\right)\\
\bar{L_{\delta_{A_r}}} &= \bar{L_{\delta_{A_{r_0}}}}\left(1+\theta_{\bar{L_{\delta_{A_r}}}}\right)
\end{aligned} \tag{7.4.3}$$

where θ_{X_Y} are all zero in the nominal case.

As before this results in optimising for a fault that technically can not occur. Real faults will however still be detected.

Using an upper linear fractional transform, the system can be written as

$$\begin{bmatrix}\dot{\beta}\\ \dot{R}\\ \dot{P}\end{bmatrix} = \begin{bmatrix}\frac{Y_\beta}{m\bar{V}_0} & -1 & \frac{Y_P}{m\bar{V}_0}\\ \frac{\bar{N}_\beta}{I_{zz}} & \frac{\bar{N}_R}{I_{zz}} & \frac{\bar{N}_P}{I_{zz}}\\ \frac{\bar{L}_\beta}{I_{xx}} & \frac{\bar{L}_R}{I_{xx}} & \frac{\bar{L}_P}{I_{xx}}\end{bmatrix}\begin{bmatrix}\beta\\ R\\ P\end{bmatrix} + \begin{bmatrix}0 & 0 & 0 & 0 & 0 & 0 & 0\\ \frac{\bar{N}_{\beta_0}}{I_{zz}} & \frac{\bar{N}_{R_0}}{I_{zz}} & \frac{\bar{N}_{\delta_{R_{l_0}}}}{I_{zz}} & \frac{\bar{N}_{\delta_{R_{r_0}}}}{I_{zz}} & 0 & 0 & 0\\ 0 & 0 & 0 & 0 & \frac{\bar{L}_{P_0}}{I_{xx}} & \frac{\bar{L}_{\delta_{A_{l_0}}}}{I_{xx}} & \frac{\bar{L}_{\delta_{A_{r_0}}}}{I_{xx}}\end{bmatrix} w$$
$$+ \begin{bmatrix}\frac{Y_{\delta_{R_l}}}{m\bar{V}_0} & \frac{Y_{\delta_{R_r}}}{m\bar{V}_0} & \frac{Y_{\delta_{A_l}}}{m\bar{V}_0} & \frac{Y_{\delta_{A_r}}}{m\bar{V}_0}\\ \frac{\bar{N}_{\delta_{R_l}}}{I_{zz}} & \frac{\bar{N}_{\delta_{R_r}}}{I_{zz}} & \frac{\bar{N}_{\delta_{A_l}}}{I_{zz}} & \frac{\bar{N}_{\delta_{A_r}}}{I_{zz}}\\ \frac{\bar{L}_{\delta_{R_l}}}{I_{xx}} & \frac{\bar{L}_{\delta_{R_r}}}{I_{xx}} & \frac{\bar{L}_{\delta_{E_l}}}{I_{xx}} & \frac{\bar{L}_{\delta_{E_r}}}{I_{xx}}\end{bmatrix}\begin{bmatrix}\delta_{R_l}\\ \delta_{R_r}\\ \delta_{A_l}\\ \delta_{A_r}\end{bmatrix} \tag{7.4.4}$$

$$z = \begin{bmatrix}1 & 0 & 0\\ 0 & 1 & 0\\ 0 & 0 & 0\\ 0 & 0 & 0\\ 0 & 0 & 1\\ 0 & 0 & 0\\ 0 & 0 & 0\end{bmatrix}\begin{bmatrix}\beta\\ R\\ P\end{bmatrix} + \begin{bmatrix}0 & 0 & 0 & 0\\ 0 & 0 & 0 & 0\\ 1 & 0 & 0 & 0\\ 0 & 1 & 0 & 0\\ 0 & 0 & 0 & 0\\ 0 & 0 & 1 & 0\\ 0 & 0 & 0 & 1\end{bmatrix}\begin{bmatrix}\delta_{R_l}\\ \delta_{R_r}\\ \delta_{A_l}\\ \delta_{A_r}\end{bmatrix} \tag{7.4.5}$$

$$B_W = \begin{bmatrix}\frac{Y_\beta}{m} & \frac{Y_R}{m} & \frac{Y_P}{m}\end{bmatrix}\begin{bmatrix}\beta\\ R\\ P\end{bmatrix} + \begin{bmatrix}\frac{Y_{\delta_{R_l}}}{m} & \frac{Y_{\delta_{R_r}}}{m} & \frac{Y_{\delta_{A_l}}}{m} & \frac{Y_{\delta_{A_r}}}{m}\end{bmatrix}\begin{bmatrix}\delta_{R_l}\\ \delta_{R_r}\\ \delta_{A_l}\\ \delta_{A_r}\end{bmatrix} \tag{7.4.6}$$

with

$$w = \begin{bmatrix}\theta_{\bar{N}_\beta} & 0 & 0 & 0 & 0 & 0 & 0\\ 0 & \theta_{\bar{N}_R} & 0 & 0 & 0 & 0 & 0\\ 0 & 0 & \theta_{\bar{N}_{\delta_{R_l}}} & 0 & 0 & 0 & 0\\ 0 & 0 & 0 & \theta_{\bar{N}_{\delta_{R_r}}} & 0 & 0 & 0\\ 0 & 0 & 0 & 0 & \theta_{\bar{L}_P} & 0 & 0\\ 0 & 0 & 0 & 0 & 0 & \theta_{\bar{L}_{\delta_{A_l}}} & 0\\ 0 & 0 & 0 & 0 & 0 & 0 & \theta_{\bar{L}_{\delta_{A_r}}}\end{bmatrix} z \tag{7.4.7}$$

7.4.4 The Disturbance Model

Next, the disturbance model is introduced. In this example the following properties will be assumed:

- Zero mean white process noise which enters the system in the same manner as the control input
- Bandwidth limited zero mean white measurement noise
- The error signal is equal to the plant output

Adding the disturbance model results in the following three port model:

$$\begin{bmatrix}\dot{\beta}\\ \dot{R}\\ \dot{P}\\ \dot{x_n}\end{bmatrix} = \begin{bmatrix}\frac{Y_\beta}{m\bar{V}_0} & -1 & \frac{Y_P}{m\bar{V}_0} & 0\\ \frac{\bar{N}_\beta}{I_{zz}} & \frac{\bar{N}_R}{I_{zz}} & \frac{\bar{N}_P}{I_{zz}} & 0\\ \frac{\bar{L}_\beta}{I_{xx}} & \frac{\bar{L}_R}{I_{xx}} & \frac{\bar{L}_P}{I_{xx}} & 0\\ 0 & 0 & 0 & c\end{bmatrix}\begin{bmatrix}\beta\\ R\\ P\\ x_n\end{bmatrix} + \begin{bmatrix}0 & 0 & 0 & 0 & 0 & 0 & 0\\ \frac{\bar{N}_{\beta_0}}{I_{zz}} & \frac{\bar{N}_{R_0}}{I_{zz}} & \frac{\bar{N}_{\delta_{R_{l_0}}}}{I_{zz}} & \frac{\bar{N}_{\delta_{R_{r_0}}}}{I_{zz}} & 0 & 0 & 0\\ 0 & 0 & 0 & 0 & \frac{\bar{L}_{P_0}}{I_{xx}} & \frac{\bar{L}_{\delta_{A_{l_0}}}}{I_{xx}} & \frac{\bar{L}_{\delta_{A_{r_0}}}}{I_{xx}}\\ 0 & 0 & 0 & 0 & 0 & 0 & 0\end{bmatrix} w$$

$$+ \begin{bmatrix}\frac{Y_{\delta_{R_l}}}{m\bar{V}_0} & \frac{Y_{\delta_{R_r}}}{m\bar{V}_0} & \frac{Y_{\delta_{A_l}}}{m\bar{V}_0} & \frac{Y_{\delta_{A_r}}}{m\bar{V}_0}\\ \frac{N_{\delta_{R_l}}}{I_{zz}} & \frac{N_{\delta_{R_r}}}{I_{zz}} & \frac{N_{\delta_{A_l}}}{I_{zz}} & \frac{N_{\delta_{A_r}}}{I_{zz}}\\ \frac{\bar{L}_{\delta_{R_l}}}{I_{xx}} & \frac{\bar{L}_{\delta_{R_r}}}{I_{xx}} & \frac{\bar{L}_{\delta_{E_l}}}{I_{xx}} & \frac{\bar{L}_{\delta_{E_r}}}{I_{xx}}\\ 0 & 0 & 0 & 0\end{bmatrix}\begin{bmatrix}\delta_{R_l}\\ \delta_{R_r}\\ \delta_{A_l}\\ \delta_{A_r}\end{bmatrix} + \begin{bmatrix}0\\ 0\\ k_P\\ -c\end{bmatrix} d \tag{7.4.8}$$

$$z = \begin{bmatrix}1 & 0 & 0 & 0\\ 0 & 1 & 0 & 0\\ 0 & 0 & 0 & 0\\ 0 & 0 & 0 & 0\\ 0 & 0 & 1 & 0\\ 0 & 0 & 0 & 0\\ 0 & 0 & 0 & 0\end{bmatrix}\begin{bmatrix}\beta\\ R\\ P\\ x_n\end{bmatrix} + \begin{bmatrix}0 & 0 & 0 & 0\\ 0 & 0 & 0 & 0\\ 1 & 0 & 0 & 0\\ 0 & 1 & 0 & 0\\ 0 & 0 & 0 & 0\\ 0 & 0 & 1 & 0\\ 0 & 0 & 0 & 1\end{bmatrix}\begin{bmatrix}\delta_{R_l}\\ \delta_{R_r}\\ \delta_{A_l}\\ \delta_{A_r}\end{bmatrix} \tag{7.4.9}$$

$$B_W = \begin{bmatrix}\frac{Y_\beta}{m} & \frac{Y_R}{m} & \frac{Y_P}{m} & k_m\end{bmatrix}\begin{bmatrix}\beta\\ R\\ P\\ x_n\end{bmatrix} + \begin{bmatrix}\frac{Y_{\delta_{R_l}}}{m} & \frac{Y_{\delta_{R_r}}}{m} & \frac{Y_{\delta_{A_l}}}{m} & \frac{Y_{\delta_{A_r}}}{m}\end{bmatrix}\begin{bmatrix}\delta_{R_l}\\ \delta_{R_r}\\ \delta_{A_l}\\ \delta_{A_r}\end{bmatrix} \tag{7.4.10}$$

$$e = \begin{bmatrix}\frac{Y_\beta}{m} & \frac{Y_R}{m} & \frac{Y_P}{m} & k_m\end{bmatrix}\begin{bmatrix}\beta\\ R\\ P\\ x_n\end{bmatrix} + \begin{bmatrix}\frac{Y_{\delta_{R_l}}}{m} & \frac{Y_{\delta_{R_r}}}{m} & \frac{Y_{\delta_{A_l}}}{m} & \frac{Y_{\delta_{A_r}}}{m}\end{bmatrix}\begin{bmatrix}\delta_{R_l}\\ \delta_{R_r}\\ \delta_{A_l}\\ \delta_{A_r}\end{bmatrix} \tag{7.4.11}$$

The values for the model parameters are provided in Appendix A.

7.4.5 Solution Synthesis and Results

Since the lateral acceleration roll model given is proper with D_{eu} of full-row rank, equation 3.2.10 applies. Now, given that the error output is equal to the

system output, the input shaping filter is given by:

$$\begin{aligned}
\dot{x_\eta} &= (A - B_u D_{eu}^{+} C_e) x_\eta + B_u a H_{\eta_0} \eta_h \\
&= \begin{bmatrix} -0.2318 & -1.003 & 0.002654 \\ 106.5 & -0.7535 & -0.6733 \\ 14.3 & 0.5627 & -5.968 \end{bmatrix} x_\eta \\
&+ \begin{bmatrix} 0.07896 & 0.07896 & -0.007165 & -0.007165 \\ -4.404 & -4.404 & 0.7341 & 0.7341 \\ 0.2023 & 0.2023 & -16.59 & -16.59 \end{bmatrix} a H_0 \eta_h \\
\eta &= -D_{eu}^{+} C_e x_\eta + I a H_{\eta_0} \eta_h \\
&= \begin{bmatrix} 0.2743 & -0.01564 & -0.003141 \\ 0.2743 & -0.01564 & -0.003141 \\ -0.6471 & 0.0369 & 0.00741 \\ -0.6471 & 0.0369 & 0.00741 \end{bmatrix} x_\eta + \begin{bmatrix} 1 & 0 & 0 & 0 \\ 0 & 1 & 0 & 0 \\ 0 & 0 & 1 & 0 \\ 0 & 0 & 0 & 1 \end{bmatrix} a H_0 \eta_h
\end{aligned} \tag{7.4.12}$$

where H_0 is a base matrix for the kernel of D_{eu}. Therefore,

$$H_0 \eta_h \in \begin{bmatrix} 1.0261 & 1.2219 & 0.4764 & 0.4764 \end{bmatrix}^T \tag{7.4.13}$$

From this input shaping filter it can be seen that the actuator mix is substantially improved over the simplified lateral dynamics case. Furthermore, it is noted that the excitation is not decoupled from the roll moment.

With reference to figures 7.18, 7.19, and 7.20 it can be seen that the auxiliary input excites all actuators and system states, but has no meaningful impact on the system output.

Suppose that the UAV suffers damage to its tail section, resulting in the following fault case

$$\Theta = \begin{bmatrix} 0 & 0 & 0 & 0 & 0 & 0 & 0 \\ 0 & -0.2 & 0 & 0 & 0 & 0 & 0 \\ 0 & 0 & -0.1 & 0 & 0 & 0 & 0 \\ 0 & 0 & 0 & 0 & 0 & 0 & 0 \\ 0 & 0 & 0 & 0 & 0 & 0 & 0 \\ 0 & 0 & 0 & 0 & 0 & 0 & 0 \\ 0 & 0 & 0 & 0 & 0 & 0 & 0 \end{bmatrix} \tag{7.4.14}$$

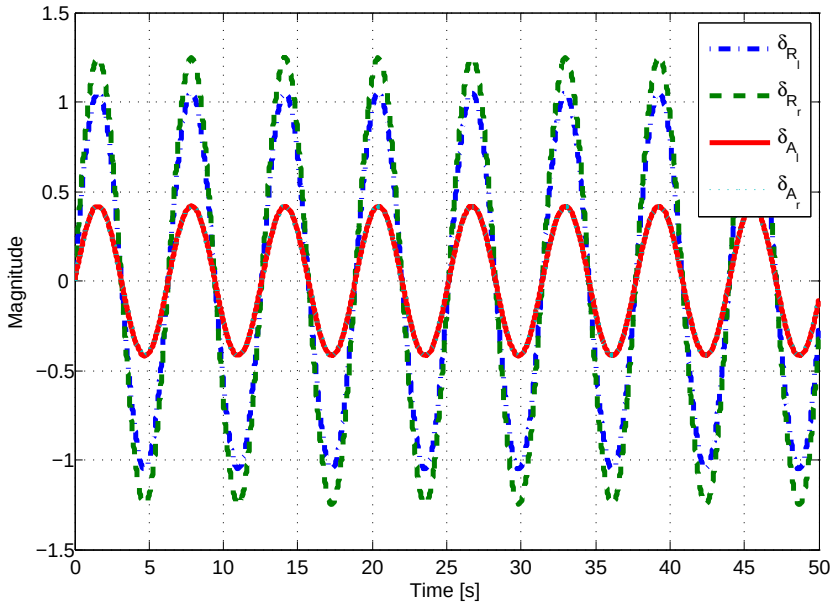

Figure 7.18: The auxiliary excitation signal. Note that both the ailerons and rudders are excited.

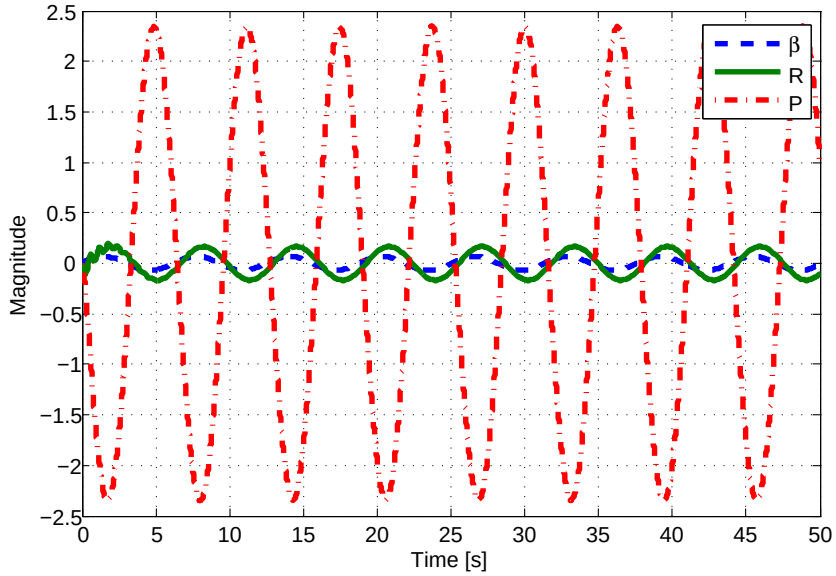

Figure 7.19: The output zeroing states. Note that both the yaw rate and side-slip angle are non-zero.

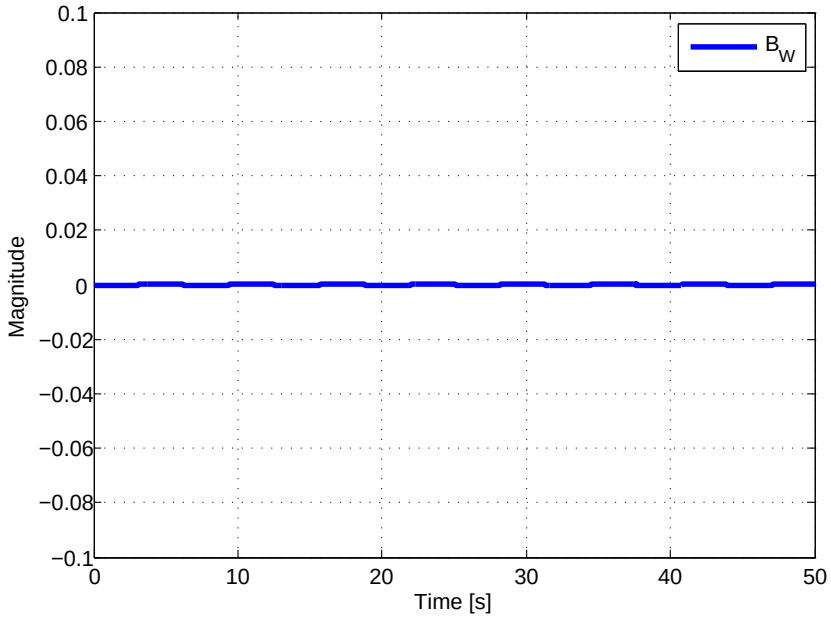

Figure 7.20: Although there is a non-zero input and non-zero states, the resulting output is zero.

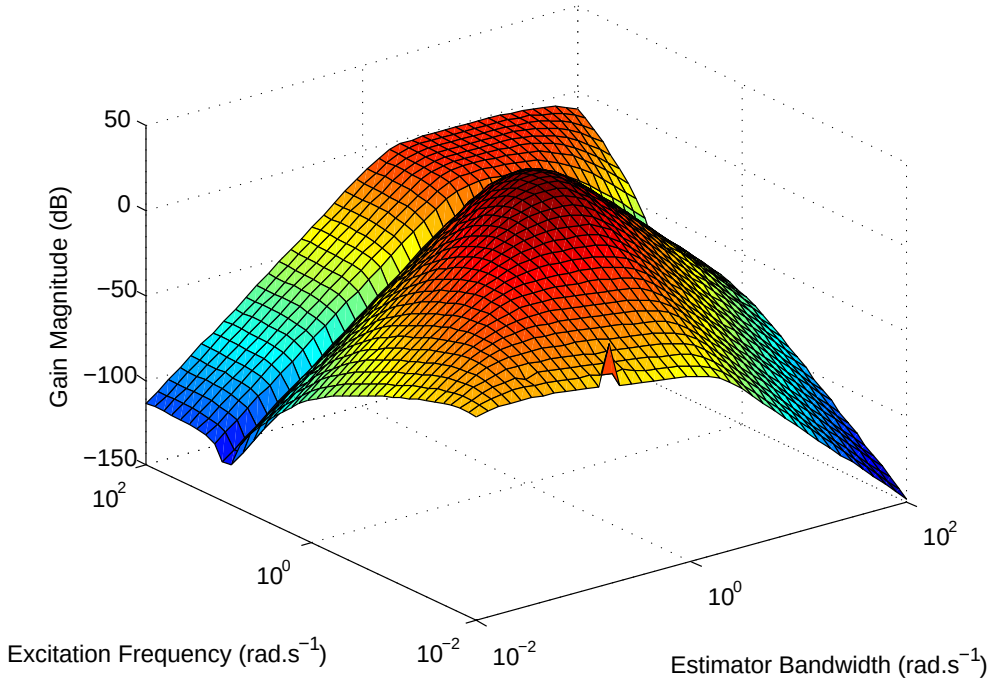

Figure 7.21: Lateral Acceleration Roll AFD performance as a function of estimator bandwidth as well as excitation frequency. As before, the optimisation is performed for a targeted detection time of 1s.

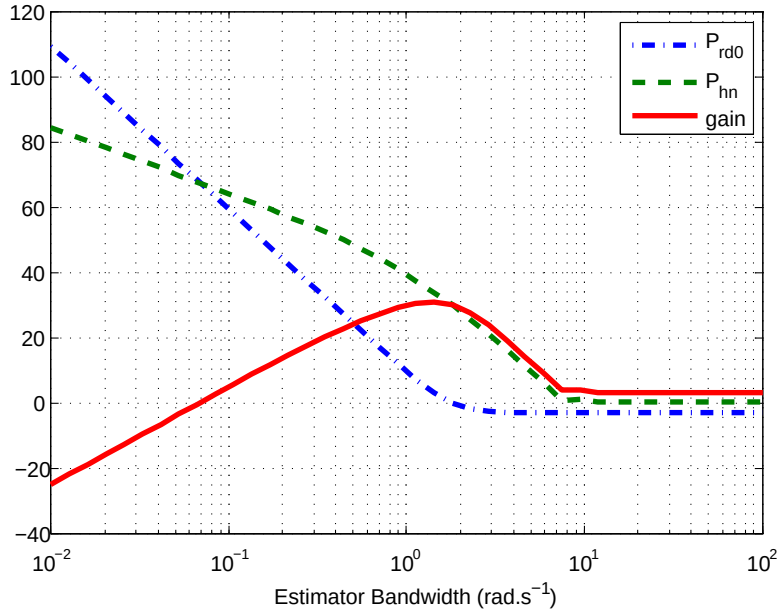

Figure 7.22: Lateral Acceleration Roll AFD performance as a function of estimator bandwidth for a targeted detection time of 1s.

Therefore, the damage results in a 20% reduction in yaw rate damping and a 10% reduction in the left rudder's yaw control authority.

It is considered acceptable to penalise fault detection times of below one second. Therefore, the targeted detection time is chosen as

$$t_d = 1s \tag{7.4.15}$$

Furthermore, the following noise model parameters are used:

$$c = -10000 \qquad k_m = 0.01 \qquad k_p = 0.1 \tag{7.4.16}$$

Using the equations derived in this work, a frequency plot showing the AFD performance as a function of the estimator bandwidth and auxiliary excitation frequency can easily be produced. The results are shown in figure 7.21. Alternatively, the optimal solution can be represented using separate estimator bandwidth and auxiliary excitation frequency related plots. The results are shown in Figure 7.22 and 7.23.

From these figures or using the solution method shown in Figure 5.3 it is possible to determine the optimal estimator bandwidth and gain as

$$\omega_{L_{opt}} = 1.4251 \text{ rad.s}^{-1} \qquad L_{opt} = \begin{bmatrix} 0.4711 & 13.5825 & 10.8363 & 0 \end{bmatrix}^T \tag{7.4.17}$$

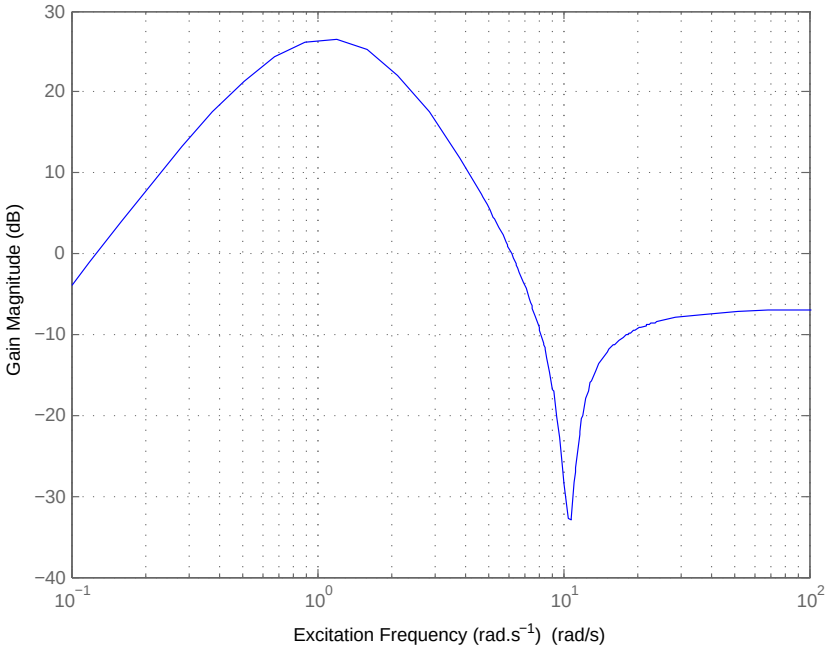

Figure 7.23: Lateral Acceleration Roll AFD performance as a function of excitation frequency for a targeted detection time of 1s and at the optimal estimator bandwidth.

and, the optimal excitation frequency as

$$\omega_{\eta_{opt}} = 1.0891 \text{ rad.s}^{-1} \tag{7.4.18}$$

7.5 Simulation

In this section, the Active Fault Detection systems designed in this chapter are tested by means of simulations. To begin with, the three decoupled simplified AFD systems are simulated. Next the full combined lateral acceleration and roll AFD system is simulated and compared with the simplified decoupled systems.

7.5.1 Simplified Roll AFD System Simulation

From the AFD system developed for the simplified UAV roll model in subsection 7.3.1 a simple simulation can be implemented. The auxiliary signal amplitude is selected such that the additional nominal system disturbance is limited to ± 1 unit on the error output.

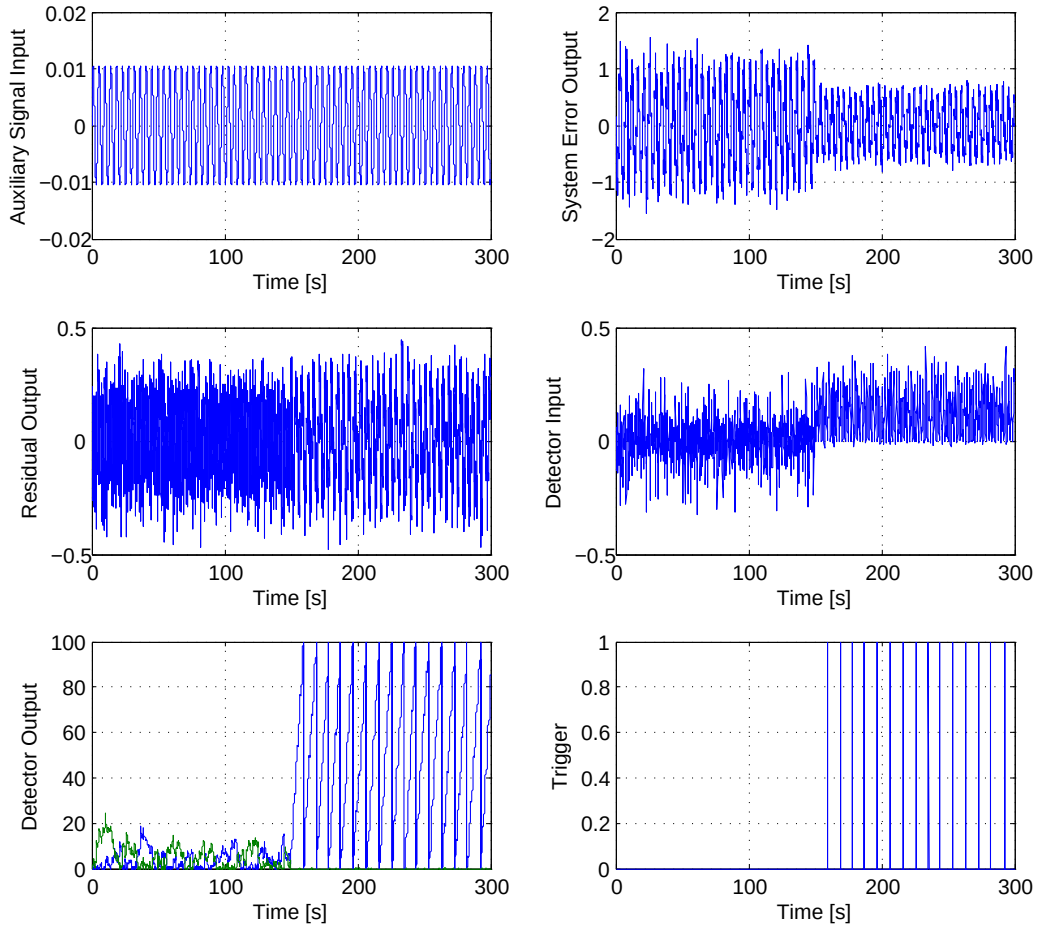

Figure 7.24: Simulation results with a moderate amount of noise in the correct ratio. Failure occurs at 150 seconds and is detected 16 seconds later. Note that each time the threshold is reached the detector is reset, and the trigger value is set to one for a single sample period.

The simulation results are shown in Figure 7.24 for moderate levels of white noise and in Figure 7.25 for high levels of white noise. In these figures the following is shown: the auxiliary excitation signal; the error output; the residual output; the detector input; the detector output; and the detector trigger. Note that the setup proves robust against white noise, while providing a substantial signal to noise gain from error signal to residual output.

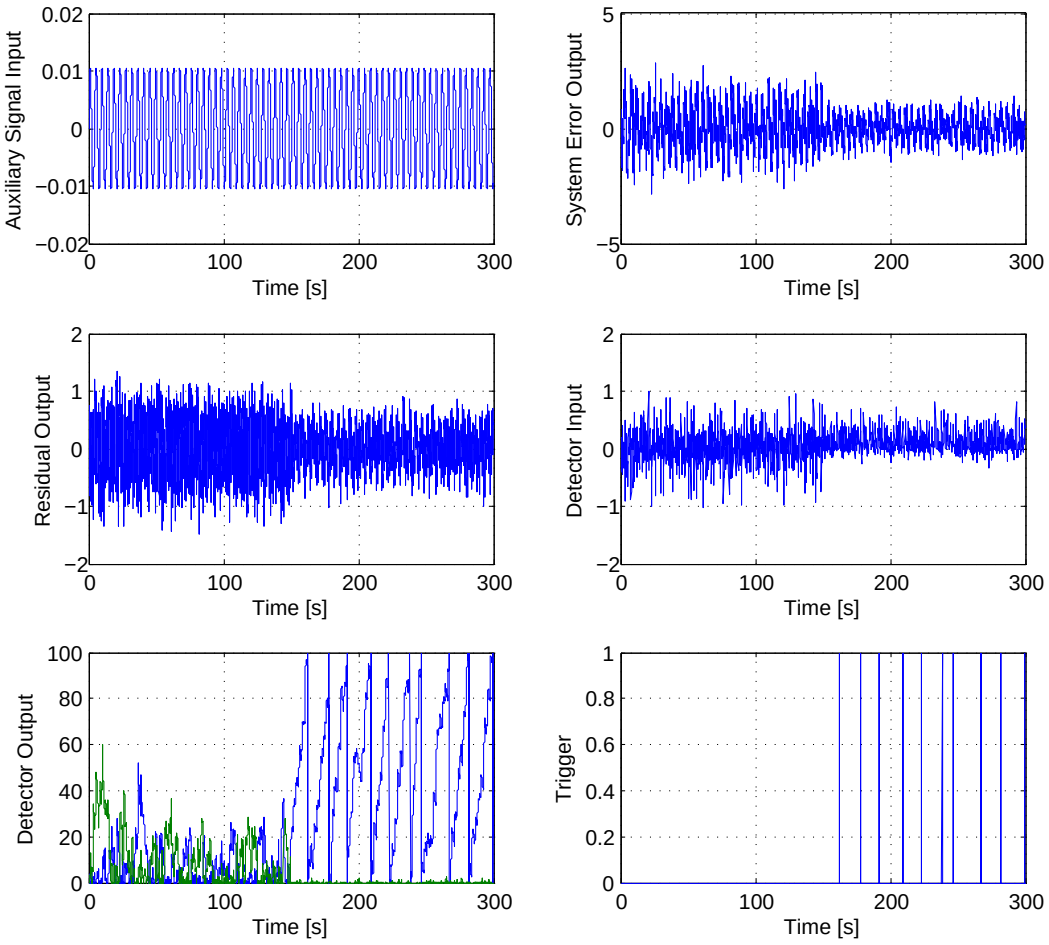

Figure 7.25: Simulation results with a large amount of noise in the correct ratio. Failure occurs at 150 seconds and is detected 9 seconds later. Note that each time the threshold is reached the detector is reset, and the trigger value is set to one for a single sample period.

7.5.2 Simplified Lateral Acceleration AFD System Simulation

From the AFD system developed for the simplified UAV lateral acceleration model in subsection 7.3.2, a simple simulation can be implemented. The auxiliary signal amplitude is selected such that the additional nominal system disturbance is limited to ± 1 unit on the error output.

The simulation results are shown in Figure 7.26 for moderate levels of white noise and in Figure 7.27 for high levels of white noise. In these figures the following is shown: the auxiliary excitation signal; the error output; the residual output; the detector input; the detector output; and the detector trigger. Note

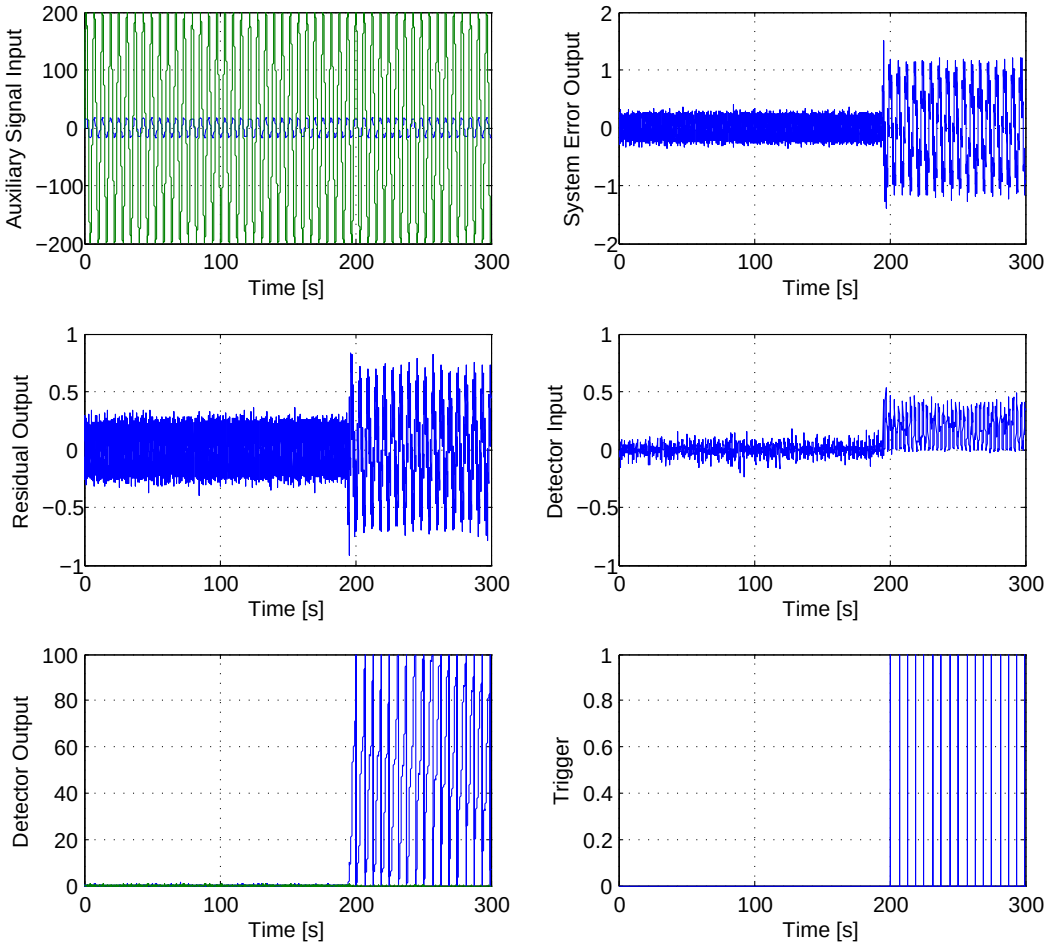

Figure 7.26: Simulation results with a moderate amount of noise in the correct ratio. Failure occurs at 195 seconds and is detected 6 seconds later. Note that each time the threshold is reached the detector is reset, and the trigger value is set to one for a single sample period.

that the setup proves robust against white noise, while inducing no additional nominal system disturbance. Furthermore, it is again noted that the excitation used for this lateral AFD system would not be practical. Ailerons are simply not effective at producing lateral acceleration, and therefore an unrealistically large aileron deviation is required in order to cancel the rudders.

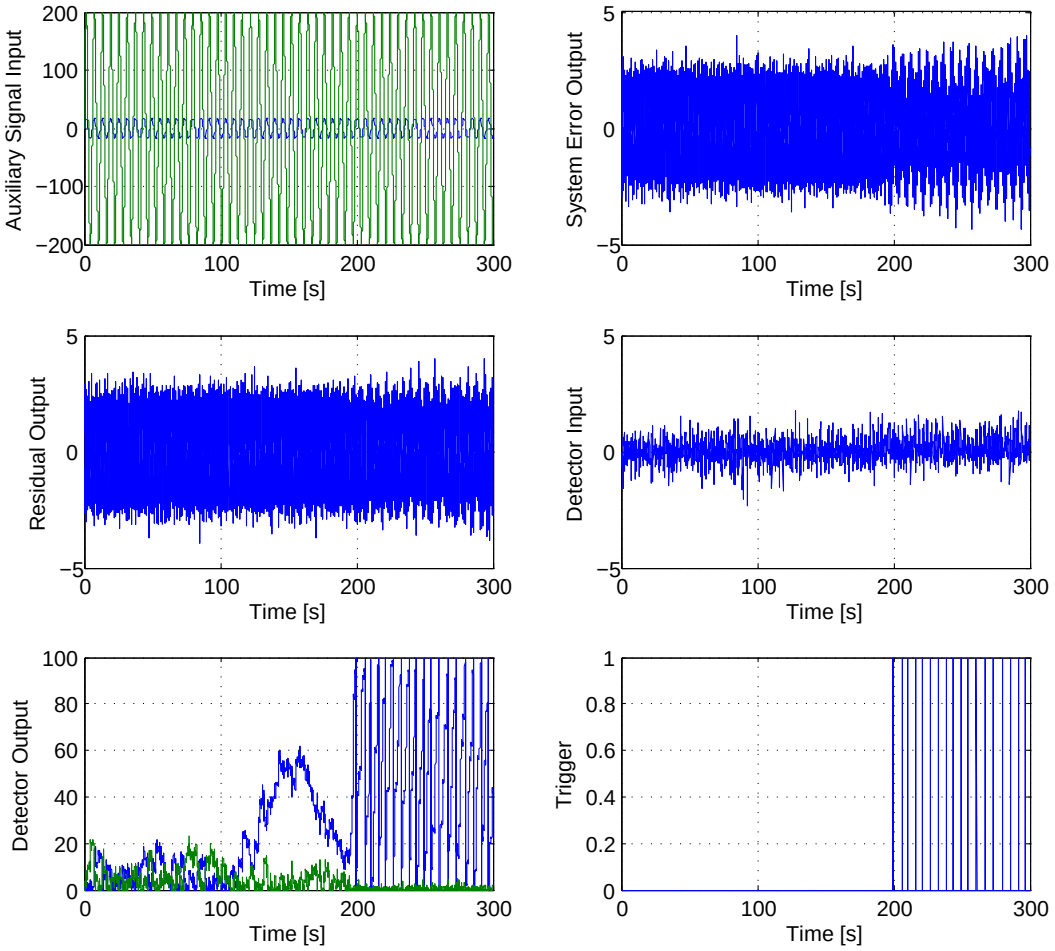

Figure 7.27: Simulation results with a large amount of noise in the correct ratio. Failure occurs at 195 seconds and is detected 5 seconds later. Note that each time the threshold is reached the detector is reset, and the trigger value is set to one for a single sample period.

7.5.3 Simplified Normal Acceleration AFD System Simulation

From the AFD system developed for the simplified UAV normal acceleration model in subsection 7.3.3, a simple simulation can be implemented. The auxiliary signal amplitude is selected such that the additional nominal system disturbance is limited to ± 1 unit on the error output.

The simulation results are shown in Figure 7.28 for moderate levels of white noise and in Figure 7.29 for high levels of white noise. In these figures the following is shown: the auxiliary excitation signal; the error output; the

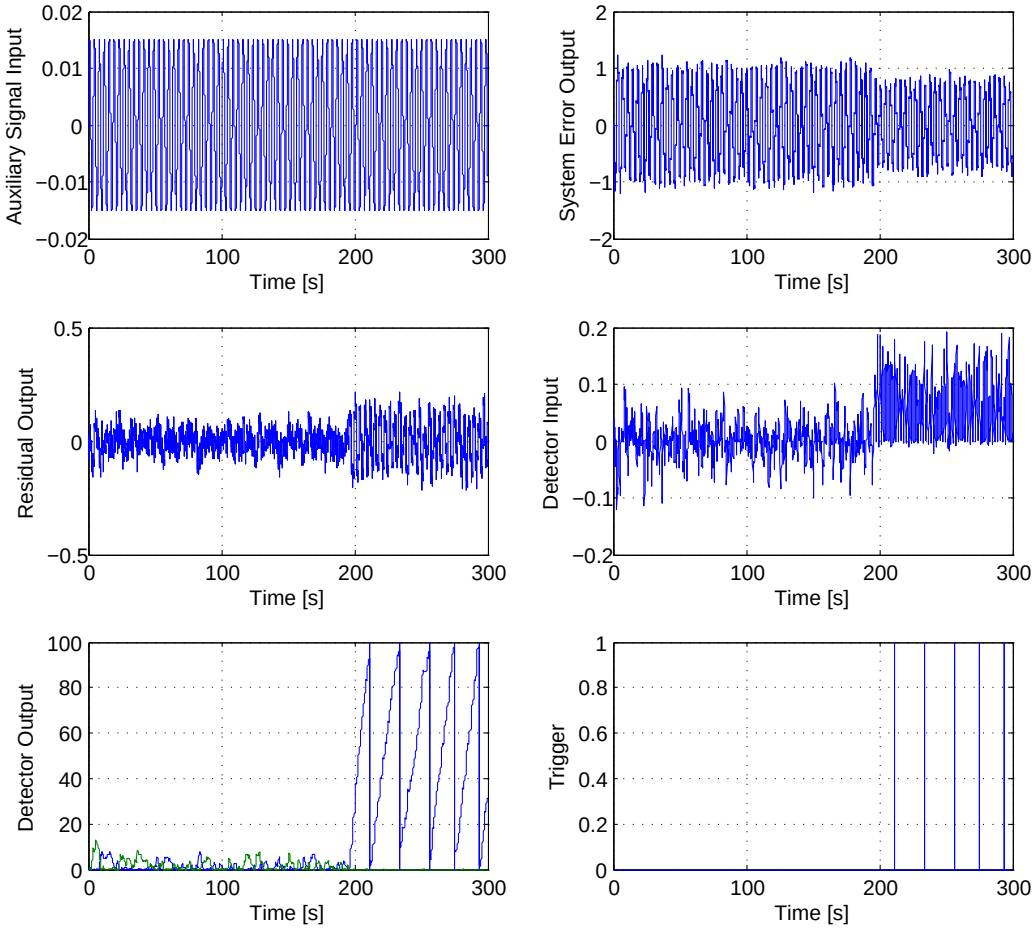

Figure 7.28: Simulation results with a moderate amount of noise in the correct ratio. Failure occurs at 195 seconds and is detected 16 seconds later. Note that each time the threshold is reached the detector is reset, and the trigger value is set to one for a single sample period.

residual output; the detector input; the detector output; and the detector trigger. Note that the setup proves robust against white noise, while providing a substantial signal to noise gain from error signal to residual output.

7.5.4 Full Lateral-Roll AFD System Simulation

From the AFD system developed for the full UAV lateral acceleration and roll model in subsection 7.4.1, a simple simulation can be implemented. The auxiliary signal amplitude is selected such that the additional faulty system disturbance is limited to ± 1 unit on the error output.

The simulation results are shown in Figure 7.30 for moderate levels of

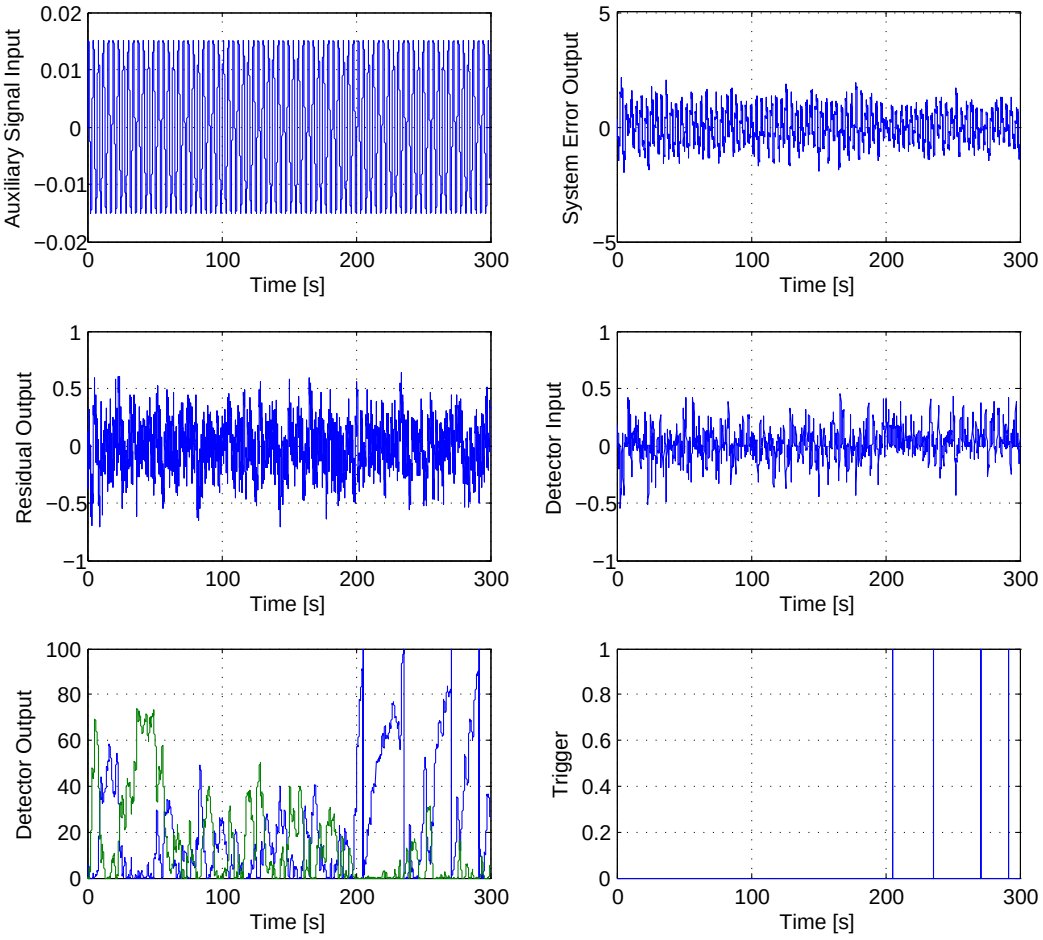

Figure 7.29: Simulation results with a large amount of noise in the correct ratio. Failure occurs at 195 seconds and is detected 11 seconds later. Note that each time the threshold is reached the detector is reset, and the trigger value is set to one for a single sample period.

white noise and in Figure 7.31 for high levels of white noise. In these figures the following is shown: the auxiliary excitation signal; the error output; the residual output; the detector input; the detector output; and the detector trigger. Note that the setup proves robust against white noise, while providing a substantial signal to noise gain from error signal to residual output.

7.6 Summary

When comparing the separate, simplified roll and lateral acceleration model AFD results to the combined model, the following is noted:

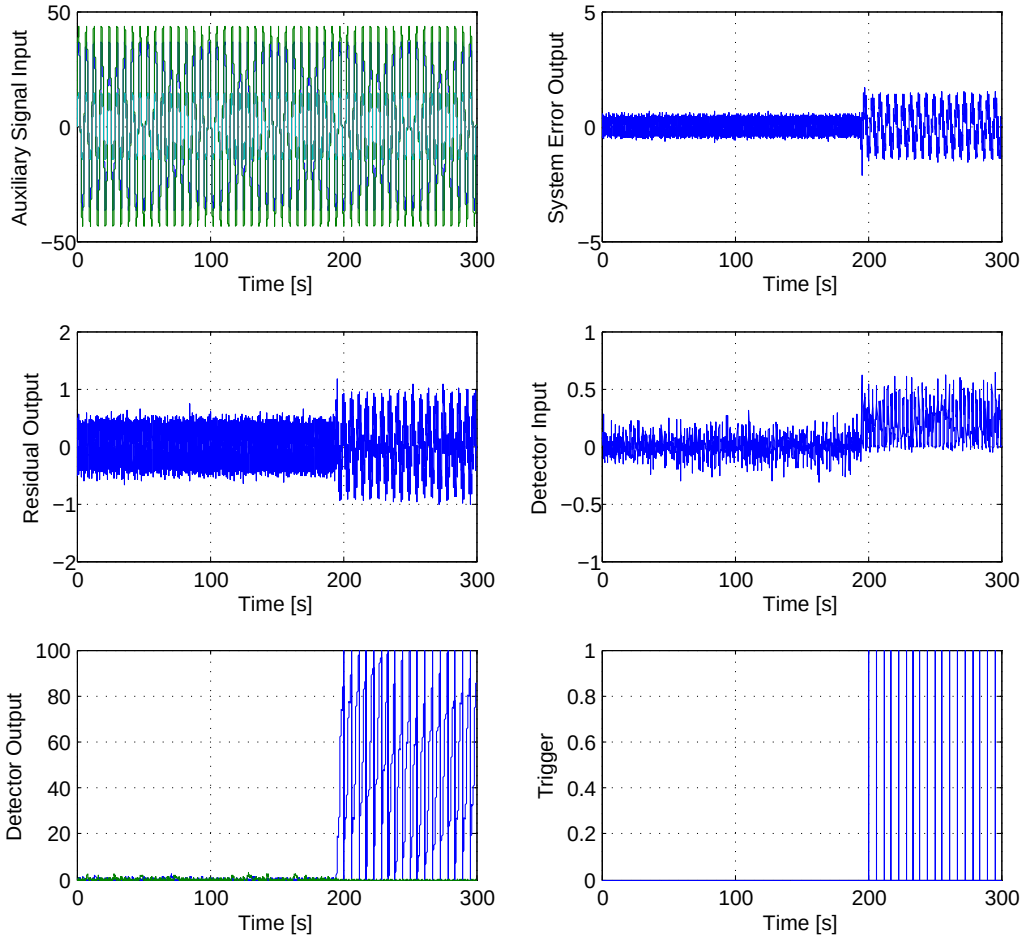

Figure 7.30: Simulation results with a moderate amount of noise in the correct ratio. Failure occurs at 195 seconds and is detected 5 seconds later. Note that each time the threshold is reached the detector is reset, and the trigger value is set to one for a single sample period.

- Both approaches result in no additional lateral acceleration being introduced into the system output.
- Both approaches excite all the actuators as well as system states.
- As was expected, the combined model results in far more balanced actuator excitation.

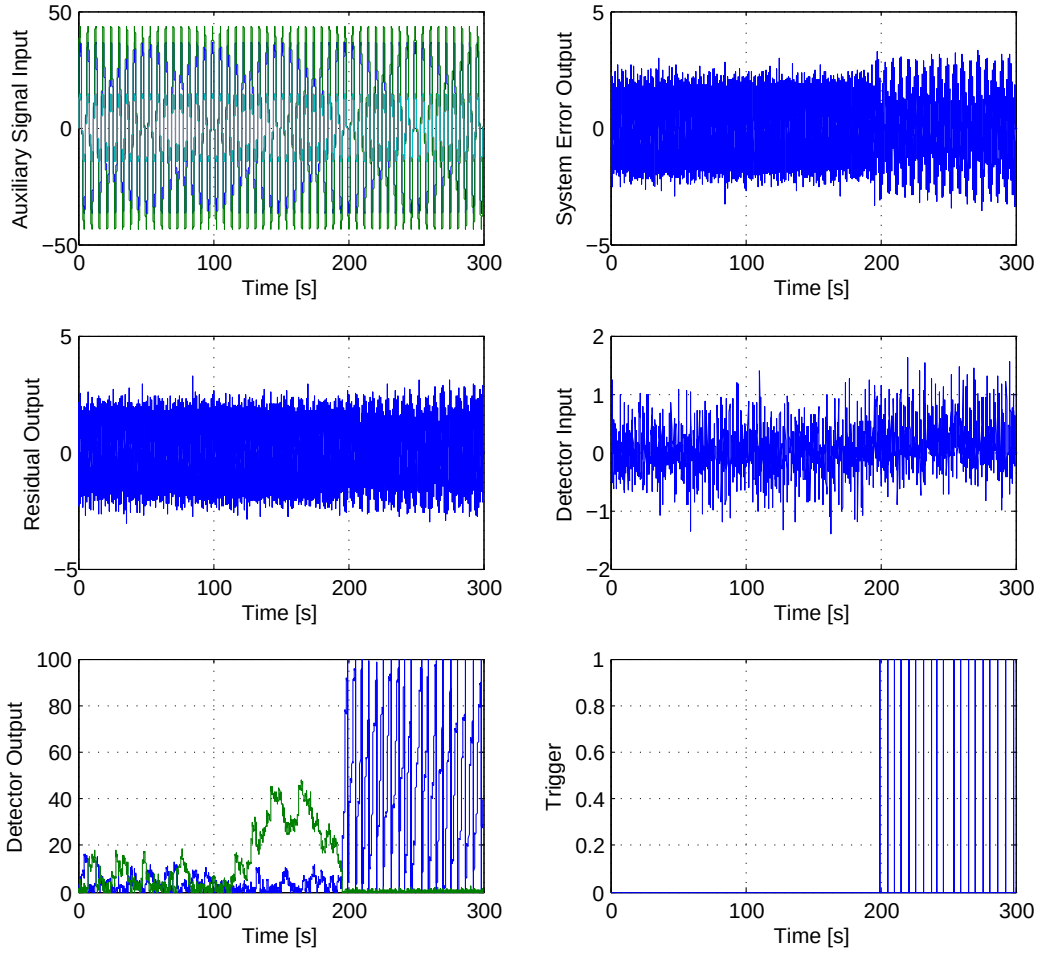

Figure 7.31: Simulation results with a large amount of noise in the correct ratio. Failure occurs at 195 seconds and is detected 4 seconds later. Note that each time the threshold is reached the detector is reset, and the trigger value is set to one for a single sample period.

Part IV

Conclusion

Chapter 8

Conclusion

Optimal open-loop active fault detection for a stable linear time-invariant system is considered. This investigation consists of: a brief literature review; the detailed development of a theoretical AFD optimisation framework; theoretical application of the framework; and the practical application of this AFD optimisation framework.

8.1 Theoretical Development

The research presented in [69], [71], [54] and [55] is simplified by considering the AFD problem in the open-loop case. The design of the estimator is considered an integral part of the AFD optimisation process instead of being a fixed controller attribute. It is therefore suggested that a separate estimator should be used for optimal state estimation, if desired. Equations are derived to minimise the noise covariance on the nominal residual output as well as to maximise the Dual Youla parameter. The framework allows the AFD optimisation to be performed for either the average- or worst-case scenario. This approach results in a novel, yet simple to apply AFD architecture.

The implications of applying the open-loop framework to stable closed-loop systems is considered and analysed. It is found that the open-loop framework can by applied to closed-loop systems, and that the performance improvement or degradation is quantifiable.

In order to realise a non-trivial solution, the open-loop theory is extended in a novel way to include dynamical effects of the detector. It is found that this

effect can be closely approximated by a second order transfer function, with a low-pass cut-off frequency determined by the minimum targeted detection time.

In an effort to decrease the complexity of applying the optimisation framework to the general MIMO case, an novel LTI pre-shaping filter is added. This filter incorporates the majority of the added MIMO complexities, thereby leaving the remainder of the system largely identical between MIMO and SISO applications.

The MIMO theory is further extended to take advantage of certain MIMO system null space properties. These system properties are used to arrive at two AFD solutions without the nominal performance penalty integral to the SISO theory. The simpler approach is applicable to systems with redundant actuators cancelling the injected disturbance at the input matrix. Alternatively, methods developed to solve the general output zeroing problem [73] are used to design a pre-shaping filter complying with the conditions stipulated in [73].

Finally, the theoretical framework is applied to a number of simple illustrative examples. These examples are designed in order to demonstrate the key AFD problem elements.

8.2 Practical Applicability

The application of active fault tolerant control to aerospace applications is discussed, and a conceptual AFTC system is designed. It is shown that such an ATFC system can be constructed from relatively simple sub-systems. The purpose of the various sub-systems including the fault detection system is discussed.

The theoretical AFD optimisation framework is applied to a small unmanned aerial vehicle. The AFD framework is first applied to simplified decoupled dynamical models. It is shown that the application is relatively simple, while providing rapid fault detection even in the presence of high levels of white noise. It is however noted that the relative actuator mix might prove problematic for the simplified lateral-acceleration case. It is finally shown that by combining the lateral-acceleration with the roll dynamics and considering all

the control surfaces independently, the rudder-aileron actuator mix problem can be adequately addressed.

8.3 Comparison to Industry Standard Methods

When comparing the method developed in this research to the commonly used multiple-model fault detection method, a number of important advantages are identified. In the multiple-model method a bank of Kalman filters is usually employed. Each one of these Kalman filters is then designed to match a postulated failure case. If a large number of non-nominal models need to be detected, this method can quickly result in a large computational load. Additionally it is difficult to envisage all possible failure cases. The method proposed here requires only a single estimator per fault class which must be optimised for. Non time-critical faults are still detected even if they were not explicitly optimised for. Detection in such cases merely occurs in a sub-optimal manner.

One major disadvantage to consider is that when a fault is detected by a multiple-model setup, the properties of the new model are immediately known. With the method presented here, system identification will need to be performed as a separate step. In a computationally constrained environment this might not be a compromise worth making.

8.4 Future Research Opportunities

The following possible future research opportunities are envisaged:

- A simplification is made by considering the system in the open-loop case. Closing a control loop around the system alters AFD performance due to the controller's disturbance rejection. Although this effect has been considered in the research presented here, future research should focus on explicitly deriving the optimised active fault detection framework for closed-loop systems.

- A major challenge with effective fault detection arises with compensating for model uncertainties without adversely effecting detection performance. The integration of an adaptive detector is therefore a possible extension to the framework presented here. This may include an adaptive estimator as well as adaptive excitation frequency and/or magnitude.

Appendices

Appendix A

Meraka Modular UAV Parameters

A.1 Engine Specifications

Parameter	Value
Engine Lag	0.4
Maximum Thrust	150
Minimum Thrust	0
Dynamic Thrust Multiplier	0.75

Table A.1: Meraka Engine Parameters

A.2 Physical Specifications

A.3 Aerodynamic Specifications

A.4 Converting Between Independent and Classic Control Derivatives

The control derivatives used in some of the research presented here, do not rely on the classic actuator definitions. Therefore, a few simple equations are needed in order to calculate the required control derivatives as a function of

Parameter	Value
Mass	26.0
Wing Span	4.0
Mean Aerodynamic Chord	0.36
Wing Reference Area	1.44
Wing Aspect Ratio	11.11
Wing Efficiency Factor	0.85
Moment of Inertia about x-axis	16.53436
Moment of Inertia about y-axis	11.58287
Moment of Inertia about z-axis	13.67195

Table A.2: Meraka Physical Parameters

Parameter	Value	Parameter	Value
C_{D_0}	0.06	C_{L_0}	0.5
C_{L_α}	5.557928	C_{L_q}	8.046991
C_{Y_β}	-0.389444	C_{Y_p}	0.049295
C_{Y_r}	0.244026	C_{M_0}	-0.05
C_{M_α}	-1.069455	C_{M_q}	-18.442581
C_{l_β}	-0.071508	C_{l_p}	-0.621899
C_{l_r}	0.194571	C_{n_β}	0.102214
C_{n_p}	-0.063578	C_{n_r}	-0.085316

Table A.3: Modular UAV Stability Derivatives

Actuator	$\mathbf{C}_{L_{\delta_x}}$	$\mathbf{C}_{Y_{\delta_x}}$	$\mathbf{C}_{l_{\delta_x}}$	$\mathbf{C}_{M_{\delta_x}}$	$\mathbf{C}_{N_{\delta_x}}$
Left Aileron	-0.47515	-0.009786	-0.16364	0.062452	0.0057296
Right Aileron	0.47515	-0.009786	-0.16364	-0.062452	0.0057296
Left Flap	0.59232	-0.010199	0.11539	-0.065031	0.003495
Right Flap	0.59232	0.010199	-0.11539	-0.065031	-0.003495
Left Elevator	0.17624	-0.028361	0.0072193	-0.6157	0.0092819
Right Elevator	0.17624	0.028361	-0.0072193	-0.6157	-0.0092819
Left Rudder	-0.03856	0.10766	0.0029221	0.13189	-0.035695
Right Rudder	0.03856	0.10766	0.0029221	-0.13189	-0.035695

Table A.4: Modular UAV Control Derivatives

the classic control derivatives. These equations are now presented for each of the actuator pairs.

A.4.1 Aileron Related Derivatives

The left and right aileron roll control derivatives are related to the classic aileron roll control derivative by

$$C_{l_{\delta_{A_l}}} = \frac{1}{2} C_{l_{\delta_A}} \tag{A.4.1}$$

$$C_{l_{\delta_{A_r}}} = \frac{1}{2} C_{l_{\delta_A}} \tag{A.4.2}$$

A.4.2 Flap Related Derivatives

The left and right flap roll control derivatives are related to the classic flap lift control derivative through

$$C_{l_{\delta_{F_l}}} = \frac{|y_F|}{2b} C_{L_{\delta_F}} \tag{A.4.3}$$

$$C_{l_{\delta_{F_r}}} = -\frac{|y_F|}{2b} C_{L_{\delta_F}} \tag{A.4.4}$$

where $|y_F|$ is the distance from the flap's centre of pressure to the roll axis.

A.4.3 Elevator Related Derivatives

The left and right elevator roll control derivatives are related to the classic elevator lift control derivative through

$$C_{l_{\delta_{E_l}}} = \frac{|y_E|}{2b} C_{L_{\delta_E}} \tag{A.4.5}$$

$$C_{l_{\delta_{E_r}}} = -\frac{|y_E|}{2b} C_{L_{\delta_E}} \tag{A.4.6}$$

where $|y_E|$ is the distance from the elevator's centre of pressure to the roll axis.

A.4.4 Rudder Related Derivatives

The left and right rudder roll control derivatives are related to the classic rudder roll control derivative by

$$C_{l_{\delta_{R_l}}} = \frac{1}{2} C_{l_{\delta_R}} \tag{A.4.7}$$

$$C_{l_{\delta_{R_r}}} = \frac{1}{2} C_{l_{\delta_R}} \tag{A.4.8}$$

Bibliography

[1] Ioannou, P. and Fidan, B.: *Adaptive Control Tutorial*. Advances in Design and Control. Society for Industrial and Applied Mathematics, 2006. ISBN 9780898716153.
Available at: https://books.google.co.za/books?id=hns365EBaZAC

[2] Safonov, M. and Fan, K.: Special issue: Multivariable stability margin. *Int. J. Robust & Nonlinear Control*, vol. 7, no. 2, pp. 97–226, 1997.

[3] Zhou, K.: *Essentials of robust control*. Prentice Hall, 1999.

[4] Tay, T.-T., Mareels, I. and Moore, J.B.: *High Performance Control*. Birkhäuser, 1997.

[5] Steinberg, M.: Historical overview of research in reconfigurable flight control. *Proceedings of the Institution of Mechanical Engineers, Part G: Journal of Aerospace Engineering*, vol. 219, no. 4, pp. 263–275, 2005.

[6] Jiang, J.: Fault-tolerant control systems: An introductory overview. *Acta Automatica Sinica*, vol. 31, no. 1, pp. 161–174, 2005.

[7] Isermann, R. and Ballé, P.: Trends in the application of model-based fault detection and diagnosis of technical processes. *Control engineering practice*, vol. 5, no. 5, pp. 709–719, 1997.

[8] Zhang, X. and Zarrop, M.: Auxiliary signals for improving on-line fault detection. In: *Control, 1988. CONTROL 88., International Conference on*, pp. 414–419. IET, 1988.

[9] Zhang, X.: *Auxiliary signal design in fault detection and diagnosis*. Lecture notes in control and Information sciences. Springer London, Limited, 1989. ISBN 9783540515593.

[10] Keresteciogl u, F.: *Change detection and input design in dynamical systems*. Research Studies Press Baldock, Hertfordshire, 1993.

[11] KERESTECIOG?LU, F. and ZARROP, M.B.: Input design for detection of abrupt changes in dynamical systems. *International Journal of Control*, vol. 59, no. 4, pp. 1063–1084, 1994.

[12] Nikoukhah, R., Campbell, S.L., Delebecque, F. *et al.*: Detection signal design for failure detection: a robust approach. 1998.

[13] Nikoukhah, R.: Guaranteed active failure detection and isolation for linear dynamical systems. *Automatica*, vol. 34, no. 11, pp. 1345–1358, 1998.

[14] Campbell, S.L. and Nikoukhah, R.: The design of auxiliary signals for robust active failure detection in uncertain systems. In: *Proceedings of the Mathematical Theory of Networks and Systems*. 2002.

[15] Campbell, S. and Nikoukhah, R.: Software for auxiliary signal design. In: *Proceedings of the American Control Conference, Boston, MA, USA*, pp. 4414–4419. 2004.

[16] Ashari, A.E., Nikoukhah, R. and Campbell, S.L.: Auxiliary signal design for robust active fault detection of linear discrete-time systems. *Automatica*, vol. 47, no. 9, pp. 1887–1895, 2011.

[17] Carstens, N.: *Development of a low-cost and low-weight flight control system for an electrically powered free-flying model helicopter*. Master's thesis, Masters dissertation, University of Stellenbosch, 2004.

[18] Peddle, I.K.: *Autonomous flight of a model aircraft*. Master's thesis, Stellenbosch: Stellenbosch University, 2005.

[19] Venter, J.: *Development of an experimental tilt-wing VTOL Unmanned Aerial Vehicle*. Master's thesis, Stellenbosch: University of Stellenbosch, 2006.

[20] Hough, W.J.: *Autonomous aerobatic flight of a fixed wing unmanned aerial vehicle.* Master's thesis, Stellenbosch: University of Stellenbosch, 2007.

[21] Roos, J.-C.J.C.: *Autonomous take-off and landing of a fixed wing unmanned aerial vehicle.* Master's thesis, Stellenbosch: Stellenbosch University, 2007.

[22] Peddle, I.K.: *Acceleration based manoeuvre flight control system for unmanned aerial vehicles.* Ph.D. thesis, Stellenbosch: Stellenbosch University, 2008.

[23] Blaauw, D.: *Flight control system for a variable stability blended-wing-body unmanned aerial vehicle.* Master's thesis, Stellenbosch: University of Stellenbosch, 2009.

[24] Gaum, D.R.: *Agressive flight control techniques for a fixed wing unmanned aerial vehicle.* Master's thesis, Stellenbosch: University of Stellenbosch, 2009.

[25] Smit, S.J.A.: *Autonomous landing of a fixed-wing unmanned aerial vehicle using differential GPS.* Master's thesis, Stellenbosch: Stellenbosch University, 2013.

[26] Kriel, S.C.: *A comparison of control systems for the flight transition of vtol unmanned aerial vehicles.* Master's thesis, Stellenbosch: University of Stellenbosch, 2008.

[27] Visser, B.J.: *Presisie landing van'n onbemande vliegtuig.* Master's thesis, Stellenbosch: Stellenbosch University, 2008.

[28] Pietersen, W.H.: *System identification for fault tolerant control of unmanned aerial vehicles.* Master's thesis, Stellenbosch: University of Stellenbosch, 2010.

[29] Basson, L.: *Control allocation as part of a fault-tolerant control architecture for UAVs.* Master's thesis, Stellenbosch: University of Stellenbosch, 2011.

[30] Basson, W.A.: *Fault tolerant adaptive control of an unmanned aerial vehicle*. Master's thesis, Stellenbosch: Stellenbosch University, 2011.

[31] Beeton, W.: *Fault tolerant flight control of a UAV with asymmetric damage to its primary lifting surface*. Master's thesis, 2013.

[32] Appel, J.-P.: *Online system identification for fault tolerant control of unmanned aerial vehicles*. Master's thesis, Stellenbosch: Stellenbosch University, 2013.

[33] Odendaal, H.M.: *An analysis and comparison of two methods for UAV actuator fault detection and isolation*. Master's thesis, Stellenbosch: Stellenbosch University, 2012.

[34] Zhang, Y. and Jiang, J.: Bibliographical review on reconfigurable fault-tolerant control systems. *Annual Reviews in Control*, vol. 32, pp. 229–252, 2008.

[35] Venkatasubramanian, V., Rengaswamy, R., Yin, K. and Kavuri, S.N.: A review of process fault detection and diagnosis: Part i: Quantitative model-based methods. *Computers & chemical engineering*, vol. 27, no. 3, pp. 293–311, 2003.

[36] Venkatasubramanian, V., Rengaswamy, R. and Kavuri, S.N.: A review of process fault detection and diagnosis: Part ii: Qualitative models and search strategies. *Computers & Chemical Engineering*, vol. 27, no. 3, pp. 313–326, 2003.

[37] Venkatasubramanian, V., Rengaswamy, R., Kavuri, S.N. and Yin, K.: A review of process fault detection and diagnosis: Part iii: Process history based methods. *Computers & chemical engineering*, vol. 27, no. 3, pp. 327–346, 2003.

[38] Frank, P.M. and Ding, X.: Frequency domain approach to optimally robust residual generation and evaluation for model-based fault diagnosis. *Automatica*, vol. 30, no. 5, pp. 789–804, 1994.

[39] Patton, R. and Chen, J.: Observer-based fault detection and isolation: robustness and applications. *Control Eng. Practice*, vol. 5, pp. 671–682, 1997.

[40] Zhang, Y. and Li, X.R.: Detection and diagnosis of sensor and actuator failures using interacting multiple-model estimator. In: *Decision and Control, 1997., Proceedings of the 36th IEEE Conference on*, vol. 5, pp. 4475–4480. IEEE, 1997.

[41] Zhang, Y. and Li, X.R.: Detection and diagnosis of sensor and actuator failures using imm estimator. *Aerospace and Electronic Systems, IEEE Transactions on*, vol. 34, no. 4, pp. 1293–1313, 1998.

[42] Zhan, Y. and Jiang, J.: An interacting multiple-model based fault detection, diagnosis and fault-tolerant control approach. In: *Decision and Control, 1999. Proceedings of the 38th IEEE Conference on*, vol. 4, pp. 3593–3598. IEEE, 1999.

[43] Gertler, J. and Singer, D.: A new structural framework for parity equation-based failure detection and isolation. *Automatica*, vol. 26, no. 2, pp. 381–388, 1990.

[44] Gertler, J.: Analytical redundancy methods in fault detection and isolation. In: *Proceedings of IFAC/IAMCS symposium on safe process*, vol. 1, pp. 9–21. 1991.

[45] Gertler, J.: Fault detection and isolation using parity relations. *Control engineering practice*, vol. 5, no. 5, pp. 653–661, 1997.

[46] Zhong, M., Ding, S.X., Lam, J. and Wang, H.: An lmi approach to design robust fault detection filter for uncertain lti systems. *Automatica*, vol. 39, no. 3, pp. 543–550, 2003.

[47] Wei, X. and Verhaegen, M.: Lmi solutions to the mixed h_-/h_∞ fault detection observer design for linear parameter-varying systems. *International Journal of Adaptive Control and Signal Processing*, vol. 25, no. 2, pp. 114–136, 2011.

[48] Edwards, C., Spurgeon, S.K. and Patton, R.J.: Sliding mode observers for fault detection and isolation. *Automatica*, vol. 36, no. 4, pp. 541–553, 2000.

[49] Tan, C.P. and Edwards, C.: Sliding mode observers for detection and reconstruction of sensor faults. *Automatica*, vol. 38, no. 10, pp. 1815–1821, 2002.

[50] Spurgeon, S.K.: Sliding mode observers: a survey. *International Journal of Systems Science*, vol. 39, no. 8, pp. 751–764, 2008.

[51] Zhang, Y. and Jiang, J.: Integrated active fault-tolerant control using imm approach. *Aerospace and Electronic Systems, IEEE Transactions on*, vol. 37, no. 4, pp. 1221–1235, 2001.

[52] Nikoukhah, R., Campbell, S.L., Horton, K.G. and Delebecque, F.: Auxiliary signal design for robust multimodel identification. *Automatic Control, IEEE Transactions on*, vol. 47, no. 1, pp. 158–164, 2002.

[53] Campbell, S.L., Horton, K.G. and Nikoukhah, R.: Auxiliary signal design for rapid multi-model identification using optimization. *Automatica*, vol. 38, no. 8, pp. 1313–1325, 2002.

[54] Niemann, H.: Active fault diagnosis in closed-loop systems. In: *Proceedings of the IFAC World Congress.* 2005.

[55] Niemann, H.: A setup for active fault diagnosis. *IEEE Transactions on Automatic Control*, vol. 51, no. 9, pp. 1572–1578, 2006.

[56] Niemann, H. and Poulsen, N.K.: Information based fault diagnosis. In: *17th World Congress, The Internation Federation of Automatic Control*, pp. 8890–8895. 2008.

[57] Poulsen, N.K. and Niemann, H.: Active fault diagnosis based on stochastic tests. *International Journal of Applied Mathematics and Computer Science*, vol. 18, pp. 487–496, 2008.

[58] Iri, M., Aoki, K., O'Shima, E. and Matsuyama, H.: An algorithm for diagnosis of system failures in the chemical process. *Computers & Chemical Engineering*, vol. 3, no. 1, pp. 489–493, 1979.

[59] Vedam, H. and Venkatasubramanian, V.: Signed digraph based multiple fault diagnosis. *Computers & chemical engineering*, vol. 21, pp. S655–S660, 1997.

[60] Kuipers, B.: The limits of qualitative simulation. In: *IJCAI*, pp. 128–136. Citeseer, 1985.

[61] Kuipers, B.: Qualitative simulation. *Artificial intelligence*, vol. 29, no. 3, pp. 289–338, 1986.

[62] Krishnamurthi, M. and Phillips, D.T.: An expert system framework for machine fault diagnosis. *Computers & industrial engineering*, vol. 22, no. 1, pp. 67–84, 1992.

[63] Liu, S. and Liu, S.: An efficient expert system for machine fault diagnosis. *The International Journal of Advanced Manufacturing Technology*, vol. 21, no. 9, pp. 691–698, 2003.

[64] da Silva, J.C., Saxena, A., Balaban, E. and Goebel, K.: A knowledge-based system approach for sensor fault modeling, detection and mitigation. *Expert Systems with Applications*, vol. 39, no. 12, pp. 10977–10989, 2012.

[65] Sorsa, T., Koivo, H.N. and Koivisto, H.: Neural networks in process fault diagnosis. *Systems, Man and Cybernetics, IEEE Transactions on*, vol. 21, no. 4, pp. 815–825, 1991.

[66] Patton, R., Chen, J. and Siew, T.: Fault diagnosis in nonlinear dynamic systems via neural networks. In: *Control, 1994. Control'94. International Conference on*, vol. 2, pp. 1346–1351. IET, 1994.

[67] Tamura, M. and Tsujita, S.: A study on the number of principal components and sensitivity of fault detection using pca. *Computers & Chemical Engineering*, vol. 31, no. 9, pp. 1035–1046, 2007.

[68] Shams, M.B., Budman, H. and Duever, T.: Fault detection, identification and diagnosis using cusum based pca. *Chemical Engineering Science*, vol. 66, no. 20, pp. 4488–4498, 2011.

[69] Youla, D., Bongiorno, J., J. and Jabr, H.: Modern wiener–hopf design of optimal controllers part i: The single-input-output case. *Automatic Control, IEEE Transactions on*, vol. 21, no. 1, pp. 3 – 13, feb 1976. ISSN 0018-9286.

[70] Youla, D., Jabr, H. and Bongiorno, J., J.: Modern wiener-hopf design of optimal controllers–part ii: The multivariable case. *Automatic Control, IEEE Transactions on*, vol. 21, no. 3, pp. 319 – 338, jun 1976. ISSN 0018-9286.

[71] Niemann, H.: Dual youla parameterisation. In: *IEE Proceedings -Control Theory and Applications*, vol. 150. 2003.

[72] Nikoukhah, R. and Campbell, S.L.: Auxiliary signal design for active failure detection in uncertain linear systems with a priori information. *Automatica*, vol. 42, no. 2, pp. 219 – 228, 2006. ISSN 0005-1098.

[73] Tokarzewski, J.: A general solution to the output-zeroing problem for mimo lti systems. *International Journal of Applied Mathematics and Computer Science*, vol. 12, pp. 161–172, 2002.

[74] Green, M. and Limebeer, D.J.: *Linear robust control*. Courier Dover Publications, 2012.

[75] Blanke, M., Kinnaert, M., Lunze, J. and Staroswiecki, M.: *Diagnosis and Fault-Tolerant Control*. Springer, 2006.

[76] Basseville, M. and Nikiforov, I.V.: *Detection of Abrupt Changes:Theory and Application*. Prentice-Hall, 1993.

[77] Van Trees, H.L.: *Detection, estimation, and modulation theory*, vol. 1. John Wiley & Sons, 2001.

[78] Toscano, R.: *Structured Controllers for Uncertain Systems: A Stochastic Optimization Approach*. Advances in Industrial Control. Springer London, 2013. ISBN 9781447151883.
Available at: https://books.google.co.za/books?id=qf3hSresSfcC

[79] Marler, R. and Arora, J.: Survey of multi-objective optimization methods for engineering. *Structural and Multidisciplinary Optimization*, vol. 26, pp. 369–395, 2004. ISSN 1615-147X. 10.1007/s00158-003-0368-6.

[80] Arora, J.S.: *Introduction to Optimum Design*. Elsevier Academic Press, 2004.

[81] Busch, R. and Peddle, I.: Active fault detection for open loop stable lti siso systems. *International Journal of Control, Automation and Systems*, vol. 12, no. 2, pp. 324–332, 2014. ISSN 1598-6446.

[82] Scheck, W.: Lawrence sperry: Autopilot inventor and aviation innovator. November 2004.
Available at: http://www.historynet.com/lawrence-sperry-autopilot-inventor-and-aviation-innovator.htm

[83] Isermann, R.: Supervision, fault-detection and fault-diagnosis methods – an introduction. *Control Engineering Practice*, vol. 5, no. 5, pp. 639 – 652, 1997. ISSN 0967-0661.

[84] Ducard, G.: *Fault-tolerant Flight Control and Guidance Systems*. Springer, 2009.